Mountain water resources, groundwater and climate change in the Peruvian Andes

Lauren D. Somers
Department of Earth and Planetary Sciences
McGill University, Montreal

April 2019

A thesis submitted to McGill University in partial fulfillment of requirements of the degree of Doctor of Philosophy.

Abstract

Mountain regions provide a disproportionately large amount of the world's fresh water resources. In the tropical Andes, a combination of glacier melt and stored groundwater feed streamflow during the dry season when there is very little precipitation. As the climate warms, glaciers in the tropical Andes are retreating faster than mountain glaciers anywhere else in the world, contributing to water stress for downstream users. Meanwhile, little research has been done to understand the mountain groundwater system despite its demonstrated importance in providing water to streams.

In this thesis, I first use a novel combination of temperature and dye tracing to characterize and quantify groundwater-surface water exchange in the Quilcayhuanca proglacial valley of the Cordillera Blanca in Northern Peru. I show that over a 4 km stream reach, ~30% of the discharge is gained from groundwater and that the moraine sections of the stream were sites of substantial exchange.

Second, I integrate glacier, surface-water and groundwater modelling to elucidate the current and future role of groundwater in the Shullcas Watershed in central Peru. My results indicate that the watershed's glaciers are likely to disappear before the end of the 21st century. While groundwater temporarily helps to buffer the loss of glacier meltwater during the dry season, it is eventually effected by decreasing groundwater recharge.

Third, I use our improved understanding of mountain groundwater processes to assess infiltration trenching as an adaptation strategy to climate change. Results show that infiltration trenching in the Shullcas Watershed slightly increases groundwater recharge by capturing overland flow. However, the small increase in infiltration results in an increase in dry season baseflow by less than 1% and would supply approximately 800 more people with municipal water.

These combined results demonstrate the growing importance of groundwater in the Andes and provide important information for water managers.

Résumé

Les régions montagneuses fournissent une quantité disproportionnément grande des ressources en eau douce du monde. Dans les Andes tropicales, l'eau de fonte des glaciers et l'eau souterraine alimentent les rivières pendant la saison sèche lors de laquelle les précipitations sont quasi inexistantes. À mesure que le climat se réchauffe, les glaciers des Andes tropicales se retirent plus rapidement que les glaciers de montagne ailleurs dans le monde, ce qui peut contribuer à des pénuries d'eau pour les utilisateurs en aval. Entre-temps, peu de recherches ont été menées pour comprendre le réseau hydrogéologique en régions montagneuses malgré la démonstration de son importance dans l'approvisionnement en eau des rivières.

Dans cette thèse, j'utilise en premier lieu une combinaison innovatrice de traceurs thermiques et de traceurs fluorescents pour caractériser et quantifier les échanges entre les eaux souterraines et les eaux de surface dans la vallée proglaciaire de Quilcayhuanca de la Cordillera Blanca au nord du Pérou. Je démontre que, sur une section de rivière de 4 km, environ 30% du débit de la rivière provient des eaux souterraines et que les sections contenant des dépôts morainiques sont des parties où des d'échanges importants ont lieus.

Deuxièmement, j'intègre des modèles de fonte glaciaire, d'eau de surface et d'eau souterraine pour élucider le rôle actuel et futur des eaux souterraines dans le bassin versant Shullcas situé dans le centre du Pérou. Mes résultats indiquent que les glaciers du bassin versant devraient probablement

disparaître complètement d'ici la fin du 21e siècle. Les eaux souterraines aident temporairement à amortir la perte d'eau de fonte des glaciers pendant la saison sèche, mais seront éventuellement affectées par une diminution de la recharge des eaux souterraines.

Troisièmement, j'utilise notre compréhension améliorée du système hydrogéologique de montagnes pour évaluer l'efficacité des tranchées d'infiltration comme stratégie d'adaptation aux changements climatiques. Les résultats montrent que les tranchées d'infiltration dans le bassin versant Shullcas augmentent légèrement la recharge des nappes phréatiques en capturant le ruissellement en surface. Cependant, cette faible augmentation d'infiltration entraîne une augmentation du débit de base lors des saisons sèches de moins de 1% et alimenterait environ 800 personnes supplémentaires en eau.

Ces résultats fournissent des informations importantes aux responsables de la gestion de l'eau et démontrent l'importance croissante des eaux souterraines dans les Andes.

Table of Contents

Abstract II
Résumé III
List of Figures VII
List of Tables X
Table of Numerical Models XI
Contribution to original knowledge XII
Acknowledgements XIII
Contribution of authors XIV
Chapter 1. Introduction and literature review 1
1.1 Glaciers and water resources 1
1.2 Tropical glaciers 2
1.3 Mountain groundwater 5
1.4 Climate and hydrological projections in the Andes 10
1.5 Hydrological climate change adaptations strategies 11
1.6 Objectives 13
Chapter 2. Quantifying groundwater-surface water interactions in a proglacial valley, Cordillera Blanca, Peru 14
2.1 Context within thesis 14
2.2 Abstract 14
2.3 Introduction 15
2.4 Study area 18
2.5 Methodology 22
2.6 Results 32
2.7 Discussion 43
2.8 Conclusion 47
2.9 Acknowledgements 49
2.10 References 49
Chapter 3. Climate impacts on Andean water resources using a mountain systems approach 57
3.1 Context within thesis 57
3.2 Abstract 57

3.3 Introduction ... 58
3.4 Methods ... 60
3.5 Results ... 64
3.6 Conclusions ... 76
3.7 Acknowledgements ... 79
3.8 Supplementary Material ... 79
3.9 References ... 93
Chapter 4. Does hillslope trenching enhance groundwater recharge and baseflow in the Peruvian Andes? ... 103
4.1 Context within thesis ... 103
4.2 Abstract ... 103
4.3 Introduction ... 104
4.4 Study Area ... 107
4.5 Methods ... 111
4.6 Results ... 119
4.7 Discussion ... 130
4.8 Conclusions ... 136
4.10 Supplementary materials ... 137
4.11 References ... 144
Chapter 5. Discussion ... 155
5.1 Challenges and opportunities ... 155
5.2 Directions for future research ... 157
Chapter 6. Conclusions and summary ... 159
References ... 162

List of Figures

(Captions abridged)

Figure 1.1: Schematic showing the different sources of streamflow for a tropical proglacial stream during the rainy and dry seasons. 1

Figure 1.2 : "Population and water risk in Andean countries" from Schoolmeester et al., (2018). 4

Figure 1.3: Precipitation versus specific discharge (river discharge divided by watershed area) for 12 glaciated and un-glaciated catchments in Nepal, from Andermann et al. (2012) 6

Figure 1.4: Hydrological fluxes in the Opabin Watershed in British Columbia, Canada, from Hood & Hayashi (2015) 7

Figure 1.5: Conceptual models for groundwater flow in valleys of the Cordillera Blanca, Peru from Glas et al. (2018). 8

Figure 2.1: (a.) Location of the Cordillera Blanca mountain range, Peru (b.) Location of the Quilcay River study section in the Quilcayhuanca Valley, (c.) KAP aerial imagery of the study area, (d.) Slope map of the study area. 19

Figure 2.2: Root mean square error contours versus groundwater temperature and total groundwater inflow described as the total change in stream discharge. 26

Figure 2.3: (a.) Stream shading versus distance downstream, (b.) Tributary width versus distance downstream, (c.) Main Channel width versus distance downstream, (d.) Observed stream temperature in space and time, (e.) Air temperature versus time (f.) Relative humidity versus time (g.) Wind speed versus time (h.) Net heat fluxes entering and leaving the stream versus time. .. 34

Figure 2.4: Simulated and measured stream temperature 39

Figure 2.5: Net and apparent stream discharge profiles (lower graph) and gross gains and losses (upper graph). 45

Figure 3.1: Maps of the Shullcas Watershed 66

Figure 3.2: Modeled stream fluxes and storage reservoirs for the Shullcas Watershed between Aug 1, 2016 and 2017 (arbitrarily selected year). 68

Figure 3.3: Climate, glacier and hydrologic projections.. 72

Figure 3.4: Conceptual model of an Andean proglacial watershed showing hydrologic pathways and future changes in hydrologic variables 78

Figure 3.5: Comparison of modeled and measured streamflow for six short-term daily stream records (panels A-F) and ANA long term stream gauge record (G).. 86

Figure 3.6: Comparison of measured outflow from Chuspicocha proglacial Lake and inflow calculated from lake level and area.. 87

Figure 3.7: Sensitivity of streamflow to selected input variables... 90

Figure 4.1: Map of study catchment within a non-glacierized basin of the Shullcas watershed. 108

Figure 4.2: a. Construction of infiltration trenches as part of the World Bank and Care funded PRAA project; b. Infiltration trench with ponded water; c. Aerial view of trenched hillslope in the Shullcas Watershed, from Google Earth™.. 110

Figure 4.3: Recharge model schematic. Red arrows indicate movement of water through the relevant hydrological processes. 113

Figure 4.4: Input variables and results for the recharge model for an idealized grassy hillslope. 120

Figure 4.5: a. Precipitation, infiltration and recharge for the base case and trenched scenarios. b. Difference in infiltration and recharge amounts for the base case and trenched case 122

Figure 4.6: Measured stream discharge compared to modeled baseflow and modeled stream discharge over the 14 month groundwater simulation period... 125

Figure 4.7: Sensitivity to trenching configuration 130

Figure 4.8: Unsaturated Zone Flow Package 2D model domain for the trenched scenario. 139

Figure 4.9: Groundwater flow model domain.. 140

Figure 4.10: Map of the study catchment showing particle path lines, as calculated using MODPATH. Travel times are indicated by the path colour. 142

Figure 4.11: Sensitivity to trenching configuration in percent difference. 143

List of Tables

Table 2.1: HFLUX input parameters.. 33

Table 2.2: Simulation results. 37

Table 2.3: Sensitivity Analysis 40

Table 2.4: Minimum gross gains and losses estimated based on HFLUX discharge profiles..... 42

Table 3.1: Changes in model fluxes between 2000-2009 and 2090-2099.................................. 75

Table 3.2: Model Setup and selected Input parameters for GSFLOW 82

Table 3.3: Model Goodness of Fit 86

Table 3.4: Sensitivity ranking for selected Input variables for GSFLOW.................................. 89

Table 3.5: Groundwater projections: 92

Table 4.1: Basin and Sub-basin properties and discharge 111

Table 4.2: Model input parameters 123

Table 4.3: Hillslope sensitivity analysis 128

Table of Numerical Models

Model	Use	Chapter
Glacier Module	Calculates glacier melt and mass given meteorological data and glacier hypsometric information.	3
GRASS-GSFLOW	Program to set up spatially distributed inputs for GSFLOW	3
GSFLOW	Coupled groundwater and surface water model used to simulate a mountain hydrological system and project climate change impacts.	3
HFLUX	Calculates stream temperature in space and time given meteorological data and groundwater inflow and temperature.	1
MODFLOW	Three-dimensional groundwater flow model used in Chapter 4 to ascertain the influence of hillslope trenching on river baseflow.	4
MODFLOW UZF Package	Unsaturated Zone Flow Package simulates vertical groundwater flow through the unsaturated zone in MODFLOW. It is used in Chapter 4 to calculate recharge in an idealized hillslope.	4
MODFLOW RIV Package	River Package simulates streamflow in MODFLOW.	4
One dimensional infiltration model	Calculates infiltration into an idealized hillslope from meteorological data and infiltration capacity for trenched and non-trenched scenarios	4

Contribution to original knowledge

This thesis represents an advance in our understanding of the role of groundwater in mountain hydrological systems. Previous research has demonstrated that groundwater contributes a large proportion of mountain streamflow during dry periods. I elucidate the spatial distribution and hydrological processes behind the contribution of groundwater to a proglacial river in the Peruvian Andes using a novel tracer approach. I then use this understanding in basin-scale numerical modelling of a proglacial Andean watershed.

Previous numerical modelling approaches in the glaciated Andes, have simplified or neglected groundwater flow processes in mountain hydrological systems and do not explore the future role of groundwater despite its hypothesized importance. My PhD research represents the first effort to incorporate process based representation of groundwater flow in projecting the hydrologic impacts of climate change in a tropical glacierized mountain watershed. Furthermore, I use our improved understanding of mountain groundwater to provide the first assessment of hillslope trenching as a groundwater-based climate change adaptations strategy. These results contribute to knowledge in an understudied environment that is simultaneously critically important for water supply.

Acknowledgements

I would like to thank my PhD supervisor, Dr. Jeffrey McKenzie, for his guidance over the last five years. Jeff fostered my creativity and helped me become an independent researcher while also providing important support and guidance through challenging periods of my PhD. Working with him has been a pleasure and I have benefitted enormously from the wonderful learning environment that he created.

It has been a privilege to be a part of an international and interdisciplinary team investigating Andean hydrology. In particular, Dr. Bryan Mark has been instrumental in facilitating my PhD research in Peru and has been a role model in leading an inclusive and collaborative team. This project would also not be possible without Dr. Pablo Lagos, who coordinated our work in the Shullcas Watershed and was a liaison with Peruvian institutions. Furthermore, Dr. Laura Lautz, Dr. Michel Baraer and Dr. Barret Kurylyk have all helped me grow as a researcher by providing advice, engaging discussions and fieldwork opportunities.

I would also like to thank my fellow EPS graduate students for their support and friendship, particularly those in the Laboratory for Advanced Hydrogeological Modelling And Stuff (LAHMAS) including Caroline Aubry-Wake, Pierrick Lamontagne-Hallé, Rob Wu, and Laura Lyon, as well as the EPS administrative team.

Finally, I would like to thank my family for their unwavering support without which this Thesis would not be possible.

Contribution of authors

This thesis is composed of three manuscripts for which I am first author, but that are written in collaboration with several colleagues. My supervisor, Jeffrey McKenzie, Project lead, Bryan Mark, and committee member Michel Baraer are co-authors on all three manuscripts for their contribution to the vision of the projects, field assistance and manuscript editing. Pablo Lagos is included as a co-author on manuscripts from Chapter 3 and 4 for his co-leadership of the Shullcas Watershed project and for supplying field and logistical support.

The first manuscript (Chapter 2) was published in *Hydrological Processes* in 2016. Laura Lautz, Ryan Gordon, Oliver Wigmore are included as coauthors for contributing to project vision, fieldwork, manuscript writing and editing. Anne Marie Glose is included for contributing to the design of the HFLUX software. Robin Glas and Caroline Aubry-Wake contributed to fieldwork and scientific discussions and Thomas Condom is included for his vision in the original conception of the wider hydrologic monitoring project.

The second manuscript (Chapter 3) will be submitted for publication to a peer-reviewed journal in 2019. Additional co-authors include Gene-Hua Crystal Ng and Andrew Wickert for their help in implementing GSLFOW modelling software, and Christian Yarleque and Yamina Silva, who provided downscaled climate projections.

The third manuscript (Chapter 4) was published in *Hydrological Processes* in 2018. Samuel Zipper is included as a co-author for his help in implementing groundwater modelling and his edits to the paper.

Chapter 1. Introduction and literature review

1.1 Glaciers and water resources

Mountains play an important role in global water supply because they receive more precipitation than lowland areas due to the orographic effect, and they contain large stores of water as snow and ice. Meltwater from mountain glaciers and snow pack, along with groundwater, provides consistent streamflow during dry periods, usually in the late summer for mid-high latitudes or during the dry season for low-latitudes (Figure 1.1) (Barnett *et al*., 2005; Viviroli *et al*., 2007; Prichard, 2017).

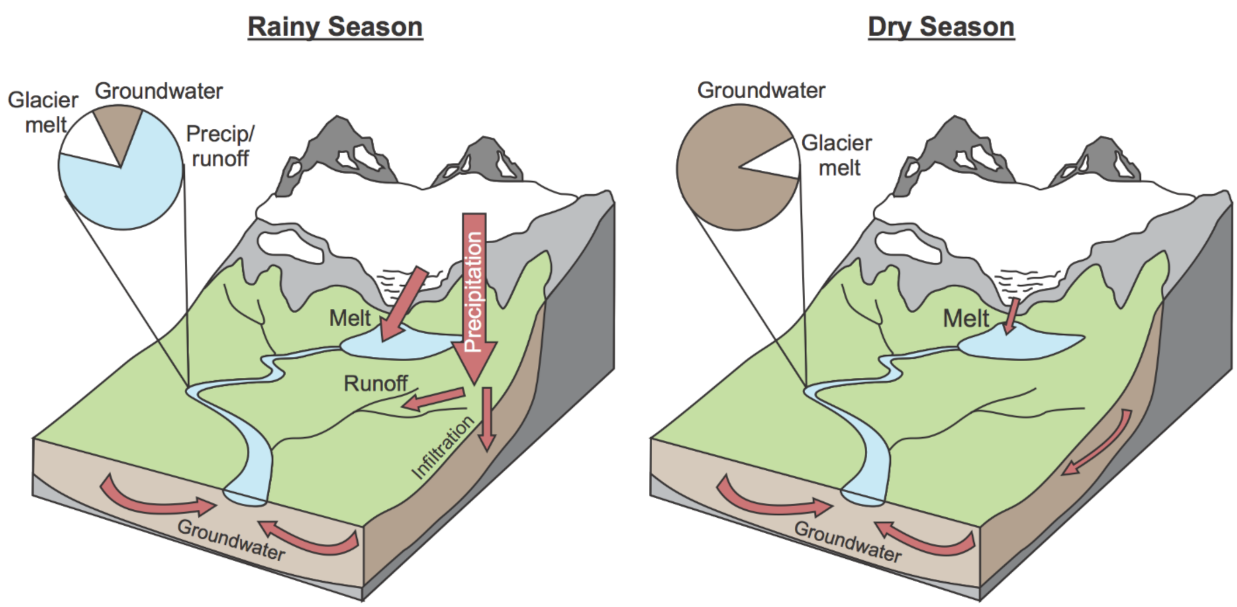

Figure 1.1: *Schematic showing the different sources of streamflow for a tropical proglacial stream during the rainy and dry seasons.*

Glaciers are sensitive indicators of climate change; they expand or retreat to remain in equilibrium with local climatic conditions. Worldwide, glaciers have experienced accelerated retreat since the 1980s due to climate change (Paul *et al*., 2004, Kaser *et al.*, 2006) with tropical alpine glaciers experiencing more rapid retreat than those at higher latitudes (Paul *et al*., 2004; Rabatel *et al.* 2013; Vuille *et al.*, 2018). Continued glacial retreat is expected for all greenhouse gas emission scenarios (Marzeion *et al*., 2018, Radic *et al.,* 2013).

Glacier recession causes a temporary increase in melt water (due to a permanent loss of ice mass), and downstream discharge, followed by a longer term decrease (Gleick and Palaniappan, 2010). The turning point, known as glacier peak water, has already passed for approximately half of large proglacial basin worldwide (Huss and Hock, 2018) and the proportion for Andean proglacial catchments is even higher (Baraer *et al*., 2012; Huss and Hock, 2018; Vuille *et al*., 2018). Following the disappearance of a glacier, the annual streamflow will return to pre-recession (equilibrium) levels but the melt season or dry season streamflow will be lower than before (Huss and Hock, 2018). This is particularly concerning for Andean proglacial catchments where the pronounced seasonality in precipitation makes them vulnerable to dry season water shortages (Bury *et al.,* 2013).

1.2 Tropical glaciers

Tropical glaciers are mountain glaciers located at high elevations at tropical latitudes (23.5°N-23.5°S). Almost all (ie. 99%) of the world's tropical glaciers are located in the Andes of South America (Rabatel *et al.,* 2013) with the remainder in eastern Africa and Indonesia. Glaciers in the Peruvian Andes have lost 40% of their area since the 1980s under increasing air temperatures (ANA, 2014).

The climatic setting and thus the melt patterns of tropical glaciers differ from higher latitude mountain glaciers. In the Peruvian Andes, there is a distinct rainy season (October-April), during which 80% of the annual precipitation occurs, and a dry season (May-September) during which very little precipitation occurs. By contrast, temperature stays relatively constant throughout the year. As a result, glaciers in the Peruvian Andes produce meltwater all year round and lack the spring freshet period that occurs in snow dominated watersheds of higher latitudes. The rainy season is both the period of maximum accumulation and maximum melt (Kaser, 2001). Furthermore, El Nino Southern Oscillation (ENSO) cycles are the main cause of interannual variability in climate in the Peruvian Andes. The warm phase (El Niño) of these 2-7 year cycles is associated with accelerated glacier retreat whereas the cool phase (La Niña) is associated with glacier growth, though the characteristics of El Niño events are not uniform across the Andes (Rabatel *et al*., 2013).

In contrast to higher latitude glaciers, sublimation is a non-negligible, and sometimes large, component of the energy balance of tropical glaciers because of the dry air, particularly in the outer tropics (Kaser, 2001). This de-coupling of melt and air temperature can present a challenge in numerical modelling of tropical glaciers using the classic temperature-index approach (Hock, 2003). This decoupling can also slow down the retreat of tropical glaciers subjected to increasing temperatures (Kaser, 2001; Hock, 2003).

The retreat of tropical glaciers poses a risk to water resources in the Andes and downstream, particularly on the arid Pacific coast. Large cities like Lima (pop: ~9.8 million (INEI, 2017)), Trujillo (pop: ~920 thousand (INEI, 2017)) and La Paz (pop: ~790 thousand (INE, 2012)) rely on Andean watersheds for their municipal water supply. Figure 1.2 highlights the intense water related risk along the arid west coast of South America and the vulnerable population centres.

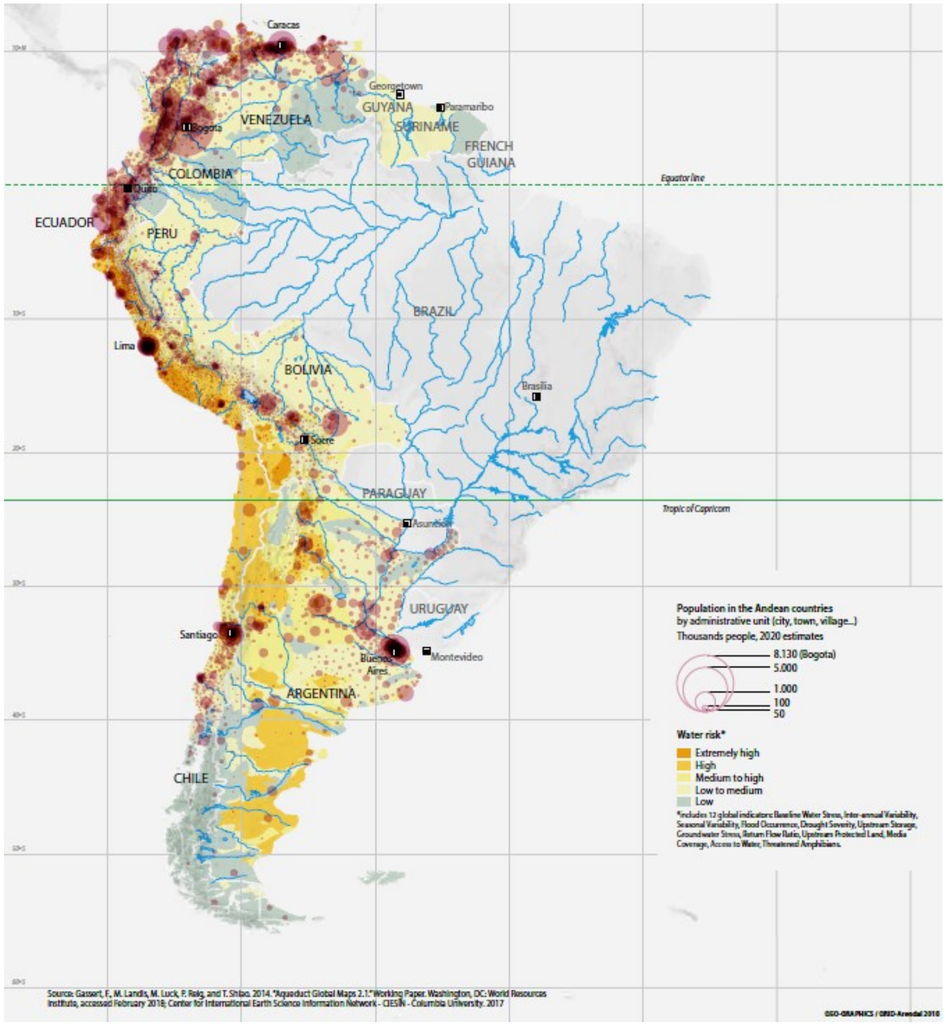

Figure 1.2 : *"Population and water risk in Andean countries" from Schoolmeester et al., (2018).*

Large agricultural developments, including the Chavimochic and Chinecas projects near Trujillo, Peru, divert water from Andean rivers to irrigate large swaths of productive desert soil (Bury *et al*., 2013). On the amazon side, water coming from the Andes is the major sediment source for the basin and shapes the geomorphic, biogeochemical and ecological regime (McClain and Naiman, 2008).

1.3 Mountain groundwater

Mountain groundwater was once considered only a minor contributor to mountain streamflow because the steep slopes and shallow soil development were hypothesized to be small and short-lived storage reservoirs for groundwater. (Liu *et al*., 2004). However, recent work has demonstrated the substantial groundwater storage and discharge in mountain watersheds and its importance in buffering streamflow during dry periods. Furthermore, it has been suggested that mountain groundwater may provide resilience against climate change impacts (Tague *et al*., 2008).

Several studies have used geochemical tracers (e.g. dissolved ions and isotopes of water) to detect groundwater discharge in mountain watersheds (Burns *et al*., 2001; Liu *et al*. 2004; Frisbee *et al*., 2011; Shaw *et al*., 2014; Baraer *et al*., 2015). Groundwater, having been in contact with geologic materials for longer periods of time, usually expresses a different hydrochemical signature than surface runoff, glacier or snow melt. This difference in hydrochemical signature can be used to quantify the contributions of different source waters.

Lui *et al*. (2004) used geochemical tracers to detect proportions of “new water”, the current year’s snow melt, and “old water”, water stored in the basin prior to that year’s snow melt, in the hydrograph of two watersheds in the Colorado Front Range, USA. They found that old water dominates streamflow for one of their two study catchments, supplying 64% of stream discharge. For example, Baraer *et al*. (2015) find that groundwater contributes 24-80 % of dry season stream discharge in 4 proglacial valleys of the Cordillera Blanca in Northern Peru.

Other studies have focused on the difference in timing between watershed inputs (precipitation, snowmelt, glacier melt) and outputs (stream discharge). The difference between these fluxes is interpreted as transient watershed storage. Andermann *et al.,* (2012) examined river discharge records from 3 large Himalayan basins and show a hysteresis in the relationship between precipitation and streamflow throughout the year that indicates transient water storage which can be explained by groundwater storage (Figure 1.3).

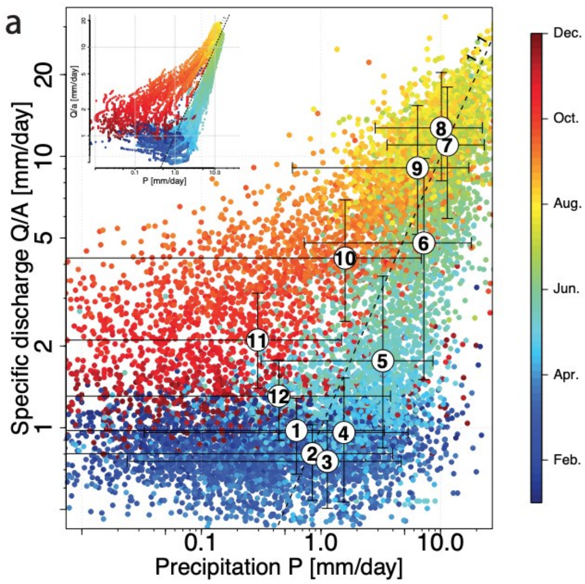

Figure 1.3: *Precipitation versus specific discharge (river discharge divided by watershed area) for the Narayani basin in Nepal, from Andermann* et al. *(2012). The colour of the points incates the time of year and the numbered circles indicate the monthly averages with error bars at the 5% and 95% quantiles. The lag between precipitation and discharge represents watershed storage.*

Similarly, Hood and Hayashi (2015) use detailed measurement of hydrological fluxes, including precipitation, snow melt and streamflow, and in a proglacial headwater catchment in the Canadian Rocky Mountains to characterize the timing of groundwater recharge, discharge and storage capacity. They show that peak groundwater storage is 60-100 mm averaged over the watershed area (Figure 1.4). This groundwater storage is much less than the peak snow water equivalent

(500-640 mm) but is significant when compared to the average fall and winter baseflow (<0.5 mm/d).

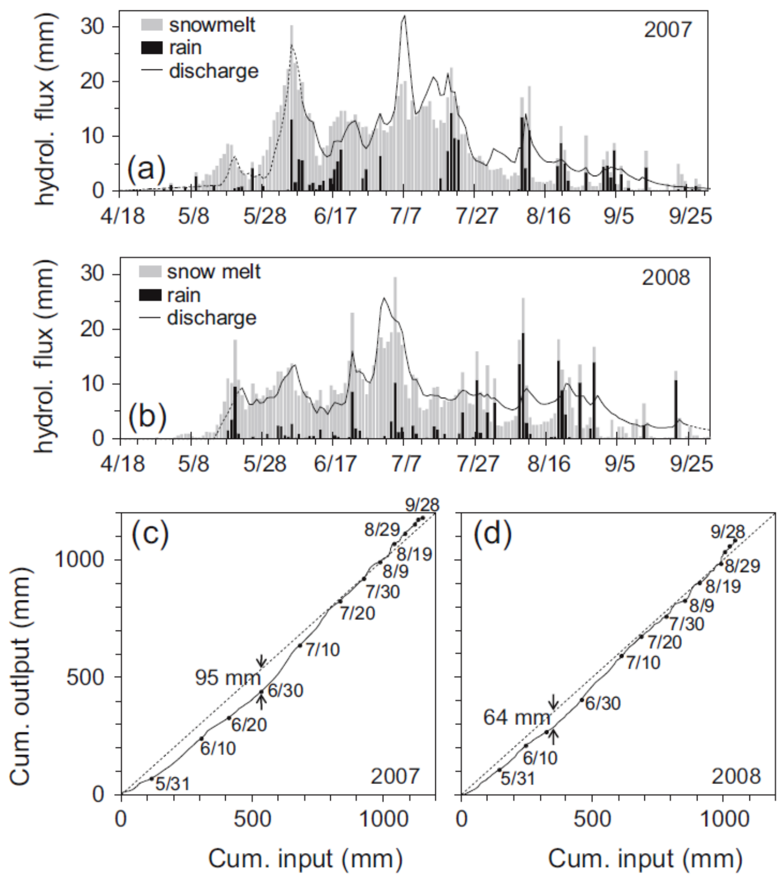

Figure 1.4*: Hydrological fluxes in the Opabin Watershed in British Columbia, Canada, from Hood & Hayashi (2015). The difference between the cumulative water inputs and outputs (C and D) quantifies the groundwater storage.*

Several studies have suggested the importance of coarse geomorphic units in storing and channeling groundwater flow in mountains. Hood and Hayashi (2015) identify proglacial moraines, composed of mostly cobbles and boulders, as important landform for groundwater storage in the Canadian Rocky Mountains. Liu *et al*. (2004) found that talus fields contributed more than 40% of the total discharge during the summer in one of their test catchments in Colorado, USA. Glas *et al*. (2018) propose a conceptual model of groundwater recharge in proglacial valleys of the Peru's Cordillera Blanca where recharge is channeled through Talus deposits beneath wetlands creating confined aquifers (Figure 1.5).

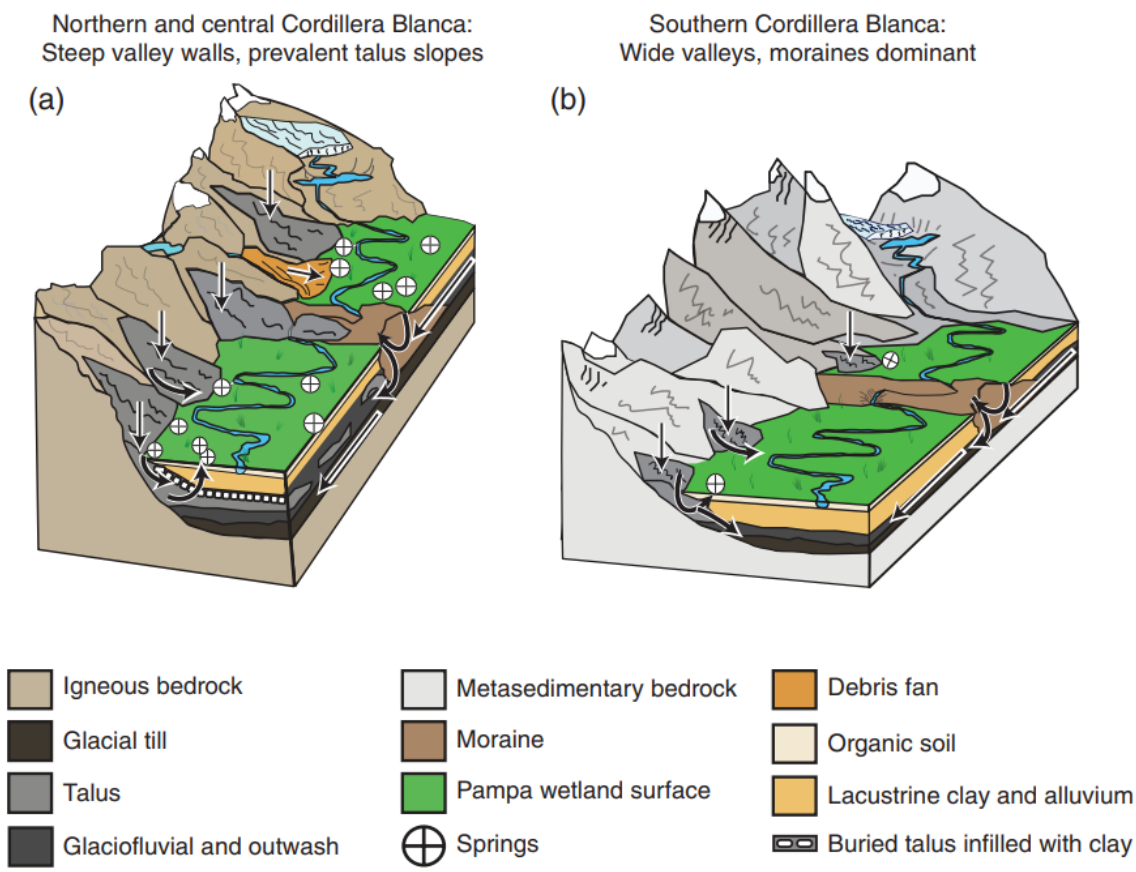

Figure 1.5: *Conceptual models for groundwater flow in valleys of the northern (a) and southern (b) Cordillera Blanca, Peru from Glas* et al. *(2018).*

Other research has focused on the division between shallow and deeper groundwater flow paths through mountain catchments. Tromp-van Meerveld *et al*. (2007) used a sprinkler plot study to quantify the recharge to bedrock in the Panola Mountain Watershed, Georgia, USA. They initially anticipated that subsurface water would flow towards the stream through the unconsolidated layer (coarse sandy loam, high permeability) above the bedrock (granodiorite, relatively low permeability), which was previously assumed impermeable. Instead, they found that 91% of the water applied to a study patch infiltrated into the bedrock layer.

Broadly speaking, water that infiltrates into mountain bedrock may follow two different paths: (1) it may flow through shallow weathered bedrock and discharge into mountain streams or (2) it may flow through deeper bedrock and eventually discharge in a central valley of the basin. The latter is known as Mountain Block Recharge (MBR, Bresciani *et al*., 2018). Welch and Allen (2012) used numerical groundwater models to investigate the partitioning of groundwater recharge between discharge to a mountain stream within a defined watershed (baseflow) and MBR. They found that 12-15% of total recharge was MBR which was eventually discharged to a higher order river in the basin, while 85-88% of recharge contributed to low-order mountain streams within the defined watershed.

Little is known about interactions between mountain glaciers and the groundwater system (Gordon et al., 2015; Baraer et al., 2015; Vuille *et al*,. 2018). Only one study to date estimates the extent to which mountain groundwater in proglacial watersheds is recharged directly by glacier melt; Saberi *et al*. (2018) use field data and numerical modelling of a proglacial headwater catchment on Volcán Chimborazo in Ecuador to estimate that 18% of groundwater discharge is sourced from glaciers which cover 34% of the watershed area.

1.4 Climate and hydrological projections in the Andes

Average global temperature has increased by 1 °C above pre-industrial levels and is expected to reach 1.5 °C between 2030 and 2052 (IPCC, 2018), with faster warming expected at higher elevations (Vuille *et al*., 2018). This phenomenon, known as elevation dependent warming, is of importance for the Andes where glaciers are located at very high elevations (Mountain Research Initiative EDW Working Group, 2015 and references therein).

Future climate change and its hydrological implications are dependent on human emission of greenhouse gasses and Representative Concentration Pathways (RCPs) are the emission scenarios used for projecting that change (IPCC, 2018). The most commonly available climate projections from General Circulation Models (GCMs) are the scenarios that could lead to radiative forcing of 4.5 W/m^2 (RCP 4.5) and 8.5 W/m^2 (RCP 8.5).

Dramatic glacier recession under a warming climate has been well documented in the Andes (ANA, 2014; Schoolmeester *et al.,* 2018 and references therein) and several studies have projected future glacier change (Vuille *et al*., 2018 and references therein, including Rabatel *et al*., 2012; Loarte *et al*., 2015). For example, Yarleque *et al*. (2018) predict the future disappearance of the Quelccaya Ice Cap in southern Peru using downscaled GCM climate projections. Under RCP 8.5, simulations show that the glacier equilibrium line will be above the ice cap summit by the end of the 21st century.

Other studies have incorporated glacier melt into hydrological models to project future changes in water resources in the Andes (Juen *et al.,* 2007; Ragettli *et al.,* 2016). Juen *et al.* (2007) model the proglacial hydrological system of Llanganuco Valley in the Cordillera Blanca, Peru, and use four climate scenarios to project future hydrological change. They project a 49 to 75% decrease in glacier area by 2080 for the lowest and highest greenhouse gas emission scenarios respectively. This decrease in glacier area is accompanied by a 44-69 % decrease in glacier melt production and a 31-56 % increase in runoff from the expanding non-glacier area. While the annual streamflow remains approximately the same, the seasonality of streamflow increases such that there is 10-26 % more discharge in rainy season discharge and 11-23% less discharge in the dry season. While the glacier melt model component is rigorous, the hydrological component of the model is simplistic and does not represent future changes in evapotranspiration, runoff-ratio or baseflow. Specifically, baseflow is calculated only as 20% of the previous month's non-glacier precipitation and does not incorporate any physically based groundwater flow processes.

Ragettli *et al*. (2016) project glacier recession and decreasing river flow throughout the 21st century based on climate projections stochastically downscaled from 12 GCMs for RCP 4.5 and 8.5 in the Juncal catchment in central Chile. Between 2001-2010 and 2091-2100, they project a 53 % (RCP 4.5) or 70% (RCP 8.5) decrease in glacier area and a 40 % (RCP 4.5) or 65% (RCP 8.5) decrease in river flow. The TOPKAPI model used by Ragettli *et al.* (2016) is a distributed and physically based hydrological model that represents marked improvement over modelling by Juen *et al*. (2007). However, a kinematic wave approximation is used for routing of groundwater flow rather than a classic finite difference groundwater flow model and the contribution and evolution of groundwater in the watershed in not investigated.

1.5 Hydrological climate change adaptations strategies

Several adaptation strategies have been suggested to combat declining glacier melt in the Andes and elsewhere. Dams are often constructed in response to seasonal water shortages but have several disadvantages. For example, dams are subject to large evaporative losses, can cause increased greenhouse gas emissions, and may mobilize contaminants like methyl mercury from the flooded land (Kelly *et al*., 1997). Dams also fragment habitats of aquatic species and change geomorphic conditions of rivers (Nilsson *et al*., 2005, Graf. W.L., 2006). A dam was proposed in the Shullcas Watershed, central Peru, one of the study watersheds for this thesis, and construction was initiated in 2016. The project was later cancelled over safety concerns involving earthquake risk at the nearby Huaytapallana geologic fault.

Adaptation strategies which increase groundwater storage for later use, known as Managed Aquifer Recharge (MAR) technologies, present a good alternative to surface water reservoirs. These technologies include enhancing groundwater recharge to aquifers via injection wells, infiltration ponds, trenches and canals (HeilWeil *et al*., 2015; Mastrocicco *et al*., 2015; Heviánková *et al*., 2016). Large swaths of land within the Shullcas Watershed, Peru, have passive infiltration trenches which aim to capture overland flow and allow more time for infiltration during the rainy season. However, little research has been done into the effectiveness of this type of MAR technology.

Another example of MAR in the Andes is being applied in the mountains near Lima, Peru. There, pre-Incan technology is being revived which diverts rainy season streamflow into infiltration canals and ponds. This technology, known as Mamanteo, is thought to increase groundwater recharge which discharges later through springs (Ochoa-Tocachi *et al.,* in review).

1.6 Objectives

Given the demonstrated importance of groundwater in mountain hydrological systems, I aim to interrogate the physical processes by which groundwater is recharged, stored and discharged in proglacial Andean watersheds. Furthermore, I aim to use this newfound process understanding to project future hydrologic change under a warming climate and assess proposed adaptation strategies which harness the storage capacity of groundwater to sustain rivers during dry periods.

Specifically, the research objectives of this thesis are to:

1. Elucidate spatial patterns of groundwater discharge to streams and rivers in a proglacial Andean valley using a multi-tracer approach (Chapter 2).
2. Characterize and quantify the role of groundwater in a proglacial Andean hydrological system using integrated glacier-surface water-groundwater numerical modeling. Project future hydrological conditions under climate change and glacier recession (Chapter 3).
3. Investigate the effectiveness of infiltration trenching as a groundwater-based hydrologic climate change adaptation strategy (Chapter 4).

Chapter 2. Quantifying groundwater-surface water interactions in a proglacial valley, Cordillera Blanca, Peru

Authors: Lauren D. Somers, Ryan P. Gordon, Jeffrey M. McKenzie, Laura K. Lautz, Oliver Wigmore, AnneMarie Glose, Robin Glas, Caroline Aubry-Wake, Bryan Mark, Michel Baraer, Thomas Condom.

2.1 Context within thesis

Previous research has established that groundwater is an important contributor to mountain rivers, as detailed in Chapter 1 (e.g. Lui *et al*., 2004; Andermann *et al*., 2012; Baraer *et al*., 2015, etc.). However, little work has been done to quantify the amount of groundwater-surface water interaction and characterize the hydrological processes and landscape features which control this interaction.

This manuscript develops a novel method for quantifying exchange between a river and the underlying valley bottom aquifer using heat and dye as tracers. I apply this method to a study site in the Quilcayhuanca Valley in the Cordillera Blanca, Peru. My results allow for a better understanding of spatial patterns of groundwater-surface water interaction and identify landforms that serve as storage reservoirs or channels for groundwater transport.

2.2 Abstract

A myriad of downstream communities and industries rely on streams fed by both groundwater discharge and glacier meltwater draining the Cordillera Blanca, Northern Peruvian Andes, which contains the highest density of glaciers in the tropics. During the dry season, approximately half the discharge in the region's proglacial streams comes from groundwater. However, due to the

remote and difficult access to the region, there are few field methods that are effective at the reach scale to identify the spatial distribution of groundwater discharge. An energy balance model, Rhodamine WT dye tracing, and high-definition kite-borne imagery were used to determine gross and net groundwater inputs to a 4 km reach of the Quilcay River in Huascaran National Park, Peru.

The HFLUX computer program (http://hydrology.syr.edu/hflux.html) was used to simulate the Quilcay River's energy balance using stream temperature observations, meteorological measurements, and kite-borne areal photography. Inference from the model indicates 29% of stream discharge at the reach outlet was contributed by groundwater discharge over the study section. Rhodamine WT dye tracing results, coupled with the energy balance, show that approximately 49% of stream water is exchanged (no net gain) with the subsurface as gross gains and losses.

The results suggest that gross gains from groundwater are largest in a moraine subreach but due to large gross losses, net gains are larger in the meadow subreaches. These insights into pathways of groundwater-surface water interaction can be applied to improve hydrological modeling in proglacial catchments throughout South America.

2.3 Introduction

Alpine watersheds supply a disproportionately large fraction of the world's water (Messerli et al., 2004, Barnett et al., 2005, Viviroli et al., 2007), with over 50% of the earth's mountainous regions providing an essential or supporting role in downstream water supply (Viviroli et al., 2007). Furthermore, approximately one sixth of the global population lives in areas where the hydrology is dominated by snow and ice melt (Barnett et al., 2005). Climate models predict warming air temperatures over the next several decades (IPCC, 2013) will lead to decreased snow and ice accumulation during winter and potential water shortages in later parts of the year. The hydrologic effects of climatic change are more severe in glacerized regions because as glaciers recede they lose stored "fossil water" on an annual basis – water which is not renewed with each winter's snowfall but is permanently lost (Barnett et al., 2005). Dry season stream flow in low-latitude, proglacial catchments is particularly vulnerable to rising air temperatures because of rapid rates of warming and because glaciers hydrologically buffer seasonal changes in stream flow by providing a consistent supply of melt water, even when precipitation is minimal (Bradley et al., 2006).

As the hydrologic buffering capacity of glaciers diminishes, groundwater storage in proglacial valleys becomes a more important source of stream water (Baraer et al., 2009). Therefore, quantification of the groundwater contribution to proglacial streams is important for better prediction of the impact of rapidly disappearing glaciers on regional water resources. Additionally, more precise methods are needed to understand the processes by which groundwater contributes to glacially fed streams on the scale of individual valleys (referred to here as reach scale), to elucidate how different geomorphic characteristics store and discharge groundwater.

One such approach to quantifying groundwater inputs at the reach scale is heat tracing or energy balance methods. For a given section of stream, the net change in thermal energy with respect to water volume must be balanced by a change in water temperature (Webb and Zhang, 1997, Westhoff et al., 2007). If all meteorological heat fluxes to and from a stream can be quantified independently and groundwater temperature is known, groundwater thermal inputs can be resolved as the necessary heat flux required to close the energy balance and match observed changes in stream temperatures through space and/or time (e.g. Becker et al., 2004). Several software tools exist for stream temperature modeling (e.g. Boyd and Casper, 2003). HFLUX (http://hydrology.syr.edu/hflux.html) is a deterministic numerical stream temperature model used to simulate changes in stream temperature as a result of the energy fluxes and groundwater entering and leaving a stream through space and time (Glose and Lautz, 2013).

Dye tracing, including dilution gauging and channel water balances, can be used to measure changes in stream discharge caused by a gain of groundwater or a loss of stream water to the subsurface. In a constant rate injection, Rhodamine WT (RWT) is released at a constant rate at the upstream end of the stream section of interest. Concentrations of RWT in the stream water are measured longitudinally and the degree to which the dye is diluted at any point downstream is used to calculate the stream discharge (Kilpatrick and Cobb, 1985, Stream Solute Workshop, 1990). Dye tracing in the Quilcayhuanca Valley in 2012 indicates that over the course of our study area, both gross gains and losses are occurring (Gordon et al., 2015). When stream water is lost to the subsurface, tracer mass is lost with it. If gains and losses happen concurrently (double dilution), the concentration of RWT will decrease while stream discharge may not change significantly.

Energy balance approaches and dye tracing methods require accurate spatial information on the studied section of stream, particularly regarding channel geometry, which can be provided by remote sensing. Unfortunately, even high-resolution (sub-meter) satellite data (e.g. GeoEye, Worldview, etc.) are often too coarse for making accurate width measurements of narrow streams. However, by using aerial small-format digital photography (collected from unmanned aerial vehicles, kites, balloons, etc.) and processing these images using structure from motion (scale invariant feature transform (SIFT) and bundle block adjustment) algorithms, very high resolution (centimeter) orthomosaics and digital elevation models (DEMs) can be generated (Fonstad et al., 2013; Harwin & Lucieer, 2012; Lowe, 2004; Turner et al., 2012; Hugenholtz et al., 2013).

The objective of this study is to combine heat tracing and dye tracing methods to quantify the groundwater contributions to the Quilcay River, and to understand the spatial variability and dominant pathways (e.g meadows, moraines and springs) of groundwater-surface water interaction in a typical proglacial valley of the Cordillera Blanca. Spatial information was collected using high definition kite-borne aerial photography, corrected with a differential global positioning system. We then used HFLUX to determine the simplified net stream discharge profile based on energy fluxes measured in the field. Dye tracing (constant rate dilution gauging) and the HFLUX results are then used together to estimate the gross gains and losses of water from the subsurface.

2.4 Study area

The Cordillera Blanca is in the northern Peruvian Andes (Figure 2.1a) and contains the highest density of glaciers in the tropics (Burns and Nolin, 2014). The majority (80%) of the annual precipitation falls during the rainy season from October to April. The highlands of the range have a relatively humid climate compared to the extremely arid coastal lowlands west of the Cordillera Blanca. Average annual air temperatures are generally between 0°C and 9°C, depending on altitude (Bury et al., 2011).

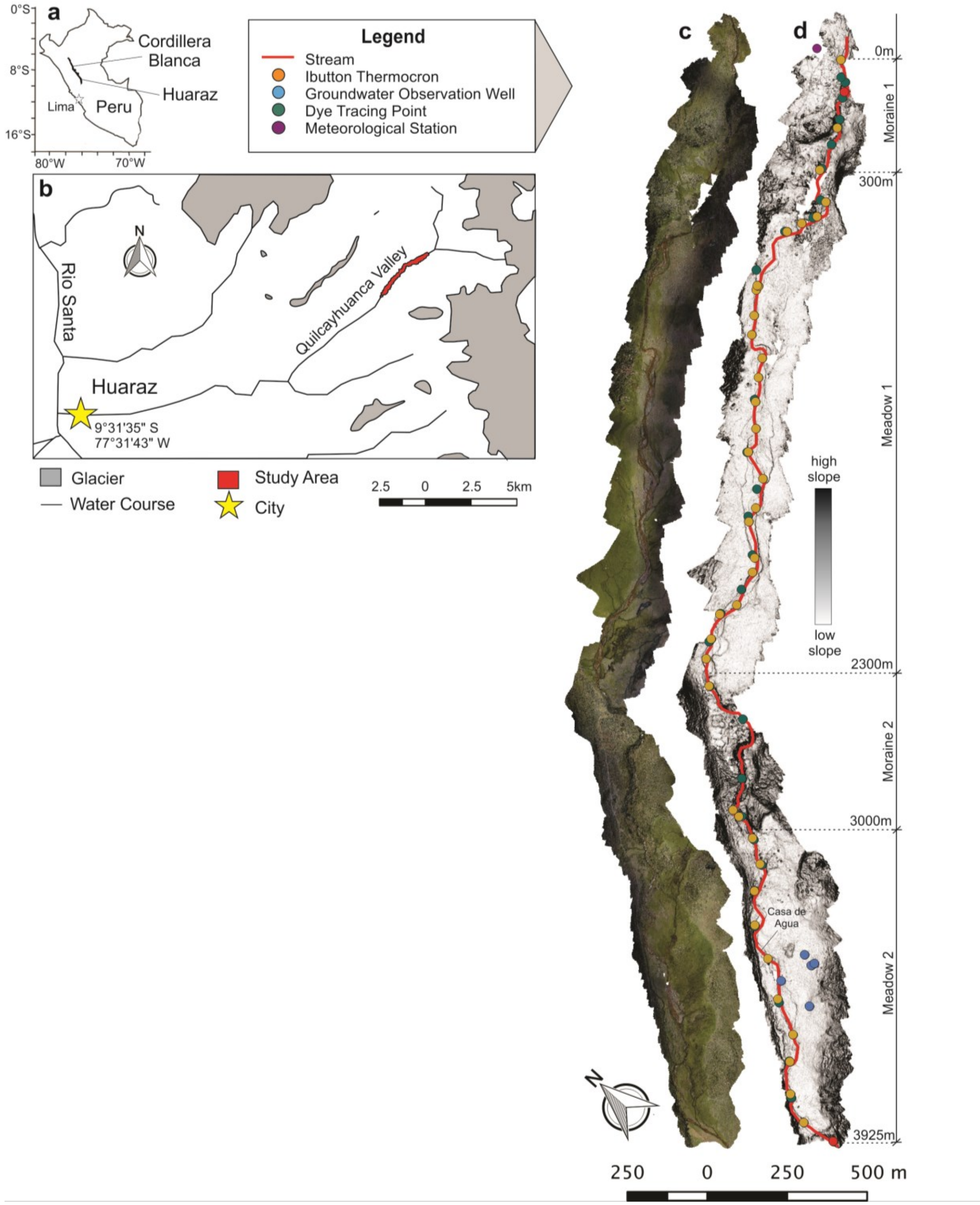

Figure 2.1: *(a.) Location of the Cordillera Blanca mountain range, Peru (b.) Location of the Quilcay River study section in the Quilcayhuanca Valley, (c.) KAP aerial imagery of the study area, (d.) Slope map of the study area.*

During the dry season, stream flow is maintained by a combination of glacial melt water and stored groundwater (Bury et al., 2011). The rivers on the western, glaciated side of the Cordillera Blanca drain to the Rio Santa, which flows northward through the Callejon de Huaylas, then through the Sechura Desert to the Pacific Ocean (Bury et al., 2013).

Approximately 267,000 people live in the upper Rio Santa Watershed between the Cordillera Blanca and Cordillera Negra, also known as the Callejón de Huaylas (Mark et al., 2005), and depend on the Rio Santa for their water supply. Additionally, these water resources are used for smallholder farming in the valleys of the Cordillera Blanca and larger scale commercial agriculture lower in the waterhshed. Here, water from the Rio Santa is used to irrigate crops in the coastal desert. Furthermore, hydroelectric power plants in the Cordillera Blanca contribute approximately 10% of the country's hydroelectric power (Bury et al., 2011; Bebbington and Bury, 2009).

Since the 1970s, approximately one third of the glacier area in the Cordillera Blanca has been lost (Burns and Nolin, 2014), with many glaciers predicted to completely disappear in the coming decades (Barnett et al., 2005). Complete disappearance of glaciers in the Cordillera Blanca would hypothetically result in a 30% reduction in average dry-season stream discharge in the upper Rio Santa (Baraer et al., 2012). Current and projected water shortages are already the subject of social and political tensions in the region, with a notable conflict in 2008 between rural farmers and a hydroelectricity company over the operation of the Lake Paron Reservoir (Vuille, 2013; Carey 2010). Understanding the hydrological system is an important step towards implementing mitigation strategies for changing water availability in the region.

This study focuses on the Quilcay River, in the Quilcayhuanca Valley (9.458°S, 77.374°W), located east of the city of Huaraz (Figure 2.1b). Quilcayhuanca has typical glacial geomorphic features including talus slopes lining the steep sided, U-shaped valley, and valley-crossing moraines or rock falls containing boulder to cobble size material. Between the moraines, low gradient meadows are thought to have formed by lake infilling and consist of organic material, lacustrine and fluvial sediments layered with heterogeneous colluvium. These high altitude meadows and wetlands, also known as pampas, are predominantly grass covered and are thought to act as storage features for groundwater, in addition to the talus slopes and moraines (Clow et al., 2003, Baraer et al., 2009). The bedrock geology is predominantly granodiorite, with some outcropping of the Chicama Formation, which consists of pyritic shale, in the headwaters (Love et al., 2004).

The 3925 m long study reach ranges between 3910 and 4040 m.a.s.l. in elevation and begins just downstream of the confluence of the Quilcay and Cayesh Rivers. Along the study reach, the river alternates between steep, single channel segments, which are heavily shaded and incised in the cross-valley moraines, and low gradient meadow segments with sinuous channel form, some braiding and very little shading (Figure 2.1c and d). Meadows and moraines are identifiable in the slope map, Figure 2.1d. For the study, the stream is divided into four reaches: Moraine 1, Meadow 1, Moraine 2, and Meadow 2. Numerous springs (visible in Figure 2.1C) are observed near the base of the moraine sections on the valley floor, as well as at the base of the lateral talus slopes. Groundwater stored in the talus slopes and moraines upwells in the meadows, forming springs, and then flows overland to join the main channel. Groundwater stored in the meadows can also reach the main stream by flowing directly from the aquifer through the streambed. Similarly, stream water can also be lost to the subsurface by flow through the streambed.

2.5 Methodology

2.5.1 Heat tracing using an energy balance model

2.5.1.1 Field methods

Data for the heat tracing analysis was acquired from June 20 through June 25, 2014. Time dependant variables were recorded for a period of 4.87 days (7010 minutes). Stream temperature data were recorded using Thermochron iButtons™ (Model DS1922L), which were installed in the water column at 37 points along the stream reach (Figure 2.1d) and recorded stream temperature at 5-minute intervals at a precision of 0.0625°C and an accuracy of +/-0.5°C. A Vantage Pro2 weather station was installed in the upper meadow, adjacent to the stream, and provided meteorological observations including incoming solar radiation, air temperature, humidity and wind speed at 10-minute intervals over the entire observation period (7010 minutes). Cloud cover values are the complementary ratio of solar radiation observed at any time, to the solar radiation on the clearest day (June 23) at the same time.

Groundwater temperature was measured hourly in five observation wells located in Meadow 2 (Figure 2.1d), using Schlumberger Mini-Diver™ pressure loggers. Streambed temperature was approximated by using data from the Yanamarey Valley (-9.6766°S, -77.2707°W) collected in 2007 at the same time of year and similar climatic and geographic conditions. The average stream bed temperature was applied to the length of the stream.

Stream discharge at the upstream end of the study section was determined by RWT dye dilution tracing (see dye tracing methodology). Stream dimensions were measured approximately every 20

m. Shading percentages were visually estimated, from kite areal photography (KAP). View to sky coefficients were estimated as 1 - shading.

2.5.1.2 Modeling methods

The energy balance for the study reach was solved using the HFLUX Stream Temperature Solver (http://hydrology.syr.edu/research/hflux/), which simulates stream temperature through space and time based on the exchange of heat energy between stream water and the environment (Glose and Lautz, 2013). The HFLUX model solves the mass and energy balance equations for heat transport using finite difference methods, and applies the heat fluxes to each stream cell at each time step. For this study, the model was run using a 10 minute time step and 10 m finite-difference stream cells.

Mass and energy balance equations are given as Equations 2.1 and 2.2 respectively (Glose and Lautz, 2013):

$$\frac{\partial A}{\partial t} + \frac{\partial Q}{\partial x} = q_L \tag{2.1}$$

$$\frac{\partial (AT_w)}{\partial t} + \frac{\partial (QT_w)}{\partial x} = q_L T_L + R \tag{2.2}$$

where Q is the discharge of the stream (m^3/s), A is the cross-sectional area of the stream (m^2), T_w is the stream temperature (°C), x is stream distance (m), t is time (s), q_L is the lateral groundwater inflow per unit stream length (m^2/s), T_L is the temperature of the groundwater (°C), and R is the temperature change resulting from the energy flux (source or sink) per unit stream length. R is defined as:

$$R = \frac{B\Phi_{total}}{\rho_w c_w} \tag{2.3}$$

where Φ_{total} is the total energy flux to the stream per surface area (W/m^2), B is the width of the stream (m), and ρ_w and c_w are the density (kg/m^3) and heat capacity (J/kg°C) of water, respectively. Φ_{total} is a function of shortwave radiation, longwave radiation (including atmospheric, land cover and back radiation off the water surface), streambed conduction, sensible heat exchange with the air, and latent heat flux (evaporation or condensation) and the stream width (Glose and Lautz, 2013). A, Q, q_L, T_L, B, and Φ_{total} are model inputs and T_w, as a function of x and t, is the model output. We infer q_L by matching modeled T_w to our observed water temperature data. Note hydraulic conductivity is not required.

A Crank-Nicolson scheme was used to solve the energy and mass balance equations. The short-wave radiation flux was calculated from direct measurements of incoming shortwave radiation, corrected for the percentage of shading and reflection based on the solar position throughout the day and Fresnel's reflectivity. The rate of evaporation, and associated latent heat flux, were calculated using the mass transfer method and the default empirical constants in the HFLUX program. The mass transfer method has been used successfully to quantify the latent heat flux in prior field-based stream energy balances (e.g. Caissie et al., 2007; Cox and Bolte, 2007; Magnusson et al., 2012). Sensible heat flux was calculated as a function of the latent heat flux, using the Bowen Ratio method. Streambed conduction is calculated from the temperature gradient between the stream water and stream bed, and the thermal conductivity of the bed. The thermal conductivity is designated in HFLUX based on bed material (cobbles in this case). Given streambed conduction is one of the smaller energy fluxes, error arising from this estimation is minimal. For the full model methodology see Glose and Lautz (2013).

The HFLUX simulations require groundwater temperature. Selecting an appropriate groundwater temperature has been identified as a challenge in heat tracing methodology (Kurylyk et al., 2015). Without information on tributary temperatures, we used a single groundwater temperature to represent the temperatures of both advecting groundwater and tributary inflow from springs. To infer this temperature, HFLUX was used to find the combination of groundwater temperature and constant groundwater inflow rate that minimizes the root mean square error (RMSE) between the simulation results and the measured data. Figure 2.2 shows how RMSE varies as a function of modeled groundwater temperature and total change in stream discharge (i.e. total amount of groundwater entering the stream over the entire reach). A minimum RMSE of 0.38 °C occurs at a groundwater temperature of 8.8 °C and a total change in stream discharge (ΔQ) of 230 l/s. However, this optimized value falls outside of the range of groundwater temperatures observed in the field (9.4 to 11.1 °C). Therefore, we selected a groundwater temperature of 9.4 °C (which corresponds to a ΔQ of 270 l/s) to use in HFLUX simulations because it represents the minimum RMSE while still being within our observed range of groundwater temperatures.

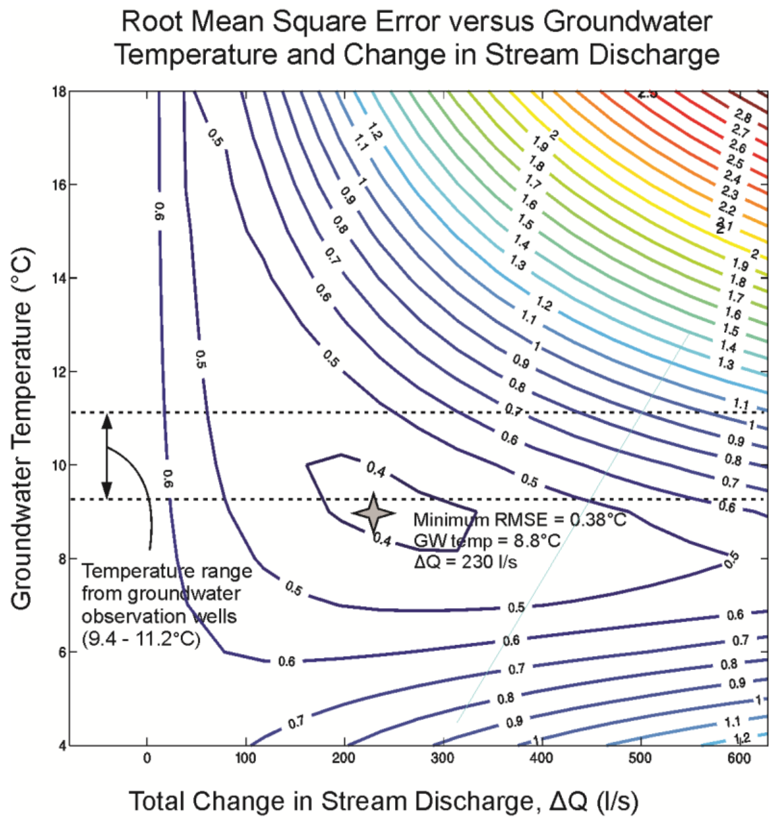

Figure 2.2: *Root mean square error contours versus groundwater temperature and total groundwater inflow described as the total change in stream discharge.*

In order to quantify the net groundwater flow to the stream, the best-fit longitudinal stream discharge profile for the river was determined through model calibration, with the discharge profile as the calibration parameter. No other input data (e.g. meteorological data) was varied from measured values, and the stream discharge profile was systematically varied, producing different simulated stream temperatures in space and time. The stream discharge profile that minimized the RMSE between the HFLUX simulated stream temperature and the measured stream temperature in space and time, was selected as the best fit. Then, longitudinal changes in stream discharge with distance were used to determine rates of groundwater base flow.

Three potential longitudinal stream profile configurations were used to calibrate the model and provide estimates of groundwater contribution to the stream. First, in Simulation A, the groundwater baseflow rate was constant over the entire 3925 m section of stream, resulting in a linear stream discharge profile. In Simulation B, the river was divided into moraine and meadow reaches, with each type of terrain having its own constant base flow rate (2 rates in total), resulting in a ramped stream discharge profile with different slopes in the moraine and meadow reaches. Finally, in Simulation C, each moraine and each meadow had its own constant base flow rate (4 rates in total), resulting in different slopes for each individual moraine and meadow reach.

2.5.1.3 Sensitivity analysis

Sensitivity analysis was done on the best-fit simulation in order to identify input variables that are particularly influential to the model output and to understand potential sources of uncertainty in our results. Model inputs are altered individually and the root mean square deviation (RMSD) between the base case model output and the perturbed model output is used to measure sensitivity:

$$RMSD = \sqrt{\overline{\left((\hat{y}(a_k) - \hat{y}(a_k + \Delta a_k)\right)^2}} \tag{2.4}$$

Where $\hat{y}$ is the modeled matrix of stream temperature in space and time (°C), a_k is the base case k^{th} input parameter and Δa_k is the increment of perturbation (modified from Zheng and Bennet, 2002). In our case, the RMSD is used because it is not only sensitive to changes in mean stream temperature, but also the amplitude of the daily temperature fluctuation as well as the timing and location shifts of temperature changes.

2.5.2 Dye tracing

2.5.2.1 Dilution gauging setup and sampling

Over a period of approximately 49 hours from June 20-22, 2014, we conducted a constant-rate tracer dilution gauging experiment (Kilpatrick and Cobb, 1985) at the same location in the Quilcay River as the heat tracing experiment. Fluorescent dye RWT was used to label stream water and estimate stream discharge and water exchange rates between the stream channel and the subsurface. On June 20 at 5:15 pm, we began injecting RWT tracer at the upstream end of the study reach (Figure 2.1d). A single injection tube outlet was suspended above the center of stream channel flow, and liquid injectate, diluted to a concentration of 25 g l^{-1} RWT, was dripped into the stream at a rate of 23 ml per minute, leading to a tracer mass injection rate, r, of 9600 µg s^{-1}. Tracer concentration in the stream was measured every 120 seconds with a Turner C3 fluorometer (Turner Designs, Sunnyvale, California) at a point downstream from the Casa del Agua flume (Figure 2.1d), approximately 3380 m downstream from the injection point. The tracer injection was abruptly stopped at 10:55 pm on June 21, but RWT concentration in the stream continued to be measured at the fluorometer location until the afternoon of June 22.

Between 7:24 pm and 9:41 pm on June 21, while the stream RWT concentration was at plateau, we collected grab samples of stream water at 29 points along the study section (Figure 2.1d) in order to construct a profile of RWT concentration with distance downstream. The concentration of RWT tracer in grab samples was measured in the lab using a GGUN-FL30 fluorometer (Albillia Co., Neuchâtel, Switzerland), calibrated using serial dilution from a sample of the injectate solution.

2.5.2.2 Discharge and water balance calculations

At a point greater than one mixing length (a short, well-mixed stream reach) downstream from the injection site, the apparent stream discharge rate, $Q*$ (l/s), can be calculated using only the tracer mass injection rate and the concentration of tracer in the stream at that point. Apparent stream discharge is the discharge rate assuming no tracer mass has been lost during transport downstream:

$$Q^* = {}^{r}/_{C} \tag{2.5}$$

where *r* is the tracer mass injection rate, and the assumed tracer load in the stream [$\mu g\ s^{-1}$] and *C* is the measured concentration of tracer [$\mu g\ l^{-1}$] at that point (Kilpatrick and Cobb, 1985).

Stream discharge fluctuates with respect to time but an average value is required for our analysis. In order to estimate average apparent discharge at the Casa del Agua flume (Figure 2.1) during the entire experiment period (day and night), a rating curve was developed using the flume stage data and the night-time discharge-through-time curves from the fluorometer. The following power law was used with best fit coefficients: α=702, β=0.518, and a=0.09.

$$Q^* = \alpha(h - a)^{\beta} \tag{2.6}$$

Where $Q*$ is apparent stream discharge and *h* is flume stage. By applying the rating curve, apparent discharge through time (day and night) at the fluorometer was estimated.

At a point downstream from the tracer injection site, true stream discharge, *Q*, can be less than apparent discharge if there has been a loss of tracer mass between the injection and sampling points due to a loss of tracer-labeled stream water to the subsurface, potentially accompanied by dilution from unlabeled water. In a stream reach that experiences concurrent or successive gross gains and losses from and to the subsurface, the net change in discharge over the reach, ΔQ, is equal to the sum of gross gains, Q_{gain} (positive), and gross losses, Q_{loss} (negative), that occur over the reach. The amount of tracer loss depends on the magnitude and the order of gross gains and losses along the stream length (Harvey and Wagner, 2000; Payn et al., 2009). At the end of a reach in which tracer mass has been lost, we can express the mass discharge rate of the tracer through the stream cross-section as fr, where f is the fraction of the original injection mass discharge remaining. True stream discharge is then given by:

$$Q = {}^{fr}/_{C} = fQ^{*} \tag{2.7}$$

In a situation where the concentration of tracer in stream water, C, as well as the true discharge, Q, is known at a series of successive points n = [0, 1, 2, …, N] downstream from the tracer injection, then ranges for gross gains and losses can be estimated in the N subreaches between each point (see Payn et al., 2009, for a related method of analyzing slug tracer injections). For each reach upstream from point n, we can calculate the minimum gross loss, for the case where all losses occur before all gains, as

$$Q_{loss,n,min} = \left(\frac{f_n}{f_{n-1}} - 1\right) Q_{n-1} \tag{2.8}$$

where

$$f_n = \frac{Q_n}{r/C_n} \tag{2.9}$$

and Q_{n-1} and Q_n are the true discharges and C_{n-1} and C_n are the tracer concentrations at the upstream and downstream ends of the reach, respectively. The minimum gross gain is then calculated by simple mass balance as

$$Q_{gain,n,min} = Q_n - Q_{n-1} - Q_{loss,n,min} \tag{2.10}$$

Equations 2.8 through 2.10 are used to estimate minimum concurrent gross gains and losses using measured tracer concentration values and hypothetical Q profiles derived from net groundwater inflow rates calculated using the calibrated HFLUX model for Simulations A, B and C.

This method combines the results of HFLUX and dye tracing. However, it should be noted that there is a potential methodological contradiction caused by the fact that the two methods do not treat groundwater-surface water exchange in the same way. HFLUX is not designed to account for simultaneous exchanges of stream water and groundwater without a net gain (or loss) in discharge, but the river temperature is still sensitive to this exchange. Therefore, it is possible that some HFLUX-perceived net discharge gain could actually be exchange or alternatively that dye tracing-perceived exchange could be over-estimated.

2.5.3. Remote sensing and imaging

We collected remote sensing imagery on June 22, 2014 using a custom-built kite aerial photography (KAP) platform (Wigmore and Mark, 2014). The camera rig was fitted with a Canon Powershot S110 camera controlled by the Canon Hack Development Kit (CHDK) firmware (Anon., 2015) and the Koh and Wich's (2012) drone.bas script to collect a photo every 10 seconds. The camera rig was suspended from a 3.4 m wingspan Delta kite by Premier Kites flown at ~60 m above the Quilcayhuanca Valley floor. Once airborne, the kite was walked up and down the valley collecting a total of 1846 RGB images over the study area. The KAP survey area is 3.5 km long and covers 0.816 km^2. Within the survey area 19 highly visible ground targets were installed and surveyed using fast static GPS methodology. The base station was a Trimble 5700 receiver (L1 and L2) with a Zephyr Geodetic antenna and the rover was a Topcon GRS-1 (L1 only) with a PG-

A1 external antenna. The base station position was occupied for 5.75 days and corrected using the NRCAN PPP web application (NRCAN, 2015), resulting in an estimated position confidence (95%) of 0.1 cm latitude; 0.3 cm longitude; 0.4 cm ellipsoid height. Survey data were post processed against this using Topcon Magnet™ Office Tools to an accuracy threshold of 0.5 cm horizontal and 1 cm vertical, for an estimated error threshold of under 1 cm horizontal and 1.5 cm vertical.

The images were processed using Agisoft Photoscan™ Professional (version 1.1.X), a photogrammetric software package for generating orthomosaics and DEM's from unordered aerial image collections (Agisoft, 2014; Fonstad et al., 2013; Lowe, 2004; Verhoeven, 2011). Maximum output pixel resolution for the orthomosaic was 2 cm. The DEM has a resolution of 25 cm pixels. Estimated vertical error for the DEM is 4.76 cm, excluding potential error from the GPS itself which could add up to 1.5 cm of additional vertical error. The generated orthomosaic and DEM were used to take detailed measurements on stream width and shading at approximately 200 points, providing input data for HFLUX.

2.6 Results

2.6.1 Field observations

Several of the HFLUX input parameters are constant in space and time. These field observations are shown in Table 2.1.

***Table 2.1**: HFLUX input parameters.*

Variable	Value	Source
Discharge (Q) at x = 0 m	657 l/s	Dye tracing
Groundwater Temperature (T_L)	9.4 °C	Average temperature in groundwater observation wells during 5-day experiment; refined through model calibration
Bed material	Cobbles	Visual observation at field site
Latitude	-9.458°S	Global Positioning System (GPS)
Longitude	-77.374°W	GPS
Average Elevation	3980 m.a.s.l.	GPS

2.6.1.1 Stream temperature, hydrology, and morphology: spatial and temporal observations

Several model input parameters change with distance along the 3.9 km experimental reach, but do not vary in time: stream shading, tributary width, and stream width (Figure 2.3 a-c). Tributary width was determined from the remote sensing imagery and is used to conceptually express the size of each tributary (n=33), most of which (>80%) are springs, in place of tributary discharge data. Tributaries range in width from 0.3 to 2.1 m and all tributaries are small relative to the main channel, which ranges in width from 2.2 m to 14.0 m. The majority of tributaries are located in the lower half of the first meadow (1.25 to 2.25 km distances in Figure 2.3).

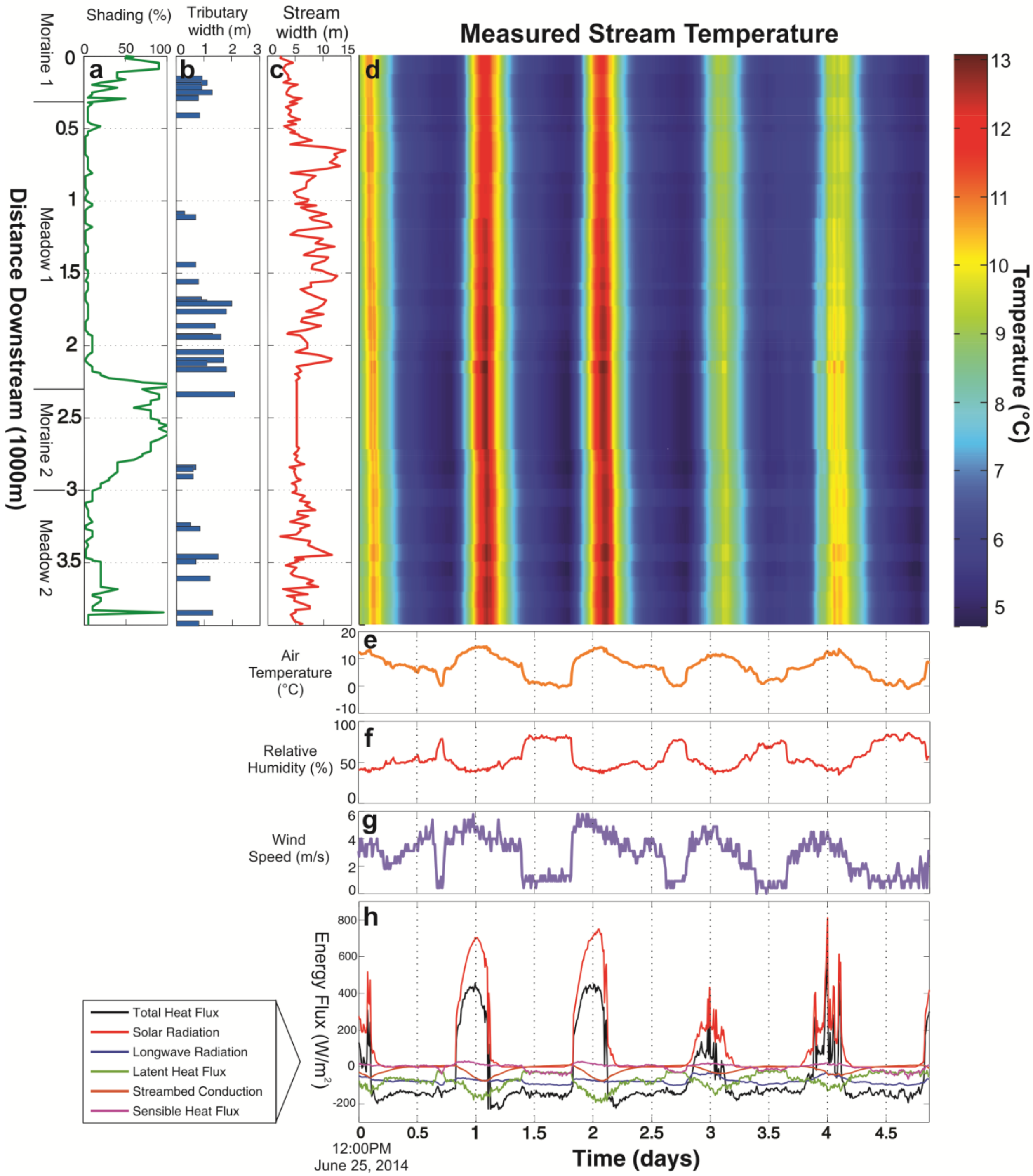

Figure 2.3: *(a.) Stream shading versus distance downstream, (b.) Tributary width versus distance downstream, (c.) Main Channel width versus distance downstream, (d.) Observed stream*

temperature in space and time, (e.) Air temperature versus time (f.) Relative humidity versus time (g.) Wind speed versus time (h.) Net heat fluxes entering and leaving the stream versus time.

Shading along the study reach varies between 2 and 100%, and high values of shading are due to river incision and dense vegetation along the two moraines, positioned at 0-0.5 km and 2.25-3.0 km along the study reach (Figure 2.3b). The stream widths across the moraines are relatively narrow (<6 m) due to river incision, while the meadows have wider stream widths due to braided sections and shallow river depths. The combination of high shading and narrow stream width reduces the potential for shortwave energy inputs in moraine segments of the experimental reach. In contrast, the meadows have higher potential for large shortwave energy inputs, but also greater potential for groundwater contributions, particularly as tributary inflows.

Meteorological input parameters (Figure 2.3 e-g), and associated energy fluxes (Figure 2.3h), change through time over the 5-day observation period, but not with distance (Figure 2.3e). Direct incoming solar radiation reaching the weather station at the field site is high, ranging from 0 to 1068 W/m^2. Solar radiation is the energy flux with the largest magnitude followed by latent heat flux (negative value indicates evaporation), long wave radiation, streambed conduction and finally sensible heat flux. The observation period included two days of intermittent clouds (June 21 and 22) and two days of full sun (June 23 and 24), providing a range of meteorological conditions during the energy balance modeling period. Cloud cover values were calculated as the ratio of the observed solar radiation, at any time of day, to the solar radiation observed on June 22 (clearest day), at the corresponding time of day. A value of 0 represents clear conditions and a value of 1 represents complete cloud cover.

Stream temperatures vary in both space and time (Figure 2.3d); we monitored stream temperatures over the 3.9 km stream reach beginning at 12:20 PM on June 20th and ending at 9:10 AM on June 25, 2014 (7010 minutes). Stream temperatures rise quickly during the day, shortly after the onset of intense, high-altitude, solar radiation, and generally peak about an hour after incoming solar radiation peaks. Stream temperatures then cool more slowly during the night. While observed air temperature is below 0 °C during the night, the minimum stream temperature is similar each night at approximately 5 °C, likely because of the warming effect of groundwater base flow to the stream.

Five groundwater observation wells provided average groundwater temperatures over the study period, which ranged from 9.4 to 11.1 °C with a mean of 10.6 °C. These measurements are evidence of the temperature of groundwater that advects directly to the stream through the streambed. However, groundwater that reaches the stream through spring flow and subaerial channels may experience some change in temperature between where it upwells in the meadow and where it reaches the main channel.

2.6.2 Heat tracing simulation results

When the incoming groundwater flux is set to 0, HFLUX has a RMSE of 0.647 °C. Groundwater inflows improve the model fit, reducing the RMSE (Figure 2.2). The three HFLUX simulations (Simulations A, B and C) provide three different estimates of groundwater discharge to the stream over the study section, shown in Table 2.2, where ΔQ is the total increase in stream discharge over the experimental reach and Q_f is the stream discharge at the downstream end of the experimental reach. Simulation C has the lowest RMSE (0.378 °C) and yields a total increase in stream discharge of 270 l/s over the 3925 m section of stream. Although the RMSE values for simulations A, B and

C are similar, the three simulations show us that when higher rates of groundwater discharge are simulated in the meadow segments, relative to the moraine segments, there is further improvement in the model fit to observed temperatures. Furthermore, Simulation C has the same total increase in stream discharge as simulation A (270 l/s), but the majority of that groundwater discharge occurs in the meadow segments. It should be noted that Simulation C has only a small improvement in model fit, but when combined with our understanding of the physical processes (e.g. Gordon et al., 2015), it seems that this is the most plausible scenario. Although the total stream experimental reach consists of 77% meadow reaches, in Simulation C 93% of the net total groundwater contribution enters the stream in the meadow reaches, indicating that the groundwater input rate is disproportionately higher in the meadows than in the moraines with respect to distance covered.

Table 2.2: *Simulation results.*

Model	Number of Variables	Groundwater Inflow rates (l/s/100m)		ΔQ (l/s)	ΔQ (%) ($\Delta Q/Q_f$)	RMSE (°C)
A	1	full experimental reach	5.8	270	29.5	0.383
B	2	Moraines:	4	230	26.2	0.382
		Meadows:	6.5			
C	4	Moraine 1:	0	270	29.4	0.378
		Meadow 1:	6.3			
		Moraine 2:	2.5			
		Meadow 2:	12.7			

2.6.2.1 Simulation error

The results of Simulation C were found to match well with the observed data. Figure 2.4a, compares the modeled and measured stream temperature through distance, averaged through time, while Figure 2.4c shows modeled and measured stream temperatures through time, averaged through distance. Figure 2.4b shows the residuals (modeled – measured stream temperature) in both space and time. The largest errors occur close to the peak daily stream temperature each day and this error is particularly pronounced downstream of 1600 m on the warmest days. The modeled peak temperatures are higher, and thus have higher amplitude, than the measured peak temperatures on days 1, 2, 3 and 5.

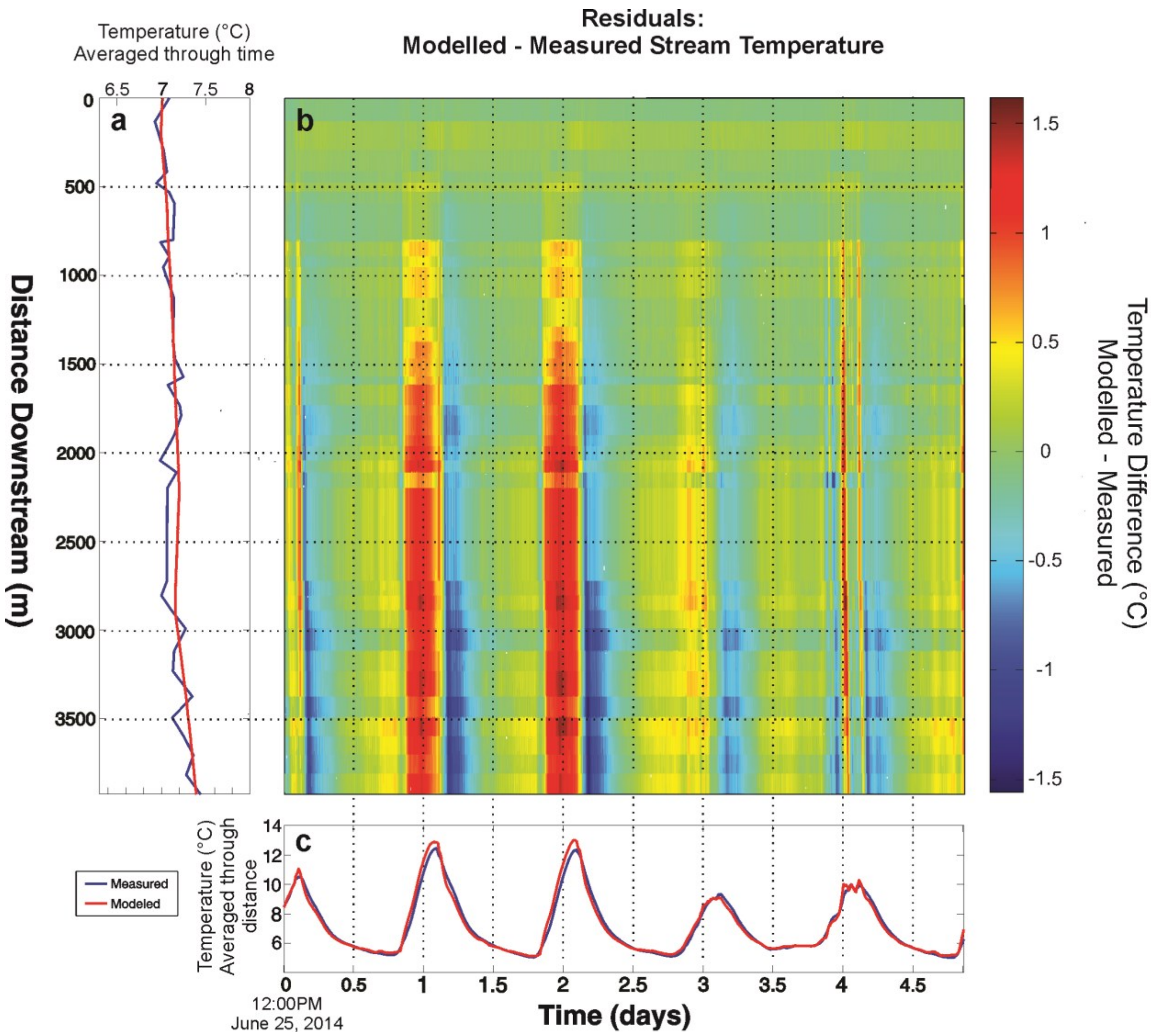

Figure 2.4: *(a.) Simulated and measured stream temperature versus distance downstream, averaged through time, (b.) Residuals between simulated and measured stream temperature (modeled – measured), (c.) Simulated and measured stream temperature versus time, averaged through distance.*

In Figure 2.4c we also note that there is a slight timing shift where the simulated stream temperature is warming up before the measured temperature. This may be because the weather station was located at the upper end of the reach and sunlight hits this area first in the morning and leaves this area first in the evening. Since weather station data was used in HFLUX, the simulated temperatures have a slight forward time shift relative to the observed temperatures.

2.6.2.3 Heat tracing sensitivity analysis

Sensitivity analysis was performed for Simulation C. Input variables were perturbed individually by increasing and then decreasing each variable as described in Table 2.3. For parameters that have a range of values through time or space, the entire range is perturbed as indicated. Where the increased and decreased RMSDs are different, the average is used to rank sensitivity.

Table 2.3: *Sensitivity Analysis*

Input Parameter Name	Absolute perturbation	Sensitivity Ranking	+RMSD	-RMSD
Groundwater temperature (T_L)	±0.47°C	1	0.068	0.068
Air temperature	±0.78°C (air temp ranges from -1.0 – 14.6°C	2	0.053	0.054
Stream width (B)	± 5% (0.11 - 0.7 m)	3	0.055	0.050
Shading	±5%	4	0.051	0.051
Short wave radiation	±5% (0 - 53.4 W/m^2)	5	0.048	0.048
Upstream discharge	±33 l/s	6	0.044	0.047
Total groundwater input	±14 l/s	7	0.054	0.016
Streambed temperature	±0.3°C	8	0.008	0.008

The model is most sensitive to groundwater temperature. This is a potential source of uncertainty in our modeling process because the range of data collected from the groundwater wells is greater than the perturbation interval. The next-most sensitive parameters are air temperature, stream width, shading, and shortwave radiation. However, all of these parameters are measured at high accuracy and are considered to be low sources of uncertainty. The upstream discharge was measured using dye tracing which has a moderate uncertainty (Schmadel et al., 2010; Winter, 1981; Briggs, 2012) and finally the model is least sensitive to changes in total groundwater input and streambed temperature.

2.6.3 Dye tracing

A dye concentration profile was recorded from synoptic sampling along the study section of the Quilcay River. As expected, the analyzed grab samples from synoptic sampling show that RWT tracer concentration decreases with distance downstream, and therefore apparent discharge, Q^*, increases with distance downstream.

RWT concentration through time was recorded at the lower fluorometer just downstream of the Casa del Agua gauging station, and was converted to apparent discharge through time using the mass injection rate. This apparent discharge-through-time curve shows a peak in discharge shortly after 8 pm both nights, with a steady decrease throughout the night.

4.3.1 Gross gains and losses from HFLUX and dilution gauging results

Using the net increases calculated with HFLUX and the apparent discharge profile from dye tracing, the maximum and minimum gross gains and losses of water from the channel were calculated. Table 2.4 lists the minimum gross gains and losses that were calculated.

Table 2.4: *Minimum gross gains and losses estimated based on HFLUX discharge profiles*

Simulation	Gross Q_{loss} (l/s)	Gross Q_{gain} (l/s)	Net ΔQ (l/s)	% Exchange
A	-461.39	723.47	262.08	51
B	-483.73	703.89	220.16	53
C	-446.88	694.06	247.18	49

Net ΔQ in Table 2.4 is the total gain in discharge over the entire study section calculated from HFLUX and is equal to the sum of the minimum gross loss and minimum gross gain. The ΔQ values are slightly smaller than those in Table 2.2 because the dye tracing experiment was conducted over a slightly smaller stretch of stream than heat tracing. These results indicate that over the study reach, a minimum of approximately 49% (Simulation C) of downstream discharge is exchanged with groundwater. In other words, 49% of the downstream discharge was lost to the subsurface and replaced with unlabeled water at some point in the study section.

A few sources of error should be noted for the dilution gauging experiment including incomplete mixing of tracer across stream cross sections, changing discharge through time, and uncertainty in tracer concentration measurements (Schmadel et al., 2010). Nonetheless, the combination of dye tracing and heat tracing allows us to better understand the processes by which a stream experiences net and gross gains of water.

2.7 Discussion

2.7.1 Heat tracing

The groundwater temperature used in the model was 9.4°C, which is between the maximum and minimum daily stream temperatures of 13.1°C and 4.7°C respectively. Therefore, groundwater discharge to the stream warms the stream during the night and cools the stream during the day, decreasing the amplitude of the daily temperature fluctuation (Webb and Zhang, 1997). This thermal dynamic is typical of low latitude regions because the daily air temperature fluctuation is greater than the seasonal change in mean air temperature (Kaser and Georges, 1999).

Having a groundwater temperature which is bracketed by daily stream temperature variation makes heat tracing more challenging because a given increase in groundwater advection to the stream will result in a smaller change in stream temperature (e.g. adding 10 °C groundwater to a 10 °C stream will not change the stream temperature). Therefore at times when the stream temperature is close to the groundwater temperature, such as around noon on days 4 and 5 (Figure 2.4), the modeled stream temperature is not sensitive to groundwater inputs. However, the model is sensitive to groundwater inputs at times of minimum and maximum stream temperature.

In both simulations B and C, the net gain in groundwater was found to be higher in the meadow sections than in the moraine sections. While the hydraulic conductivity in the moraines is thought to be higher than in the meadows, the meadow sections have numerous springs that contribute to steam flow while the moraines have none. These springs may be an important pathway by which groundwater reaches the stream (Baraer, 2015; Mark, 2005). Quantification of spring water tributaries to the main channel is needed to confirm the hypothesis that springs are potentially a main pathway for groundwater to enter the main channel. If this is correct, a combination of diffuse and point sources of groundwater could be used to more accurately represent field conditions in heat tracing.

When determining groundwater contribution based on stream temperature, one limitation is that we cannot distinguish between warming caused by either a loss of stream water from the channel to the subsurface, or by a gain in warmer groundwater. In our case, however, we can generally rule out large losses of stream water, as a significant net loss would be required to achieve the observed warming downstream. Additionally, while HFLUX is able to model losses of stream water to the subsurface (Glose and Lautz, 2013), it does not have the capacity to model concurrent gains and losses. This could be modified to improve future versions of the model.

2.7.2 Dye tracing

The dye tracing results of this study can be compared to the discharge profile measured over the lower moraine in the Quilcayhuanca Valley in 2012 by Gordon et al. (2015). For the same section of stream, gross gains and losses were found to be larger in 2012 than in 2014, particularly at the boundary of the lower moraine and lower meadow where 2012 results indicate significant tracer dilution occurs. This difference may be a result of different precipitation amounts in 2012 than 2014. In both 2014 and 2012, a loss and subsequent gain in stream discharge over the lower moraine was observed. Stream water is lost to the subsurface in the upper half of a moraine reach and then gained towards the bottom of the moraine, resulting in only a small net change in discharge.

One source of uncertainty for dye tracing is the potentially non-conservative behaviour of RWT where it may sorb to suspended sediment, porus media and organics in natural stream channels (Runkel, 2015). Significant decay of RWT in our experiment would result in an over estimate of dye dilution and therefore of groundwater-surface water exchange. However, since we are not using RWT as a tracer through the hyporheic zone, stream water has limited contact with sediment and sorption is not through to have a significant impact on the observed dye concentrations.

Figure 2.5 compares the apparent discharge profile from dilution gauging to the discharge profile from Simulation C (from heat tracing) on the primary axis. On the secondary axis, the minimum calculated gross gains and losses are shown for each of the four sections. The minimum gross gains and losses represent the amount of dilution needed for the heat tracing discharge profile to match the apparent discharge profile. The gross gains and losses have been normalized by dividing by the length of the reach.

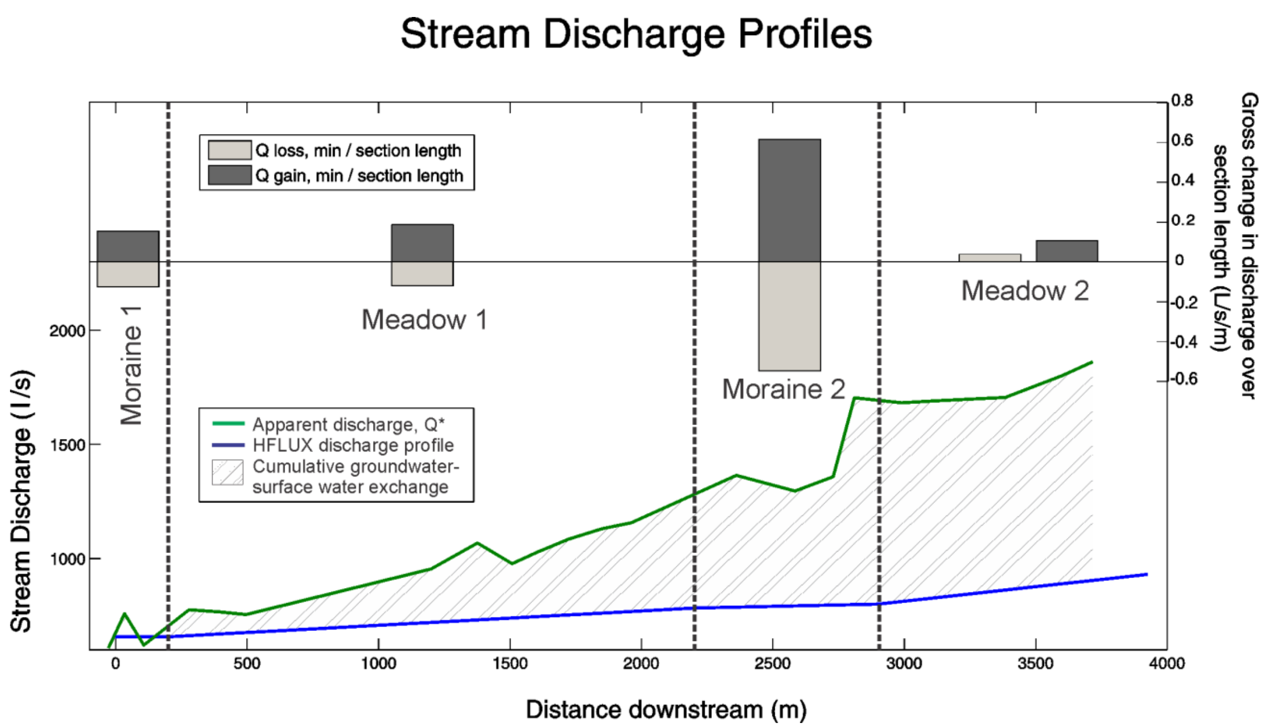

Figure 2.5: *Net and apparent stream discharge profiles (lower graph) and gross gains and losses (upper graph). In the upper graph, positive values indicate a gross increase in stream*

discharge, and negative values indicated a gross decrease in stream discharge. Positive gross loss shown in Meadow 2 are a result of dye tracing error.

From Figure 2.5 we see that the largest gross gains and losses occur over the lower moraine, suggesting that greater exchange of groundwater and surface water occurs here. This agrees with the suggestion of previous research (Gordon et al., 2015; Clow et al., 2003), which found that the moraines have larger and more heterogeneous particle sizes and therefore are thought to have a higher hydraulic conductivity. The meadows experience the smallest gross gains and losses but the largest net gains in stream flow due to the contribution of springs.

It should be acknowledged that the contribution of groundwater to stream flow likely changes throughout the dry season as well as from year to year. Inter-annual variability in both precipitation and glacier melt influence the degree of subsurface saturation and the amount of water stored in the valley.

2.7.3 Comparison between methods

In this paper, heat tracing and dye tracing are used to complement each other, with heat tracing providing information on net gains, and dye tracing providing information on gross gains and losses. However, these two methods have some differences in a.) the nature of the tracer used and b.) how they quantify groundwater exchange.

Using heat as a tracer is methodologically appealing because it requires little to no disruption to the environment, though it does require both time and substantial data collection. However, heat can be transmitted in several different ways. For example, in the hyporheic zone water lost to the subsurface can travel advectively within or out of the hyporheic zone. Alternatively, conductive heat transfer can occur in this zone, not only within the groundwater but also with the subsurface material, adding uncertainty to the thermal regime of the area below the streambed. The thermal regime below the streambed is important because it determines the temperature of groundwater which is being contributed to the stream.

Unlike heat, there is only one source of dye in our study area – the injection site. At the time scale of our experiment, it is assumed that when dye is lost to the subsurface it is not stored and later re-contributed to the stream in any significant proportion.

As mentioned in section 3.2.2, there is a potential methodological contradiction in the way that the two methods deal with groundwater–surface water exchange. Thermally, the calculated exchange should result in a stronger influence of groundwater on the temperature of the stream than that which is observed. Therefore, the exchange calculated from dye tracing may be overestimated.

We believe this two-step approach is desirable because it goes beyond what either method can do in isolation and provides a way to investigate groundwater exchange.

2.8 Conclusion

Heat tracing results suggest that over the 3925 m study reach, the Quilcay River experiences a net gain of approximately 29% of its outflow discharge from groundwater during the dry season. The meadow sections experience more net gain in groundwater than the moraine sections. This suggests that springs, which upwell in the meadows, are a significant pathway for groundwater reaching the stream. These groundwater contributions from the HFLUX simulations are similar to the 24% groundwater contribution presented by Baraer et al. (2015), determined using hydrochemical mixing analysis in a similar study area in the Cordillera Blanca.

The apparent discharge profile from dye tracing was used, in combination with the heat tracing results, to calculate gross gains and losses of water along the stream section. These results indicate that 49% of the stream discharge at the section outlet, is exchanged with the subsurface, while producing no net gain in stream discharge. Gross gains and losses were larger over the moraine sections, particularly the lower moraine, indicating that more groundwater–surface water exchange occurs in the moraine sections.

The stream heat budget in combination with dye tracing techniques is a viable way to quantify groundwater contributions at the reach scale in a remote catchment. These methods are complementary, allowing us to investigate both net and gross groundwater-surface water interactions.

These results suggest that groundwater in the Quilcayhuanca Valley of the Cordillera Blanca provides a net contribution to stream flow during the dry season as well as significant exchange between the stored precipitation in the groundwater and the glacial melt derived surface water. Along with the work of Gordon et al. (2015) and Baraer et al. (2015), these findings support the paradigm that groundwater is an important contributor to stream flow in proglacial valleys of the Cordillera Blanca. As glaciers recede, groundwater will become increasingly important for water supply. The results from this study indicate that the amount of groundwater exchanged between the river and subsurface is substantial, and suggests that stored groundwater is recharged from not only precipitation (as is often assumed) but also partially from glacier melt derived stream-water. This creates complex feedbacks in predicting the impact of glacier melt on valley hydrology and further investigation is needed to determine if decreased glacial melt water may also lead to decreased groundwater- surface water exchange.

2.9 Acknowledgements

The authors would like to thank the Huscarán National Park for access to the study site. This work was supported by the National Science Foundation under Grant Nos. EAR-0901480, EAR-1316429, EAR-1316432 and DEB-1010384, Natural Sciences and Engineering Research Council of Canada, and McGill University. Some of this material is based on data or equipment, services provided by the UNAVCO Facility with support from the National Science Foundation (NSF) and National Aeronautics and Space Administration (NASA) under NSF Cooperative Agreement No. EAR-0735156.

2.10 References

Agisoft., 2014. Agisoft PhotoScan User Manual Professional Edition, Version 1.1.0. AgiSoft LLC.

Anon., 2015. Canon Hack Develpoment Kit. Retrieved June 10, 2014, from Wikia: http://chdk.wikia.com/wiki/CHDK

Baraer, M., McKenzie, J.M., Mark, B.G., Bury, J., Knox, S., 2009. Characterizing contributions of glacier melt and groundwater during the dry season in a poorly gauged catchment of the Cordillera Blanca (Peru). *Advances in Geosciences* 22: 41–49, doi: 10.5194/adgeo-22-41-2009.

Baraer, M., et al., 2012. Glacier recession and water resources in Peru's Cordillera Blanca. *Journal of Glaciology* 58 (207): 134-150.

Baraer M., J. McKenzie, B. Mark, R. Gordon, J Bury, T. Condom, J. Gomez, S. & Knox, S. Fortner, 2015. Contribution of groundwater to the outflow from ungauged glacierized catchments: a multi-site study in the tropical Cordillera Blanca, Peru. *Hydrological Processes* 29 (11): 2516-2581.

Barnett, T.P., Adam, J.C., Lettenmaier, D.P., 2005. Potential impacts of a warming climate on water availability in snow-dominated regions. *Nature* 438 (7066): 303–309, doi: 10.1038/nature04141.

Bebbington, A.J., Bury, J.T., 2009. Institutional challenges for mining and sustainability in Peru. *Proceedings of the National Academy of Sciences of the United States of America* 106(41): 17296–17301, doi: 10.1073/pnas.0906057106.

Becker, M.W., Georgian, T., Ambrose, H., Siniscalchi, J., Fredrick, K., 2004. Estimating flow and flux of ground water discharge using water temperature and velocity. *Journal of Hydrology* 296(1-4): 221–233, doi: 10.1016/j.jhydrol.2004.03.025.

Bradley, R.S., Vuille, M., Diaz, H.F., Vergara, W., 2006. Threats to Water Supplies in the Tropical Andes. *Science* 312 (5781): 1755–1756.

Briggs M.A., Lautz L.K., McKenzie J.M., Gordon R.P., Hare D.K., 2012. Using high-resolution distributed temperature sensing to quantify spatial and temporal variability in vertical hyporheic flux. *Water Resources Research, 48*(2) doi:10.1029/2011WR011227

Burns, P., Nolin, A., 2014. Using atmospherically-corrected Landsat imagery to measure glacier area change in the Cordillera Blanca, Peru from 1987 to 2010. *Remote Sensing of Environment* 140: 165–178, doi: 10.1016/j.rse.2013.08.026.

Bury, J., Mark, B.G., Carey, M., Young, K.R., Mckenzie, J.M., Baraer, M., French, A., Polk, M.H., 2013. New Geographies of Water and Climate Change in Peru : Coupled Natural and Social Transformations in the Santa River Watershed. *Annals of the Association of American Geographers* 103 (October 2012): 363–374, doi: 10.1080/00045608.2013.754665.

Bury, J.T., Mark, B.G., McKenzie, J.M., French, A., Baraer, M., Huh, K.I., Zapata Luyo, M.A., Gómez López, R.J., 2011. Glacier recession and human vulnerability in the Yanamarey watershed of the Cordillera Blanca, Peru. *Climatic Change* 105 (1): 179–206, doi: 10.1007/s10584-010-9870-1.

Caissie, D., Satish, M.G., El-Jabi, N., 2007. Predicting water temperatures using a deterministic model: Application on Miramichi River catchments (New Brunswick, Canada). *Journal of Hydrology.* 336, 303–315.

Carey M., 2010. *In the shadow of melting glaciers: Climate change and andean society* (pp. 1-304) doi:10.1093/acprof:oso/9780195396065.001.0001

Clow, D.W., Schrott, L., Webb, R., Campbell, D.H., Torizzo, A, Dornblaser, M., 2003. Groundwater occurrence and contributions to stream flow in an alpine catchment: Colorado Front Range. *Ground Water* 41937e950, 7: 937–950.

Cox, M.M., Bolte, J.P., 2007. A spatially explicit network-based model for estimating stream temperature distribution. *Environmental Modelling & Software.* 22, 502-514.

Fonstad M.A., Dietrich J.T., Courville B.C., Jensen J.L., & Carbonneau P.E., 2013. Topographic structure from motion: A new development in photogrammetric measurement. *Earth Surface Processes and Landforms, 38*(4), 421-430. doi:10.1002/esp.3366

Glose, A.M., & Lautz, L.K., 2013. Stream heat budget modeling with HFLUX: model development, verification, and applications across contrasting sites and seasons. Syracuse University, Syracuse, NY. In review.

Gordon, R.P., Lautz, L.K., McKenzie, J.M., Mark, B.G., Chavez, D., & Baraer, M., 2015. Sources and pathways of stream generation in tropical proglacial valleys of the Cordillera Blanca, Peru. *Journal of Hydrology* 522, 628–644, doi: 10.1016/j.jhydrol.2015.01.013.

Harvey, J.W., Wagner, B.J., 2000. Quantifying hydrologic interactions between streams and their subsurface hyporheic zones. In Jones, J.A., and Mulholland, P.J. (Eds), *Streams and Ground Waters,* Academic Press, San Diego. p. 3-44.

Harwin, S., Lucieer, A., 2012. Assessing the accuracy of georeferenced point clouds produced via multi-view stereopsis from unmanned areal vehicle (UAV) imagery. *Remote Sensing.* 4(6): 1573-1599.

Hugenholtz, C. H., Whitehead, K., Brown, O.W., Barchyn, T.E., Moorman, B.J., LeClair, A., Riddell, K., Hamilton, T., 2013. Geomorphological mapping with a small unmanned aircraft system (sUAS): Feature detection and accuracy assessment of a photogrametrically-derived digital terrain model. *Geomorphology.* 194: 16-24.

Intergovernmental Pannel on Climate Chance (IPCC), 2013. *Climate Change: The Physical Science Basis, Working group 1 Contribution to the Fifth Assessment Report of the Intergovernmental Panel on Climate Change*. Cambridge University Press, Cambridge, United Kingdom.

Kaser, G., Georges, C., 1999. On the mass balance of low latitude glaciers with particular consideration of the Peruvian Cordillera Blanca. *Geografiska Annaler* 81 (40)

Kurylyk, B.L., Moore, R.D., MacQuarrie, T.B., 2015. Scientific briefing: quantifying streambed heat advection associated with groundwater-surface water interactions. *Hydrological Processes*. doi: 10.1002/hyp.10709

Love, D. a., Clark, A.H., Glover, J.K., 2004. The lithologic, stratigraphic, and structural setting of the giant antamina copper-zinc skarn deposit, Ancash, Peru. *Economic Geology* 99 (5): 887–916, doi: 10.2113/gsecongeo.99.5.887.

Lowe, D., 2004. Distinctive image features from scale-invariant keypoints. *International Journal of Computer Vision*, 60 (2): 91-110.

Magnusson, J., Jonas, T., Kirchner, J.W., 2012. Temperature dynamics of a proglacial stream: Identifying dominant energy balance components and inferring spatially integrated hydraulic geometry. *Water Resources Research.* 48, W06510.

Mark, B.G., McKenzie, J.M., Gómez, J., 2005. Hydrochemical evaluation of changing glacier meltwater contribution to stream discharge: Callejon de Huaylas, Peru / Evaluation hydrochimique de la contribution évolutive de la fonte glaciaire à l'écoulement fluvial: Callejon de Huaylas, Pérou. *Hydrological Sciences Journal* 50 (6): 975–988, doi: 10.1623/hysj.2005.50.6.975.

Messerli, B., Viviroli, D., Weingartner, R. , 2004. Mountains of the World : Vulnerable Water Towers for the 21st Century. *Ambio* 33, SPEC. ISS.:, 29–34.

Payn, R. a., Gooseff, M.N., McGlynn, B.L., Bencala, K.E., Wondzell, S.M., 2009. Channel water balance and exchange with subsurface flow along a mountain headwater stream in Montana, United States. *Water Resources Research* 45 (11): doi: 10.1029/2008WR007644.

Runkel, R.L., 2015. On the use of rhodamine WT for the characterization of stream hydrodynamics and transient storage. *Water Resources Research.* 51: 6125-6142, doi: 10.1002/2015WR017201

Schmadel, N.M., Neilson, B.T., Stevens, D.K., 2010. Approaches to estimate uncertainty in longitudinal channel water balances. *Journal of Hydrology* 394 (3-4): 357–369, doi: 10.1016/j.jhydrol.2010.09.011.

Stream Solute Workshop, 1990. Concepts and Methods for Assessing Solute Dynamics in Stream Ecosystems. *Journal of the North American Benthological Society* 9 (2): 95–119, doi: 10.2307/1467445.

Turner, D., Lucieer, A., Watson, C., 2012. An automated technique for generating georectified mosaics from ultra-high resolution unmanned aerial vehicle (UAV) imagery, based on structure from motion (SFM) point clouds. *Remote Sensing*. 4(5): 1392-1410.

Verhoeven, G., 2011. Taking computer vision aloft--archaeological three-dimensional reconstructions from aerial photographs with photoscan. *Archaeological Prospection*, 18 (1): 67-73.

Viviroli, D., Dürr, H.H., Messerli, B., Meybeck, M., Weingartner, R., 2007. Mountains of the world, water towers for humanity: Typology, mapping, and global significance. *Water Resources Research*, 43 (7): 1–13, doi: 10.1029/2006WR005653.

Voss, F.D., Curran, C.A., Mastin, M.C., 2006. Modeling water temperature in the Yakima River, Washington, from Roza Diversion Dam to Prosser Dam. *USGS Scientific Investigations Report* 2008-5070.

Vuille, M., 2013. *Climate Change and Water Resources in the Tropical Andes*. Interamerican Development Bank, Environmental Safeguards Unit, Technical Note No. IDB-TN-515, 35pp. Retrieved June 2015 from http://idbdocs.iadb.org/wsdocs/getdocument.aspx?docnum=37571430

Wagner, B.J., Harvey, J.W., 2001. Analysing the capabilities and limitations of tracer tests in stream-aquifer systems. *IAHS-AISH publication* 269: 191-198.

Webb, B.W., Zhang, Y., 1997. Spatial and seasonal variability in the components of the river heat budget. *Hydrological Processes* 11: 79 – 101.

Westhoff, M.C., Savenije, H.H.G., Luxemburg, W.M.J.., Stelling, G.S., van de Giesen, N.C., Selker, J.S., Pfister, L., Uhlenbrook, S., 2007. A distributed stream temperature model using high resolution temperature observations. *Hydrology and Earth System Sciences.* 11(4): 1469–1480,

Wigmore, O., Mark, B., 2014. High Resolution Aerial Photogrammetry and DEM Generation in the Peruvian Andes: Evaluation of a Kite Based Platform. *Presented at 2014 AAG Annual Meeting, R.S. Tarr Student Illustrated Paper Competition.* Tampa, FL.Winter, T. C., 1981.

Uncertainties in estimating the water balance of lakes. *Water Resources Bulletin* 17(1): 82-115.

Zheng, C., Bennett, G.D., 2002. *Applied Contaminant Transport Modeling, 2 nd ed.* John Wiley and Sons Inc., New York, NY. 343-347.

Chapter 3. Climate impacts on Andean water resources using a mountain systems approach

Authors: Lauren D. Somers, Jeffrey M. McKenzie, Bryan G. Mark, Pablo Lagos, Gene-Hua Crystal Ng, Andrew Wickert, Christian Yarleque, Michel Baraer, Yamina Silva

3.1 Context within thesis

Hydrochemical mixing analyses by others (Baraer *et al*., 2015; Crumley *et al*., 2015) and work presented in Chapter 2 provide "snap shots" in time, which demonstrate groundwater's importance in the mountain hydrological system and elucidate the processes and pathways involved. Numerical hydrological modelling is commonly used to transform this process understanding into a temporally continuous representation of hydrological conditions and also to project future hydrological change under climate change. Additionally, glaciers, surface water and groundwater systems are often modelled in isolation but, in mountain settings, these three systems are tightly coupled and interact to shape water resources.

In this manuscript, I integrate glacier melt, surface water and groundwater modelling approaches to gain a holistic understanding of the hydrologic dynamics of the Shullcas Watershed in central Peru. I then use the calibrated model in combination with climate projections to project future glacier recession and changes in the amount and timing of stream discharge.

3.2 Abstract

Mountains act as vital water towers for downstream populations because the buffering capacity of snow and ice helps to sustain water resources during dry periods (Barnet *et al*, 2005; Viviroli *et al*, 2007; Prichard, 2017). Under a warming climate, glaciers in the tropical Andes are retreating faster than mountain glaciers anywhere else on earth (Paul *et al*., 2004; Bradley *et al*., 2006;

Rabatel *et al.* 2013; Vuille *et al.*, 2018). Climate, glacier, surface water and groundwater systems are usually considered in isolation when assessing the impact of climate change on Andean hydrology (e.g. Juen *et al*., 2007; Huss & Hock, 2018; Yarleque *et al.,* 2018). Here we show that the interactions between these systems shape the response of mountain water resources to climate change and that groundwater has an important and nuanced role to play. We use a novel mountain-systems modelling approach to elucidate water storage and discharge dynamics in a proglacial Andean watershed and project the future impacts of climate change. For all climate scenarios, glacier coverage in the Shullcas Waterhsed, central Peru, is likely to disappear completely by 2100. The loss of glacier melt water is buffered to some extent by consistent groundwater discharge which only receives minor recharge (<2%) from glacier melt. However, increasing temperature and changes in precipitation act to decrease groundwater recharge in the long term, leading to decreased groundwater inputs to streams, particularly for "business as usual" carbon emission scenario RCP 8.5.

3.3 Introduction

Glaciers worldwide have been experiencing accelerated retreat since the 1980s due to climate change (Paul *et al*., 2004, Kaser *et al.*, 2006) with tropical alpine glaciers experiencing the most rapid retreat (Paul *et al*., 2004; Bradley *et al*., 2006; Rabatel *et al.* 2013; Vuille *et al.*, 2018). 70% of the world's tropical glaciers are in the Peruvian Andes where glacier coverage has decreased by over 40% since the 1970s (Autoridad Nacional del Agua, 2014). Communities and industries in the Andes and on the Arid Pacific coast are vulnerable to intensifying climate-driven, dry season (May-September) water shortages (Vuille *et al*., 2018) as 80% of annual precipitation falls during the austral summer in the Peruvian Andes (Bury *et al*, 2013).

Recent studies in the Peruvian Andes have demonstrated the importance of groundwater for mountain streamflow generation (Baraer *et al*., 2015; Gordon *et al*., 2015; Somers *et al*., 2016; Glas *et al*., 2018) and are echoed in other high mountain environments including the Canadian (McClymont *et al*., 2010; Hood and Hayashi, 2015) and American Rocky Mountains (Liu *et al*., 2004; Frisbee *et al.,* 2011), and Himalayas (Anderman *et al*., 2012). These studies suggest that mountain groundwater, previously considered a minor contributor to streamflow, may provide resilience to climate change impacts (Tague *et al*., 2008). However, groundwater is frequently neglected or over simplified in hydrological modelling of proglacial mountain catchments due to the computational intensity of joint modelling and a lack of observational groundwater data (Juen *et al*., 2007; Ragettli *et al*., 2014). Unlike previous research, our contribution integrates lateral groundwater flow by integrating distributed groundwater modelling with surface water, and glacier melt modelling. We combine our extensive field observations with a systems modelling approach to elucidate the role of groundwater in a proglacial mountain hydrological system and assess the capacity of mountain groundwater to buffer the hydrological impacts of climate change and glacier recession.

The Shullcas Watershed, central Peru, is a typical proglacial Andean watershed comprised of steep alpine grasslands and flatter valley bottom wetlands. It is underlain by glacio-fluvial soils above metamorphic rock of the Huaytapallana Complex in the north and weakly metamorphosed sedimentary rock of the Mitu, Cabanilla and Pucara Groups in the south (Chew *et al*., 2016). The Shullcas River is partially fed by glaciers of the Cordillera Huaytapallana, which have retreated 55% between 1984 and 2011 (Lopez-Moreno *et al.,* 2014). The outflow river is the primary water source for the city of Huancayo (population: 365K; Instituto Nacional de Estadistica y Informatica, 2012) which frequently experiences water shortages during the dry season (Mark *et al.,* 2017). The social and economic importance of this watershed and availability of climate, glacier, hydrologic and hydrogeological data, make the Shullcas Watershed an ideal test site to use a parsimonious (Voss, 2011) systems approach to assess the impact of climate change on Andean hydrology.

3.4 Methods

3.4.1 Field data collection and processing

We obtained monthly streamflow data at the watershed outlet from 1985 to 2009 from the Peruvian National Water Authority (ANA). Daily meteorological records, including maximum and minimum air temperature, and precipitation, are from the National Meteorology and Hydrology Service of Peru (SENAMHI) for two primary meteorological stations (Huaytapallana, 4684 masl, and Shullcas, 3839 masl; Figure 3.1a) within the watershed from 2008 to 2018. (https://www.senamhi.gob.pe/?&p=estaciones). Two additional weather stations (Huayao and Santa Ana) located within 20 km of the watershed and data from NASA's Tropical Rainfall Measurement Mission (TRMM version 3B42 RR, Huffman and Bolvin, 2018) at 0.25 degree resolution, were used to extend temperature and precipitation inputs, respectively, back to 1998 and fill data gaps using linear regression to the primary stations. To account for orographic effects, precipitation and temperature were spatially distributed across the model domain based on elevation lapse rates calculated from the two main stations within the watershed.

In June, 2015 we installed 5 stream discharge gauges and 2 lake level gauges (3 years of data available). In July 2016 we installed an additional stream gauging station and 7 shallow (<2.5m) groundwater table wells (2 years of data available, Figure 3.1a). Streamflow at each station is calculated based on stage observations and a calibrated rating curve. Both streamflow and water table depth were recorded at a minimum frequency of one hour across all gauges and are compensated for barometric pressure changes.

3.4.2 Integrated groundwater-surface water modelling

We use GSFLOW (Markstrom *et al*., 2008) version 2.0.0, a combined surface water and groundwater numerical model created by the U.S. Geological Survey, which we couple to a glacier melt module, to simulate the hydrological system of the Shullcas Watershed. The surface water component is based on the Precipitation Runoff Modeling System (PRMS) and discretized into hydrologic response units (HRUs). HRUs exchange water with the finite difference groundwater model, MODFLOW, a widely used groundwater flow model. MODFLOW-NWT, which employs a Newtonian formulation for solution, is used to improve model convergence in the steep topography of the study site. Input files are prepared using GRASS-GSFLOW version 1.0.0 (Ng *et al*, 2018).

The ASTER Global Digital Elevation Model with 30-m resolution (Tachikawa *et al*., 2011) is used to define the watershed boundaries and topography. Land cover types and associated inputs are assigned for the HRUs based on separate analysis of Landsat satellite imagery of the Shullcas Watershed (Sadler *et al*., in review). Input parameters are based on field measurements where possible, or literature values, if not. A table of selected input parameters and GSFLOW input files are included in the Supplementary Materials, Table 3.2.

3.4.3 Glacier melt module

A semi-distributed, modified temperature-index model is used to simulate glacier melt and mass balance for the Huaytapallana glaciers. The glacier area is divided into 100 m elevation bands. Temperature and precipitation lapse rates are calculated from the two weather stations in the Shullcas Watershed and are applied to calculate the temperature and precipitation for each elevation band per time step. Seasonal melt factors are calibrated to match glacial lake outflow for the Chuspicocha lake. For projection runs, glacier area observations by Lopez-Moreno (2014) are used to validate the calibrated glacier module. Simulated glacier melt is applied to the GSFLOW model as precipitation.

Temperature-index modelling is not ideal for tropical glaciers because the seasonality of humidity and solar radiation can de-couple melt from air temperature (Hock, 2003). In our case, lack of humidity and radiation data makes energy balance modelling impossible. Therefore, we employ seasonal melt factors, where the dry and rainy season have different melt factors (after Quick and Pipes, 1977, see equation 3.1 in supplementary materials), to help account for this limitation. Our temperature index model was able to reproduce general trends in glacier melt and retreat.

3.4.4 Model setup and calibration

The model has a daily time step and uses a steady state spin up followed by a 30-year, transient spin up period. The transient spin up repeats weather from 2001 when annual precipitation was close to the long-term average. We confirm that the model is stabilized after the spin up period by comparing the saturated groundwater storage for the last two years of the spin up, and find less than 0.5% difference. Furthermore, three constant head MODFLOW cells are placed downstream of the watershed outlet point to allow for some groundwater out of the modeled domain. This boundary flow is very small compared to groundwater discharge to the stream.

The joint GSFLOW and glacier model is calibrated using an aggregate error metric that combines multiple data sources to ensure process representation of the model. The aggregate error metric is calculated based on the root mean square error of the model output to the long-term monthly streamflow record and 6 short-term stream flow records (locations shown in Figure 3.1a) and is formulated such that downstream gauges are weighted more heavily, proportional to discharge. 20 key parameters were manually calibrated within a range of probable values. A detailed description of the aggregate error metric and parameter calibration procedure are included in the supplementary materials.

The model is run over 2 time periods: The first is from 1998 to 2018 where the model is driven by meteorological observations from within the Shullcas Watershed. This time period is used for model calibration and analysis of hydrograph components. The second is from 1961 to 2099 where the model is driven by the downscaled GCM outputs and is used for hydrologic projections.

3.4.5 Sensitivity analysis

Given limited computational capacity, a one-at-a-time sensitivity analysis (Zheng and Bennet, 2002) is performed to assess the uncertainty of the results. We select 4 sets of input parameters of high uncertainty and define a range of extreme possible values and run the model using each one. We then calculate the RMSE between the altered and base case stream discharge from 2015 to 2018, the period of record for our 6 daily stream gauges (Table 3.4). The resulting conservative estimate of uncertainty on modeled streamflow is ± 23% ($p=0.05$), calculated by adding the resulting RMSE together and defining the confidence interval assuming normally distributed model outputs (See supplementary materials).

3.4.6 Climate projections

Climate projections were generated from the regional dynamic ETA model (Chou et al., 2014a; 2014b) by the Center for Weather Forecasting and Climate Studies (CPTEC) at the Brazilian National Institute for Space Research (INPE). The ETA model uses the MIROC5, CanESM2, and BESM GCMs under historical, and future (RCP4.5 and RCP8.5) downscaling scenarios with a spatial resolution of 20 km and a daily time step from 1961 to 2099. The regional simulations were obtained by request at http://projeta.cptec.inpe.br.

The atmospheric variables required for hydrologic modelling include maximum and minimum temperature, and precipitation. Daily temperatures were corrected using the (classical) additive bias correction technique (Bordoy and Burlanto 2013; Hawkins *et al*., 2012), while daily precipitation raw data were corrected in two steps. First, Linear scaling (Smitha et al 2018) or multiplicative shift (Ines and Hansen 2006) bias correction was used, with a 3-months sliding windows precipitation. Second, the Quantile mapping bias correction technique (Ines and Hansen, 2006) was applied following the Grillakis *et al*. (2013) procedure.

3.5 Results

Daily measurements of precipitation, and maximum and minimum temperature from two meteorological stations within the watershed and several others nearby are used to calculate lapse rates and force the model between 1998 and 2018. Input parameters for integrated modelling were selected through field observation and literature search (Supplementary Materials, Table 3.2). Given the large number of parameters, we manually calibrate (>100 calibration runs) selected input parameters to long-term monthly streamflow records at the watershed outlet from 1998 to 2009 and daily streamflow records at six stations within the watershed from 2015 to 2018 (Figure 3.1a and Figure 3.4). The glacier melt module is manually calibrated to outflow from the glacial Chuspicocha Lake from 2015-2018. Dry and rainy season melt factors of 2.8 and 3.0 mm $d^{-1}°C^{-1}$ respectively yielded the best fit to observed meltwater production. The relatively low melt factors are consistent with the dry, high radiation setting where more of the energy for melt is partitioned to sublimation (Hock, 2003; Fernandez and Mark, 2016). Sensitivity analysis is then used to assess the impact of parameter selection on our results.

Nash-Sutcliffe Model Efficiency (E_{N-S}) for stream discharge ranged from -0.46 to 0.74 (See supplementary material Figure 3.5, Table 3.2), with 4 of the 6 gauging stations having E_{N-S} greater than 0.5 (A hydrological model is often considered to adequately represent observed data if E_{N-S} > 0.5; Moriasi *et al.,* 2007). Operation of a small dam at gauge 1 and road construction upstream of gauge 5 may have led to interference with the natural hydrograph and explain the low model efficiency at these locations (discussed further in supplementary materials). Average modeled water table depth matched well with observations from our two groundwater table well clusters with root mean square errors (RMSE) of 0.20 and 1.50 m for the Chuspicocha and Huacracocha areas respectively from 2016 to 2018. The model underestimates the range in water table fluctuations due to the comparatively large grid-cell size.

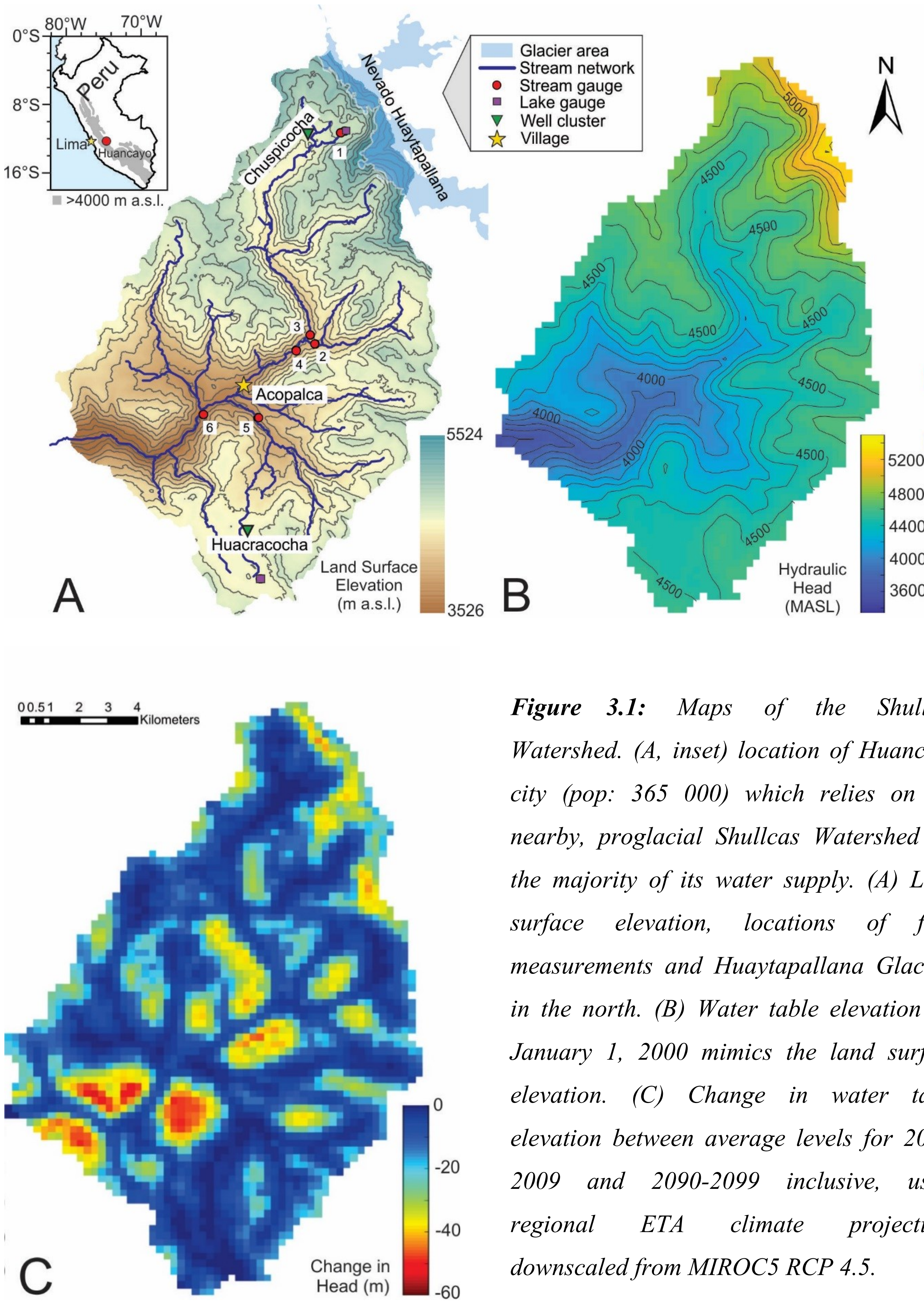

Figure 3.1: *Maps of the Shullcas Watershed. (A, inset) location of Huancayo city (pop: 365 000) which relies on the nearby, proglacial Shullcas Watershed for the majority of its water supply. (A) Land surface elevation, locations of field measurements and Huaytapallana Glaciers in the north. (B) Water table elevation for January 1, 2000 mimics the land surface elevation. (C) Change in water table elevation between average levels for 2000-2009 and 2090-2099 inclusive, using regional ETA climate projections downscaled from MIROC5 RCP 4.5.*

3.5.1 Groundwater dominates dry season streamflow

The calibrated model allows us to continuously quantify sources and pathways of streamflow generation. On average, modeled glacier melt contributes only 8.0% of Shullcas River outflow discharge from 1998 to 2018. As additional validation, hydrochemical mixing analysis by Crumley (2015) found that between 8.9 and 17% of Shullcas River outflow from July 10-22, 2014 was sourced from glacier melt and the remainder from groundwater. Over the same time period, our results indicate an average glacier melt contribution of 11% of the outflow stream discharge with maximum and minimum on individual days of 12 and 8.5% respectively, increasing confidence in our results.

Figure 3.2a shows the breakdown of the modeled hydrograph at the watershed outlet for one sample year (2016-2017). Over the modeled period from 1998 to 2018, modeled groundwater discharge from the saturated zone to the stream ranges from -4.4 to 93 % of total outlet stream discharge. Negative groundwater discharge indicates that the stream is recharging the groundwater system, which occurs on days with very high precipitation. During the dry season, groundwater from the saturated zone contributes, on average, 72% of stream discharge and is the dominant pathway for streamflow generation. Interflow (shallow, preferential flow through the unsaturated zone) to the stream ranges from 6.9 to 100% of outlet stream discharge and dominates (60%) during the rainy season.

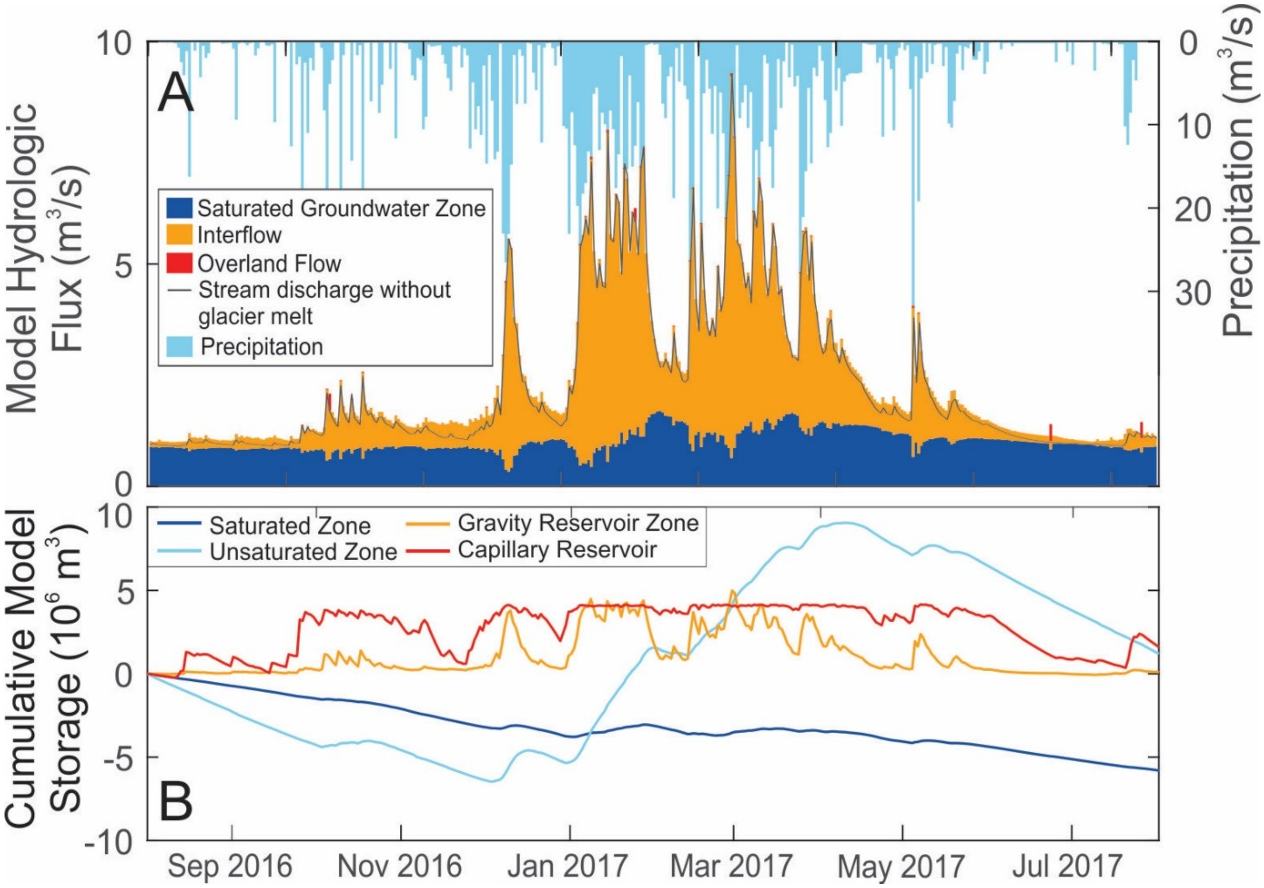

Figure 3.2: *Modeled stream fluxes and storage reservoirs for the Shullcas Watershed between Aug 1, 2016 and 2017 (arbitrarily selected year). (A) plot of precipitation, and stacked plot of stream flow contribution pathways. Streamflow without glacier melt is shown by the black line separately form the stacked plot since glacier melt can contribute through overland flow, interflow or groundwater discharge. (B) Cumulative change in water storage for modeled reservoirs. The capillary reservoir, gravity reservoir and unsaturated zone storage have a net storage change that is close to zero while the saturated zone storage has a net negative storage change, indicating that it is dominated by multi-year trends in recharge.*

3.5.2 Glacier melt contributes little to groundwater recharge

While glacier area accounted for 2.4% of the watershed area in 2015, only 1.9% of saturated zone groundwater discharge to the stream was originally sourced from glacier meltwater. This is attributed to the high (overland) runoff ratio of bare rock near the glacier termini and suggests that glacier sourced groundwater recharge is localized to the area near the glacier. The low contribution of glacier melt to groundwater suggests that overall, groundwater recharge in this watershed will be resilient to a reduction in glacier meltwater input.

To our knowledge, the only other quantitative estimate of glacier melt contribution to groundwater comes from a headwater catchment on Volcán Chimborazo in Ecuador, where 18% of groundwater discharge is sourced from glaciers which cover 34% of the watershed area (Saberi *et al*., 2019). This may suggest a useful relationship between glacier coverage as a proportion of watershed area, and glacier sourced groundwater discharge, similar to the relationship proposed by Baraer *et al*. (2015) between glacierized area and glacier melt contribution to streamflow. However, this relationship likely varies with climate and topography, and requires more estimates in different basins to expound.

Our results show that 37% of total annual streamflow reaches the stream through the saturated groundwater zone. These results complement work by others (Hood and Hayashi, 2015) to demonstrate that mountain groundwater is an important contributor to streamflow, including Andermann *et al*., (2012) who estimate that groundwater accounts for 2/3 of annual river discharge of three Himalayan basins.

An analysis of simulated groundwater head distribution (Figure 3.1b) shows the water table remains close to the ground surface in valley bottoms and near streams, but drops well below the unconsolidated surficial aquifer (0-20 m below ground surface (bgs)) in highland and steep areas (as low as 176 m bgs). Therefore, much of the modeled groundwater flow towards the streams occurs, at least partially, through the fractured bedrock aquifer, as suggested in other mountain hydrological studies (Clow and Sueker, 2000; Liu *et al*., 2004; Andermann *et al*., 2012). The longer and slower flow paths through bedrock allow groundwater to contribute to streamflow year round.

3.5.3 Soil water and unsaturated zone storage fluctuate seasonally while saturated groundwater storage follows multi-year trends

Soil zone storage (i.e. the sum of capillary storage and gravity storage calculated in GSFLOW), and unsaturated and saturated groundwater zone storage all fluctuate seasonally as they are recharged during the rainy season and drained during the dry season. Figure 3.2b shows the cumulative storage change in the model reservoirs for the 2016-2017 hydrologic year. The range in cumulative storage change (i.e.annual storage) is largest in the unsaturated groundwater zone (0.0158 km^3), followed by the soil zone (0.0095 km^3) and the saturated groundwater zone (0.0060 km^3). For reference, a city the size of nearby Huancayo uses approximately 0.023 km^3 of water per year based on the population and an average Peruvian water usage of 175L/day (United Nations Development Report, 2006).

However, the timing of changes in storage is an important parameter for water resources. While the unsaturated and soil zones have large annual storage, these reservoir are quickly depleted after the end of the rainy season. Annual storage in the saturated groundwater zone is smaller, but continues to drain throughout the dry season. The negative net change in saturated storage in this particular year (Figure 3.2b) illustrates the multi-year time scales on which groundwater acts and its ability to buffer inter annual climatic variability. It also supports the characterization of groundwater as a resource with a long memory (Cuthbert et al., 2019), even in a mountain environment where hydraulic gradients are high.

3.5.4 Rapid projected climate warming causes disappearance of Huaytapallana Glaciers

We simulate future hydrologic conditions using dynamically downscaled climate projections from three general circulation models (GCMs): MIROC5, CanESM2 and BESM under historical and future (RCP4.5 and 8.5) scenarios from 1961 to 2099. The ETA regional climate model (RCM) (Chou et al., 2014a; 2014b) is used for downscaling and results are corrected to historical data from the Huayao meteorological station (1975-2005).

Observed historical warming at the Huayao Meteorological station from 1975 to 2005 was 0.42°C per decade. The projected rates of warming from the ETA RCM over the 21st century were 0.46 and 0.88 °C per decade for RCP 4.5 and 8.5 emission scenarios respectively (Figure 3.3a). For the RCP 4.5 scenario, minimum and maximum temperature begin to stabilize around 2070. The high projected rate of warming is consistent with elevation dependent warming (EDW) that has been observed and projected in areas of high elevation (Urrutia and Vuille, 2009; Seth et al., 2010; Mountain Research Initiative EDW Working Group, 2015). For RCP 4.5, little change is projected in precipitation and the GCMs disagree on the direction of change, whereas RCP 8.5 projects more negative trends in precipitation.

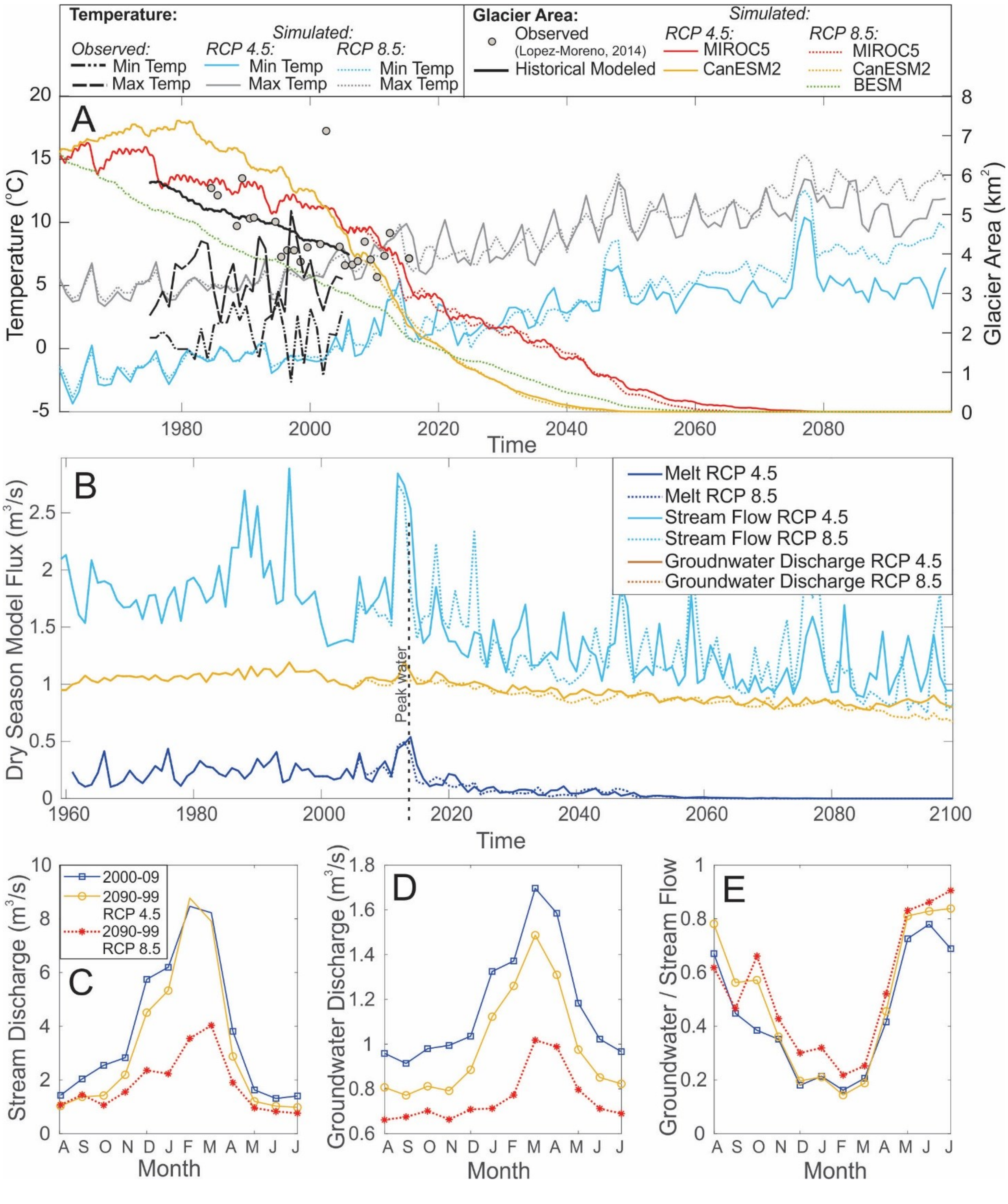

Figure 3.3: *Climate, glacier and hydrologic projections. (A) Projected change in maximum, minimum temperature and glacier area from 1960 to 2099 and observed glacier areas reprocessed*

from Lopez-Moreno, 2014. (B) Modeled dry season streamflow, groundwater discharge and glacier melt. Peak glacier runoff occurs in 2017. (C) Change in mean monthly streamflow between the first and last decade of the 21st century. (D) Change in groundwater discharge between the first and last decade of the 21st century. (E) The proportion of streamflow that comes from groundwater discharge, where a value of 1 means that all streamflow is sourced from groundwater discharge.

We reanalyzed remote sensing results from Lopez-Moreno *et al*. (2014) and determine that the glacier area within the Shullcas Watershed decreased by 30% between 1984 and 2011. Figure 3.3a shows that the simulated glacier area for the historical period compares well with remote sensing observations ($R^2 = 0.67$).

All emission scenarios and GCMs run through our glacier melt module project the complete disappearance of the Huaytapallana glaciers by the end of the 21st century (Figure 3.3a) with the most conservative scenario projecting disappearance (glacier area <100m^2) in 2085. These projections are comparable to equilibrium line elevation projections for the Quelccaya Ice cap, approximately 400 km to the southeast of our study area with a summit elevation of 5680 m a.s.l. (Yarleque et al., 2018) (Huaytapallana summit elevation is 5557 m a.s.l.). Though climatic settings vary, approximately 2330 glaciers in the Peruvian Andes have summit elevations of less than 5500 m a.s.l (as of 2014, Calculated from ANA, 2014) and therefore likely face similar outlooks.

The glacier melt module uses a temperature-index scheme to calculate melt and therefore is insensitive to possible changes in humidity and solar radiation (Hock, 2003). However, lacking both historical data or future projections of humidity and solar radiation, the temperature index approach serves as a good estimate of future glacier melt (Fernández & Mark, 2016). Furthermore, the glacier module does not include edge effects feedbacks, where longwave radiation from rock surrounding the glacier plays an increasingly important role as the glacier retreats (Aubry-Wake *et al.,* 2015); or elevation feedbacks, where glacier thinning lowers the elevation of the glacier surface and is subjected to higher temperatures (Weertman, 1961) making our glacier melt projections conservative.

3.5.5 Groundwater temporarily buffers loss of glacier melt under future climatic conditions

As glaciers recede, meltwater production initially increases to a maximum, known as "peak water", before dropping off as the glacier continues to retreat (Gleick and Palaniappan, 2010). Glacier peak water has passed for approximately half of glaciered drainage basins globally (Huss and Hock, 2018) and an even higher proportion in the Andes (Baraer *et al*., 2012). Our results show modelled glacier meltwater production peaks when glacier areal retreat is fastest, around 2013, during a relatively warm period in the climate projections, then steadily drops off until it becomes zero when the glacier disappears.

The projected decrease in glacier melt in turn affects the stream discharge. During the dry season, glacier melt contribution to streamflow steadily decreases after peak water but groundwater discharge to the stream remains relatively constant (Figure 3.3b), thereby maintaining a buffer to stream flow during the dry season when downstream water stress is at a maximum. However, as temperature increases, so does potential evapotranspiration (PET), calculated using a Priestley-Taylor approach, which reduces groundwater recharge. The effect of increasing ET can be seen in the gradual decreasing trend in dry season groundwater discharge (Figure 3.3b). This effect is more severe in the RCP 8.5 scenario where temperature continues to increase through 2099 and there is a severe reduction in precipitation for some GCMs.

Table 3.1 and Figure 3.3c,d,e summarize modeled changes in climatic and hydrological variables between the first and last decade of the 21st century. Though both RCP 4.5 and 8.5 predict complete loss of glacier melt water, there is a marked difference in streamflow between the scenarios. RCP 8.5 has lower stream flow and groundwater discharge year round due to both lower precipitation and higher ET. These projections do not account for changes in vegetative community and increases in the vertical vegetation threshold that may further increase ET. Furthermore, 2000-2009 was, in general, dryer than other decades, meaning that the changes in precipitation, ET and streamflow may be understated. Both future scenarios project that a larger proportion of streamflow will come from groundwater (Figure 3.3e).

Table 3.1: *Changes in model fluxes between 2000-2009 and 2090-2099*

Model Flux	**RCP 4.5**			**RCP 8.5***		
	2000-2009	**2090-2099**	**% change**	**2000-2009**	**2090-2099**	**% change**
Precipitation (m^3/d)	563 079	529 630	-5.94	518 658	375 939	-27.5
Evapotranspiration (m^3/d)	211 772	250 567	+18.3	210 809	231 848	+10.0
Glacier melt (m^3/d)	26 220	0	-100	26 839	0	-100
Stream flow (m^3/d)	349 480	278 011	-20.5	314 713	156 527	-50.3
Dry season	132 801	97 053	-26.9	129 431	87 516	-32.4
Rainy season	504 249	407 266	-19.2	447 058	205 821	-54.0
Groundwater discharge to stream (m^3/d)	103 905	85 651	-17.6	101 408	65 523	-35.4

* Excluding BESM simulations so that RCP 4.5 and 8.5 are averaging the same number of runs

All of the modeled climate scenarios project a decrease in water table elevation and groundwater storage (Supplementary Materials Table 3.5). On average, the groundwater table drops by 8.8 and

13.4 m for RCP 4.5 and 8.5 respectively, over the 21st century. The loss of groundwater storage in the watershed is not spatially uniform. Figure 3.1c shows the change in water table between the beginning and end of the 21st century for the MIROC5 RCP 4.5 scenario. The greatest changes in head occur beneath the Huaytapallana glaciers where the loss of meltwater decreases groundwater recharge, and beneath the steepest hillslopes in the watershed where hydraulic gradient is greatest. The least amount of change occurs near the stream network and in the high flat areas of the watershed. Spatial patterns between climate scenarios differ slightly and are described in Supplementary Materials Table 3.5. Similarly, groundwater projections in a forested watershed in eastern Canada also exhibit the largest water table changes beneath topographic highs (Cochand *et al.,* 2018).

3.5.6 Uncertainty of results

A one-at-a-time sensitivity analysis indicates that model results are most sensitive to the priestly-Taylor α coefficient for calculating ET, followed by the hydraulic conductivity of the fractured bedrock layer, the interflow coefficient and the glacier melt factors (see Supplementary Materials, Table 3.4). The uncertainty associated with the climate projections is larger than the uncertainty associated with any individual hydrological input parameters, consistent with other studies (Teng *et al*., 2012) and the difference between GCMs is greater than the difference between RCPs 4.5 and 8.5. However, since our analysis is limited to the 3 GCMs in the regionally focused ETA model, we cannot comprehensively quantify the associated uncertainty.

3.6 Conclusions

Though historically considered a minor component of mountain streamflow (Liu *et al.,* 2004), our results demonstrate the current and future importance of groundwater in the mountain system. We use a distributed, deterministic approach to show that groundwater is the dominant source of streamflow throughout the dry season in the Shullcas watershed, a typical proglacial Andean watershed. Furthermore, though glacier melt contributes approximately 8% of streamflow, glacier melt contributes little (<2%) to groundwater recharge, making watershed groundwater storage resilient to decreases in glacier melt. By applying an ensemble of climate models, we project the complete disappearance of the Huaytapallana glaciers by 2085. In the near term, consistent groundwater discharge mediates the loss of glacier melt. But, in the long term, increasing ET and decreasing precipitation decrease groundwater recharge, particularly for the high carbon emission scenarios. These hydrologic projections results in decreases in dry season streamflow of 27% (RCP 4.5) to 32% (RCP 8.5) over the 21st century. Figure 3.4 is a conceptual representation of projected hydrologic changes in a proglacial Andean watershed under climate change.

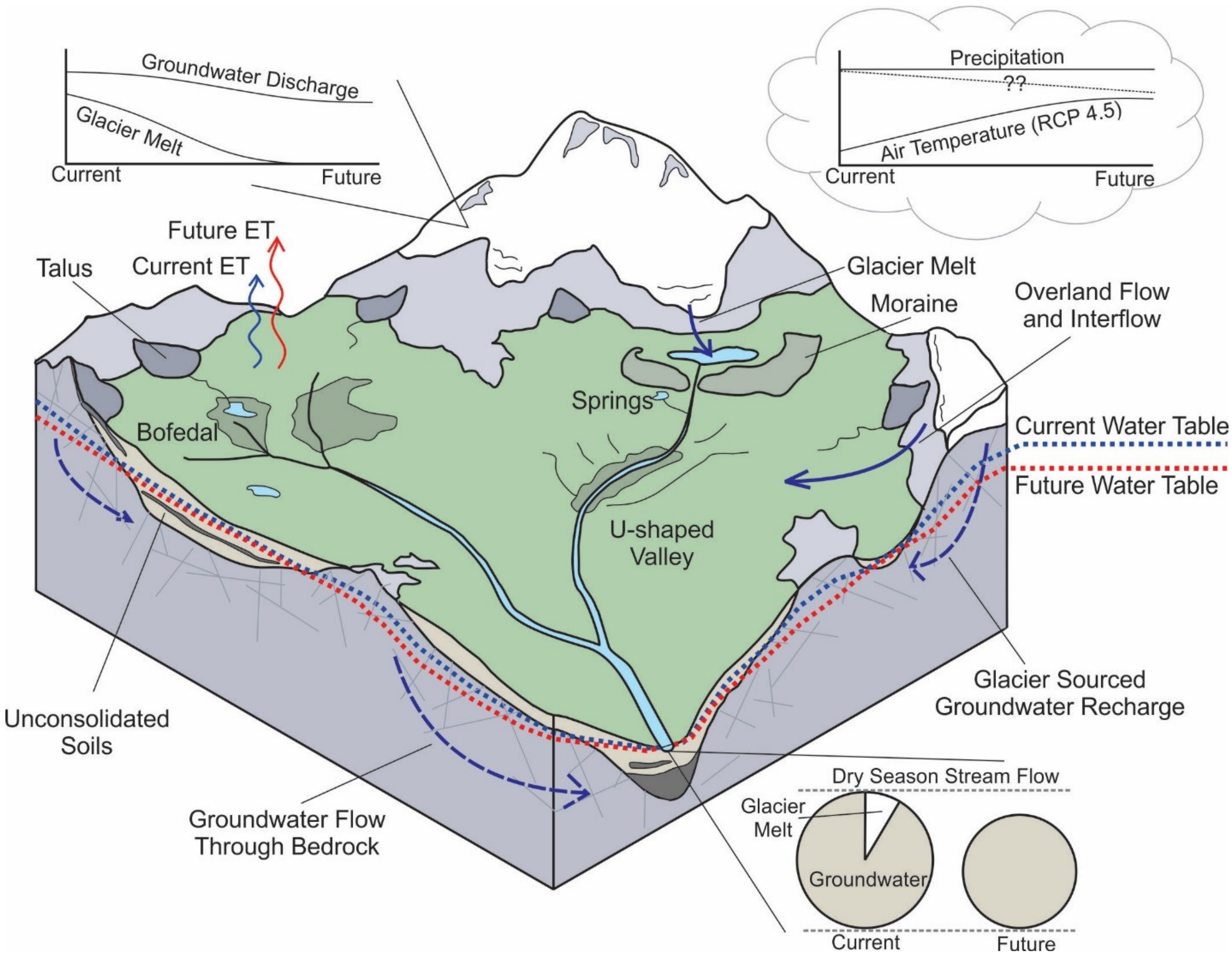

Figure 3.4: *Conceptual model of an Andean proglacial watershed showing hydrologic pathways and future changes in hydrologic variables including groundwater storage (i.e. lower water table), glacier melt, dry season streamflow.*

Recent global-scale glaciological studies (e.g. Huss and Hock, 2018) provide critical information about future glacier change and the timing of glacier peak water. However, our findings contribute important context to these glacier projections and show that water resource response to climate change in proglacial mountains is shaped, not only by glacier change but by surface and groundwater hydrological processes.

3.7 Acknowledgements

The authors would like to thank SENAMHI and IGP for the collection of meteorological data. The National Science Foundation and United States Agency for International Development provided finding as part of the NSF-USAID PEER Program (Project 3-127), NSF EAR-1316432, as well as the Natural Science and Engineering Research Council of Canada. We would also like to thank Richard Niswonger for technical advice in implementing GSFLOW and acknowledge the help of our field assistants: Américo and Alvaro González Caldua, Oliver Wigmore, Pierrick Lamontagne-Hallé, Nadine Shatilla and Emilio Mateo.

3.8 Supplementary Material

3.8.1 Glacier melt module

The glacier melt module employs a modified temperature-index approach which calculates melt, m, for each band, *b*, as:

$$m_b = \begin{cases} MF_s(T - T_{crit}), & T > T_{crit} \\ 0, & T \leq T_{crit} \end{cases} \tag{3.1}$$

(e.g. Where MF_s is the melt factor of a given season, *s* (dry or rainy), *T* is the average daily temperature and T_{crit} is the minimum temperature where melt is possible (0 in this case), both in degrees Celsius.

At each time step, *t*, the mass balance of the glacier, *Mass*, is calculated as:

$$Mass_t = Mass_{t-1} + \rho \sum_1^b (Sn_b - m_b - Sub_b) * A_b \tag{3.2}$$

Where ρ is the density of water, 1000kg/m^3, *Sn* is the total daily snow fall in meters of water equivalent, *Sub* is the daily sublimation in meters and *A* is the area of the elevation band in square meters. Sublimation is included since it represents an important energy flux for tropical glaciers. It is calculated in the same way as glacier melt using Equation 3.2 but using sublimation factors that are one tenth of the melt factors since sublimation requires approximately ten times as much energy as melt.

Net change in glacier mass, calculated with Equation 3.2, is applied to the glacier where 20% of the mass change comes from the thickness and 80% of the change is from the glacier margin. As the glacier recedes, mass is lost from the bottom most elevation band until there is no mass remaining. For the sake of simplicity, there is no accounting for glacier flow.

Given the available data, this methodology provides a realistic though approximate estimate of glacial retreat. However, glacier retreat is likely to respond to changes in incoming solar radiation and humidity that are beyond the scope of our study.

3.8.2 Selection of GSFLOW model input parameters

Selected input variables and the range of calibration values where applicable, are included in Table 3.2 to facilitate comparison with other studies. Further details on specific input parameters are listed below.

<u>Hydraulic conductivity</u> of the upper layer is assigned using the *createSpatialHydCond* function in GRASS-GSFLOW which distributes hydraulic conductivities according to the distance from the stream network (Ng. *et al*., 2018). This assumes higher hydraulic conductivities closer to the stream network where subsurface materials are coarser and fluvial in origin, and lower further

from the stream at higher elevations where bedrock is closer to the surface. To simplify model calibration, hydraulic conductivity of the bedrock layer is constant across geologic facies.

Shallow boreholes in two flat wetland areas in Chuspicocha and Huacracocha valleys (Figure 3.1a) showed a mixture of silty clay with sand and gravel seams. Road cuts approximately 10 m deep showed poorly sorted glacial soils ranging from boulders to silt. See Sadler *et al*., (in review) for complete description of soil profiles. These field observations provided a starting point for estimation of hydraulic conductivities from literature values (Heath, 1983).

Subsurface layer thickness for the unconsolidated upper layer is 20m based on road cut observations that expose over 10 m of poorly sorted soils. The fractured bedrock layer extends 180 m below the unconsolidated layer under the assumption that bedrock can be considered impermeable below that depth. Though this approach allows for a parsimonious model structure, it is limited in that it does not allow for deep groundwater circulation (Frisbee *et al*., 2017). Future work should seek to elucidate model sensitivity to the inclusion of this process.

The Priestley-Taylor α coefficient is used to calculate PET. A value of 1.26 is often considered a default for mid-latitudes. However, a value of 1 or lower is used in the literature to represent alpine grasslands and arctic tundra due to moisture limitations (Saunders et al., 1997; Eaton et al., 2001; Hood and Hayashi, 2015) and values as low as 0.35 have been reported for bare soil (Khaldi and Hamimed, 2014). For HRUs which represent a mixture of glacier and rock, a value of 0.1 is used to represent the limited evaporation from rock surfaces in these areas since sublimation is calculated in the glacier module.

Table 3.2: Model Setup and selected Input parameters for GSFLOW

	Input Parameter	GSFLOW variable name	Value (Calibration Range if applicable)	Notes, Source and References
MODFLOW Subsurface Zone				
	Number of layers	NLAY	2 (1-2)	Upper layer represents unconsolidated material. Lower layer represents fractured bedrock.
	Subsurface Layer Thickness (m, Top, bottom)	DZ	20, 180	Estimation of unconsolidated layer thickness supported by road cut observations
	Number of rows	NROW	90	
	Number of columns	NCOL	63	
	Width, Length of MODFLOW cells (m)	DELR, DELC	242.3 m, 245.8 m	
Upper Layer	Horizontal Hydraulic Conductivity (m/d)	HK	0.05-0.2 (0.005-0.5)	Unconsolidated glacial and fluvial sediments. Higher hydraulic conductivities closer to stream network representing deeper soil development.
Upper Layer	Vertical hydraulic conductivity (m/d)	VKS	0.025-0.1 (0.0025-0.25)	Anisotropy = 2
Upper Layer	Specific Yield	Sy	0.35 (0.2-0.35)	
Upper Layer	Specific Storage	Ss	2 e-6	*
Lower Layer	Horizontal Hydraulic Conductivity (m/d)	HK	0.01 (0.01-0.2)	Fractured metamorphic bedrock
Lower Layer	Vertical hydraulic conductivity (m/d)	VKS	=HK	Anisotropy = 1
Lower Layer	Specific Yield	Sy	0.15 (0.15-0.35)	
Lower Layer	Specific Storage	Ss	2 e-6	*
	Spin-up recharge (m/d)	FINF	0.0007 (0.00025-0.0007)	Approximately equal to average daily precipitation * 0.25
	Brooks-Corey Epsilon	EPS	3.5	*
MODFLOW Streamflow Routing				
	Manning's n	ROUGHCH	0.035	For combination gravel, cobbles and boulder bed river
	Overbank Manning's n	ROUGHBK	0.060	For grassland
	Channel Width (m)	WIDTH	3	Average field Measurement
	Number of stream Segments	NSEG	59	
PRMS Soil Zone				
	Number of HRUs	nhru	45	Generated using GRASS-GSFLOW (Ng *et al*., 2018)

Priestly-Taylor α Glacier and Rock Moraine Humid grassland Grassy hillslope	pt_alpha	 0.1 0.5 0.8 0.9	A PT-α value of 1.26 is often considered a default for mid-latitudes. However a value of 1 or lower is used in the literature to represent the alpine grasslands and arctic tundra due to moisture limitations (Saunders et al., 1997; Eaton *et al*., 2001; Hood and Hayashi, 2015) and values as low as 0.35 have been reported for bare soil (Khaldi and Hamimed, 2014).
Vegetation threshold (m asl)		4700	Approximate elevation above which there is no vegetation
Soil Type for ET calculation	soil_type	Loam (2), sand (1)	Field observation from boreholes, shallow excavations and road cuts
Land cover type	Cov_type	Grasses (1), Shrubs (2)	Field observation and remote sensing by Sadler *et al*., (in review)
vegetation cover density (summer, winter)	covden_sum, covden_wi	0.8 (0.6-0.8)	Field observation*
Rain interception capacity (inches, summer, winter)	Srain_intcp, Wrain_intcp	0.05	*
Maximum capillary storage (in)	soil_moist_max & soil_rechr_max	1-1.5 (1-12)	*
Linear coefficient to compute transfer from PRMS to MODFLOW	Ssr2gw_rate	0.05 (rock and glacier) – 0.15 (other) (0.04-4)	*
Exponent to compute transfer from PRMS to MODFLOW	Ssr2gw_exp	0.75	*
Decimal fraction of soil zone available for preferential flow	pref_flow_den	0.05 (0.05 - 0.3)	*
Soil zone saturation threshold (in)	sat_threshold	3-4 (3-20)	*
Linear coefficient for slow interflow (per day)	slowcoef_lin	0.015 (0.001-0.02)	*
Non-linear coefficient for slow interflow (per inch day)	slowcoef_sq	0.05 (0.001-0.1)	*
Linear coefficient for fast interflow (per day)	fastcoef_lin	0.1 (0.05-0.4)	*
Non-linear coefficient for fast interflow (per inch day)	fastcoef_sq	0.1-0.15 (0.01-0.6)	*

* Values from Sagehen example in Markstrom *et al*. (2008) were used or used as a starting point for parameter calibration

3.8.3 Coupled model calibration

The climatic setting of the Shullcas watershed lends itself well to the calibration of a joint surface water and groundwater model. Since very little precipitation falls during the dry season, the baseflow recession pattern and dry season streamflow serves as an excellent calibration target for the groundwater flow parameters. Meanwhile, the rainy season hydrograph serves as a good calibration target for the interflow parameters.

In order to calibrate the joint glacier-surface-groundwater model, we calculate an aggregate performance metric which includes our six, three-year, daily streamflow records and the 11 year monthly streamflow record (Figure 3.5). The root mean square error (RMSE) is calculated for each available record and the aggregate error is calculated as follows:

$$E_{Agg} = \frac{E_{1985-2009} + E_1 + E_2 + \cdots + E_6}{7} \tag{3.3}$$

Where E_{Agg} is the aggregate error, $E_{1985\text{-}2009}$ is the RMSE of the monthly discharge record from ANA, and $E_{1\text{-}6}$ are the calculated RMSR for each of the six daily discharge stations between 2015 and 2018. This scheme weights errors proportionally to the discharge such that, downstream gauges are more heavily weighted than headwater gauges.

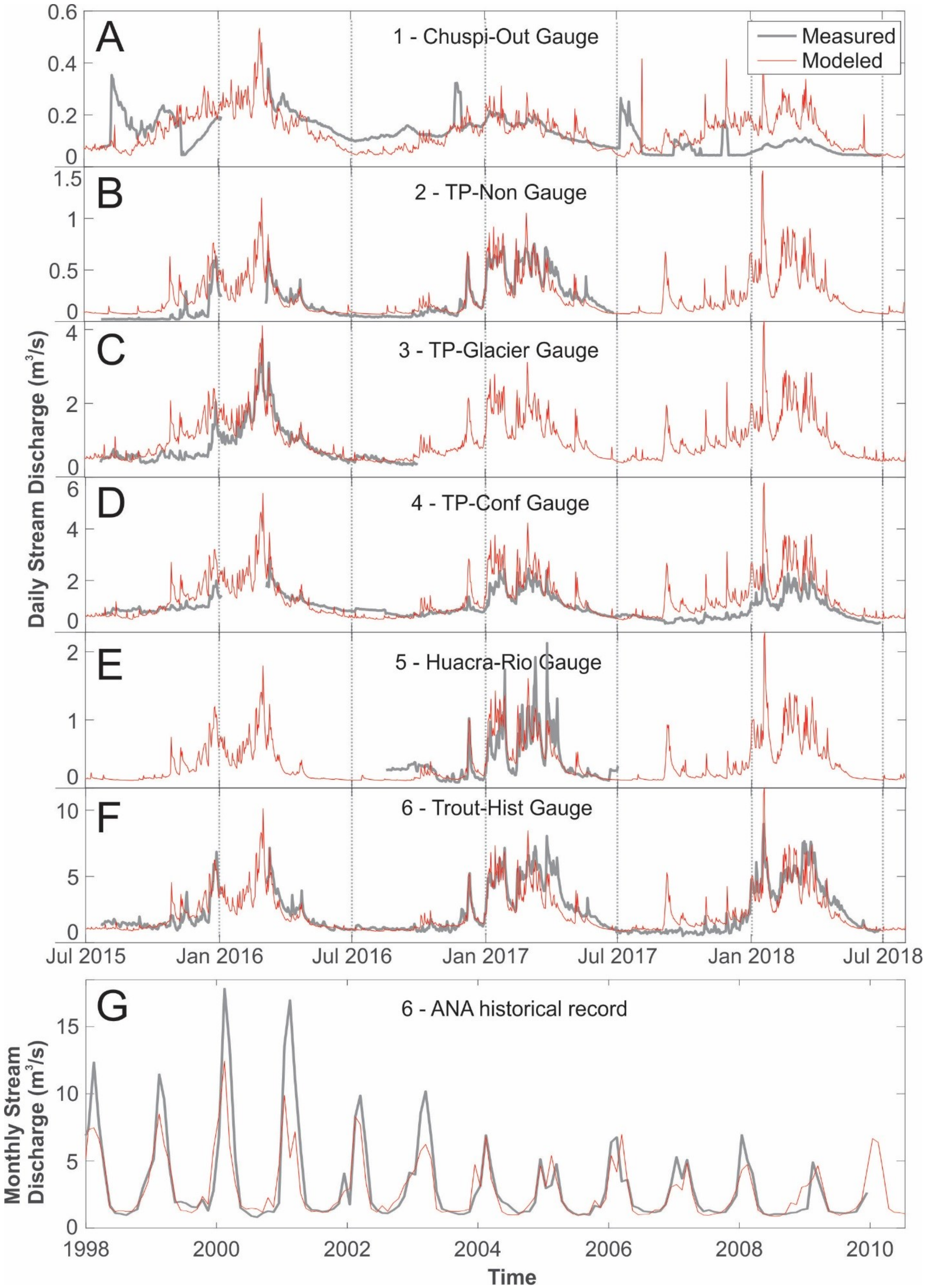
A
1 - Chuspi-Out Gauge
Measured
Modeled
B
2 - TP-Non Gauge
C
3 - TP-Glacier Gauge
D
4 - TP-Conf Gauge
E
5 - Huacra-Rio Gauge
F
6 - Trout-Hist Gauge
Daily Stream Discharge (m³/s)
Jul 2015
Jan 2016
Jul 2016
Jan 2017
Jul 2017
Jan 2018
Jul 2018
G
6 - ANA historical record
Monthly Stream Discharge (m³/s)
1998
2000
2002
2004
2006
2008
2010
Time

Figure 3.5: *Comparison of modeled and measured streamflow for six short-term daily stream records (panels A-F) and ANA long term stream gauge record (G). Note the impact of the operation of a small dam at gauge 1 in sudden changes in discharge.*

We use the Nash-Sutcliffe Efficiency ($E_{N\text{-}S}$) to express model fit where:

$$E_{N-S} = \frac{\sum_{i=1}^{n}\left(Q_i^{obs} - Q_i^{sim}\right)^2}{\sum_{i=1}^{n}\left(Q_i^{obs} - \overline{Q_{obs}}\right)^2} \tag{3.4}$$

Q^{obs} and Q^{sim} are observed and simulated stream discharge respectively at any time step, *i*. $E_{N\text{-}S}$ for all streamflow records are listed in Table 3.3.

Table 3.3: *Model Goodness of Fit*

Map Location	Gauge Name	Time Period	Nash-Sutcliffe Efficiency ($E_{N\text{-}S}$)
1	Chuspi_Out	2015-2018	-0.4688
2	TP_Non	2015-2017	0.5522
3	TP_Galcier	2015-2016	0.7082
4	TP_Conf	2015-2018	0.3648
5	Huacra_Rio	2016-2017	0.5517
6	Trout_Hist	2015-2018	0.7397
6	ANA_Hist	1998-2009	0.7040

Simulated discharge at gauge 1 performs poorly compared to measured discharge in part because a small security dam at the Chuspicocha glacier lake outflow is occasionally operated as a water supply reservoir during the measured time period. To mitigate this challenge, we initially installed a gauge in the Chuspicocha proglacial like. By comparing lake level and outflow we are able to calculate the inflow to the lake, neglecting evaporation. However, the lake level had a greater range than expected meaning that for certain periods, the sensor was out of the water, while at other times the lake level was too high for the gauge to be downloaded, leading to data gaps,. Figure 3.6 compares the lake inflow and outflow, and demonstrates that they follow similar trends since the dam is usually opened in response to high water levels. Given that the time series for the outflow is more complete than the inflow, we elected to use it for calibrating the glacier melt factors but this does decrease model efficiency.

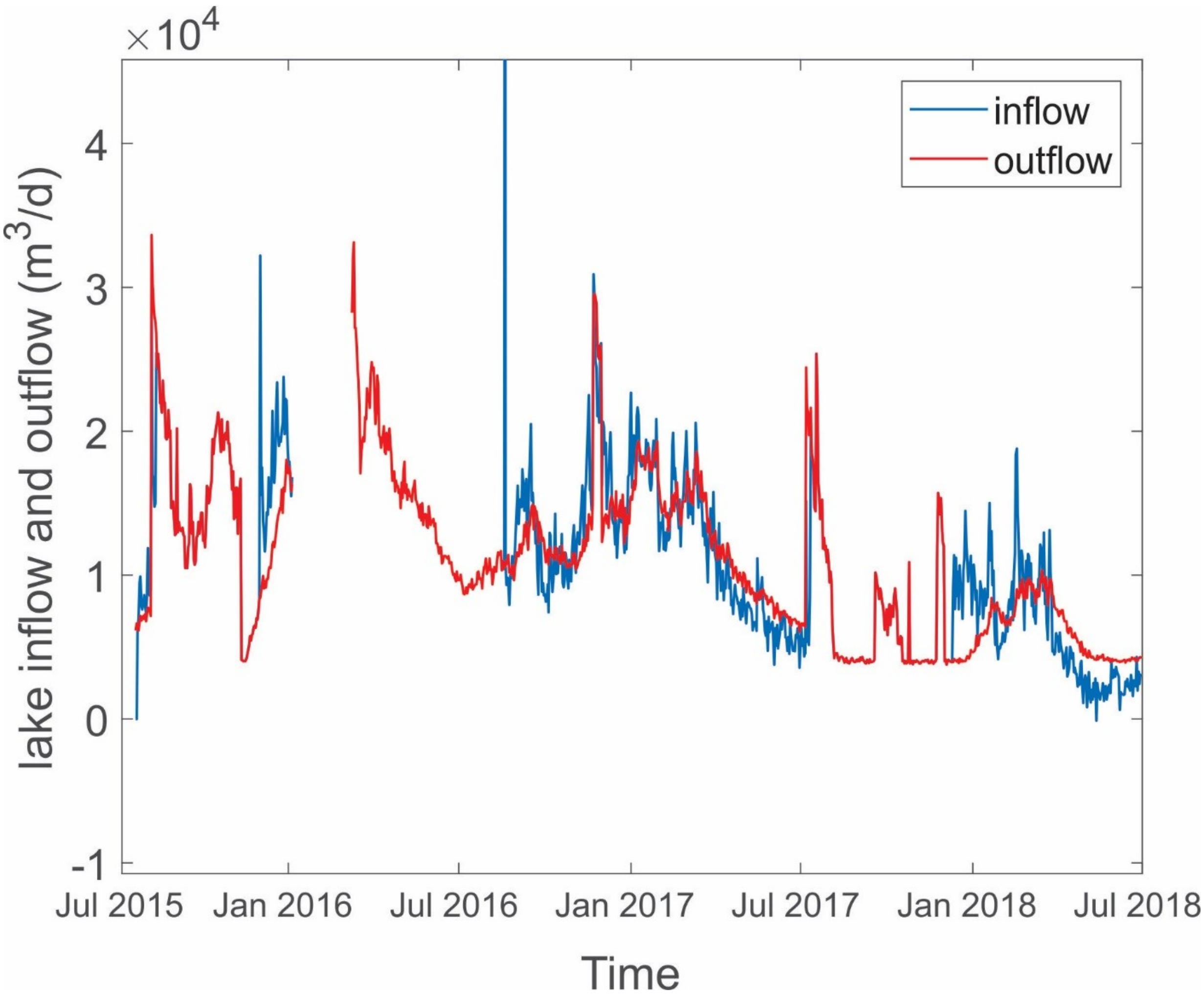

Figure 3.6: *Comparison of measured outflow from Chuspicocha proglacial Lake and inflow calculated from lake level and area.*

3.8.4 Sensitivity analysis

Our research utilizes projections of future hydrological conditions that depend upon our chosen parameters which each have some uncertainty. Integrated modelling inevitably introduces additional variables and therefore increases the sources of uncertainty in numerical modelling. Therefore, we perform sensitivity analysis to gauge the sensitivity of our modeled streamflow to four key groups of parameters that we identified during calibration as relatively uncertain given our inability to measure them across the modeled domain (Forster & Smith, 1988): (1) vertical and horizontal hydraulic conductivity of bedrock, (2) Priestly-Taylor α coefficients which are used to calculate PET, (3) interflow coefficients, and (4) glacier melt factors.

Given already long model run times, a Monte-Carlo style sensitivity analysis (e.g. Wilby, 2005) is not possible. Instead, we select an offset of the final calibrated values that represents a broad range of possible values based on a literature search. The joint model is run using one perturbed parameter at a time (Figure 3.7) and the RMSE to the base case streamflow from 2015 to 2018 is calculated and ranked in Table 3.4.

Table 3.4: *Sensitivity ranking for selected Input variables for GSFLOW*

Sensitivity Ranking	Parameter	Calibrated value	Perturbation	RMSE	
				+	-
1	PT α (unitless)	0.85	± 0.25	0.6358	0.4036
2	Hydraulic Conductivity (m/d)	0.01	*/ 5	0.1523	0.1502
3	Fast Interflow coefficients (per day)	0.1	*/ 4	0.1043	0.0897
4	Glacier melt factors (unitless)	Dry season: 2.8 Rainy season: 3.0	± 1.5	0.0491	0.0589

*/ signifies multiplied by and divided by

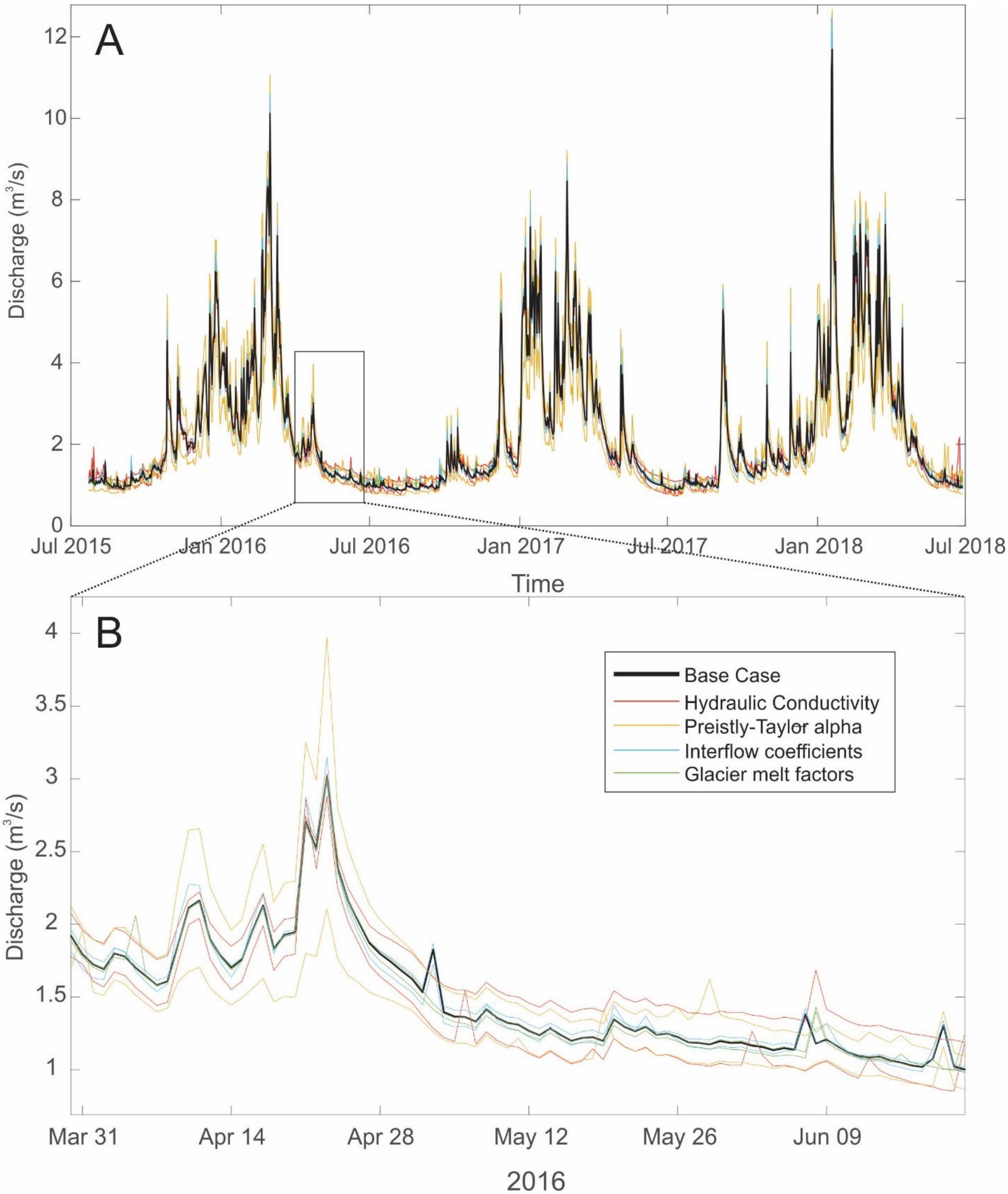

Figure 3.7: *Sensitivity of streamflow to selected input variables. (A) Streamflow at gauge 7 from 2015 to 2018. (B) Close up section of streamflow using different input variables which are perturbed by the amounts indicated in Table 3.4.*

We can produce a conservative estimate of uncertainty in modeled streamflow based on several assumptions: (1) the range of possible inputs is normally distributed and result in normally distributed outputs. (2) Our selected perturbed values are 3 standard deviations from the mean or "true" value and therefore represent 99.7% of possible values, and (3) the sum of the resulting uncertainties represents all combinations of inputs. This is a very conservative estimate of total uncertainty since many combinations of different inputs will act in opposite directions, or will otherwise interact, and would almost certainly be less than the sum.

Using those assumptions, the total RMSE (averaged for the positive and negative perturbations) is 0.82 m^3/s at Gauge 7 or 0.5351 m^3/s at a 95% confidence. Given an average daily streamflow over this period of 2.30 m^3/s, the streamflow uncertainty is ± 23% ($p=0.05$). This is notably less than the difference in projected streamflow between RCP 4.5 and 8.5 (~30%) implying that the uncertainty in climate projections is larger than that of the hydrological inputs.

3.8.5 Spatial patterns in groundwater projections

As mentioned in the main text, there are slight variabtions in the spatial patterns in groundwater table change for the different GCMs. Table 3.5 describes the different spatial patters. Figure 1c shows the spatial pattern for the MIROC 4.5 climate model.

Table 3.5: *Groundwater projections:*

GCM	Change in water table head between 2000-2009 and 2090-2099	Spatial Patterns
MIROC5 4.5	-14.14	Largest water table declines beneath topographically steep areas and glacier
MIROC5 8.5	-16.97	“
CanESM2 4.5	-3.33	Largest water table declines in steep areas. Magnitude of decrease is less than MIROC5, particularly in high flat planes near streams.
CanESM 8.5	-9.74	“
BESM	-5.27	Largest water table declines beneath high glaciated peaks and near the watershed outlet. Some decline in topographically steep areas.

3.9 References

Andermann, C., Longuevergne,L., Bonnet, S., Crave, A., Davy, P. & Gloaguen, R. (2012). Impact of transient groundwater storage on the discharge of Himalayan rivers. *Nature Geoscience,* Vol 5, 2012. DOI: 10.1038/NGEO1356.

Aubry-Wake, C., Baraer, M., McKenzie, J.M., Mark, B.G., Wigmore, O., Hellström, R. A. & Lautz, L. (2015). Measuring glaciersurface temperatures with ground-basedthermal infrared imaging. *Geophys. Res.Lett*., 42, 8489–8497, doi:10.1002/2015GL065321.

Authoridad Nacional del Agua (2014). *Inventario de glaciares del Peru*. Ministerio de agricultura y riego, Huaraz, Peru.

Baraer, M., Mark, B.G., McKenzie, J.M., Comdom, T., Bury, J., Huh, K., Portocarrero, C., Gomez, J. & Rathay, S. (2012). Glacier recession and water resources in Peru's Cordillera Blanca. *Journal of Glaciology,* 58(207): 134-149.

Baraer, M., McKenzie, J., Mark, B.G., Gordon, R., Bury, J., Condom, T., Gomez, J., Knox, S. & Fortner, S.K. (2015). Contribution of groundwater to the outflow from ungauged glazierized catchments: a multi-site study in the tropical Cordillera Blanca, Peru. *Hydrol. Proc*. 29 (11), 2561–2581.

Barnett, T.P., Adam, J.C., & Lettenmaier, D.P. (2005). Potential impacts of a warming climate on water availability in snow-dominated regions. *Nature*, 438, 7066: 303–309, doi: 10.1038/nature04141.

Bordoy, R., & P. Burlando (2013). Bias Correction of Regional Climate Model Simulations in a Region of Complex Orography. *Journal of Applied Meteorology and Climatology*, doi: 10.1175/JAMC-D-11-0149.1.

Bradley R S, Vuille M, Diaz, H. F. & Vergara W. (2006). Threats to water supplies in the tropical andes. *Science* 312, 1755–6

Braun, L.N., Grabs, W. & Rana, B. (1993). Application of a conceptual precipitation-runoff model in the Langtang Khola basin, Nepal Himalaya. In: Young, G.J., (Ed.), *Snow and Glacier Hydrology, Proceedings of the Kathmandu Symposium 1992: IAHS* Publ. no. 218, pp. 221–237

Cochand, F., Therrien, R. & Lemieux, J-M (2018). Integrated Hydrological Modelling of Climate Impacts in a Snow-Influenced Catchment. Groundwater, Vol.57 (1): 3-20. Doi:10.1111/gwat.12848

Chew, D.M., Pedemonte G., Corbett, E. (2016). Proto-Andea evolution of the Eastern Cordillera of Peru. *Gondwana Research* 35(2016) 59-78. DOI:10.1016/j.gr.2016.03.016

Chou, S.C, Lyra, A. , Mourão, C. , Dereczynski, C. , Pilotto, I. , Gomes, J. , Bustamante, J. , Tavares, P. , Silva, A. , Rodrigues, D. , Campos, D. , Chagas, D. , Sueiro, G. , Siqueira, G. , Nobre, P. & Marengo, J. (2014a) Evaluation of the Eta Simulations Nested in Three Global Climate Models. *American Journal of Climate Change*, 3, 438-454. doi:10.4236/ajcc.2014.35039.

Chou, S.C, Lyra, A. , Mourão, C. , Dereczynski, C. , Pilotto, I. , Gomes, J. , Bustamante, J. , Tavares, P. , Silva, A. , Rodrigues, D. , Campos, D. , Chagas, D. , Sueiro, G. , Siqueira, G.

& Marengo, J. (2014b) Assessment of Climate Change over South America under RCP 4.5 and 8.5 Downscaling Scenarios. *American Journal of Climate Change*, 3, 512-527. doi: 10.4236/ajcc.2014.35043.

Crumley, R. (2015). Investigating glacier melt contribution to stream discharge and experiences of climate change in the Shullcas River Watershed in Peru. Masters Thesis, The Ohio State University, Columbus, USA.

Cuthbert, M.O., Gleeson, T., Moosdorf, N., Befus, K.M., Schneider, A., Hartmann, J. & Lehner, B. (2019). Global patterns and dynamics of climate-groundwater interactions, *Nature Climate Change*, Volume 9(2019): 137-141. Doi: 10.1038/s41558-018-0386-4.

Fernàndez, A. & Mark, B.G. (2016). Modeling modern glacier response to climate changes along the Andes Cordillera: A multi-scale review, *J. Adv. Model. Earth Syst.*, 8, 467-495, 2016.

Forster, C. & Smith, L. (1988). Groundwater Flow Systems in Mountainous Terrain 2. Controlling Factors. *Water Resources Research*, 24(7): 1011-1023.

Frisbee M.B., Phillips, F.M., Campbell, A.R., Liu, F. & Sanchez, S.A. (2011). Streamflow generation in a large, alpine watershed in the southern Rocky Mountains of Colorado: Is streamflow generation simply the aggregation of hillslope runoff responses? *Water Resour. Res.* 47(6) W06512. doi :10.1029/2010WR009391

Frisbee, M. D., Tolley, D.G. & Wilson, J.L (2017). Field estimates of groundwater circulation depths in two mountainous watersheds in the western U.S. and the effect of deep circulation on solute concentrations in streamflow. *Water Resour. Res.*, 53,2693–2715, doi:10.1002/2016WR019553.

Glas, R., Lautz, L., McKenzie, J., Mark, B., Baraer, M., Chavez, D. & Maharaj, L. (2018). A review of the current state of knowledge of proglacial hydrogeology in the Cordillera Blanca, Peru, *WIREs Water* 5:c1299. doi: 10.1002/wat2.1299

Gleick, P. H. & Palaniappan, M. (2010). Peak water limits to freshwater withdrawal and use. *Proc. Natl Acad. Sci*. USA 107, 11155–11162.

Grillakis, M. G., A. G. Koutroulis, & I. K. Tsanis (2013). Multisegment statistical bias correction of daily GCM precipitation output. *Journal of Geophysical Research*: atmospheres, 118, 3150-3162, doi:10.1002/jgrd.50323.

Hawkins, E., T. M. Osborne, C. K. Ho, & A. J. Challinor (2012), Calibration and bias correction of climate projections for crop modelling: An idealised case study over Europe. *Agricultural and Forest Meteorology*, 170, Pages 19-31, doi:10.1016/j.agrformet.2012.04.007.

Hock, R. (2003). Temperature index melt modelling in mountain areas. *Journal of Hydrology* 282 2003) 104-115. DOI:10.1016/S0022-1694(03)00257-9

Hood J. & Hayashi, M. (2015). Characterization of snowmelt flux and groundwater storage in an alpine headwater basin. *Journal of Hydrology* 521 (2015) 482-497. DOI: 10.1016/j.jhydrol.2014.12.041.

Huffman G.J., Bolvin D.T. (2013). TRMM and other data precipitation data set documentation. Greenbelt USA, National Aeronautics and Space Administration (NASA).

Huss, M. & Hock R. (2018). Global-scale hydrological response to future glacier mass loss. *Nature Climate Change.* 8, 135-140. DOI:10.1038/s41558-017-0049-x

Ines, A. V. M., & J. W. Hansen (2006), Bias correction of daily GCM rainfall for crop simulation studies. , 138, 1-4, 44-53.

Instituto Nacional de Estadisticas y Informaticas – Perú, (2012). *Estiamciones y Proyecciones de Población por sexo, según Departamento, Provincia y Distrito, 2000 – 2015*, Lima, Peru.

Juen, I., Kaser, G., Georges, C. (2007), Modelling observed and future runoff from a glacierized tropical catchment (Cordillera Blanca, Peru). *Global and Planetary Cange.* 59(2007): 37-48. Doi:10.1016/j.gloplacha.2006.11.038

Liu, F., Williams, M.W., Caine, N. (2004). Source waters and flow paths in an alpine catchment, Colorado Front Range, United States. *Water Resources Research* 40. DOI: 10.1029/2004WR003076.

López-Moreno, J.I., Fontaneda, S., Bazo, J., Revuelto, J., Azorin-Molina, C., Valero-Garcés, B., Morán-Tejeda, E., Vicente-Serrano, S.M., Zubieta, R., & Alejo-Cochachín, J. (2014). Recent glacier retreat and climate trends in Cordillera Huaytapallana, Peru. *Global and Planetary Change* 112(1-11).

Mark, B.G., French, A., Baraer, M., Carey, M., Bury, J., Young, K.R., Polk, M.H., Wigmore, O., Lagos, P., Crumley, R., McKenzie, J.M. & Lautz, L (2017). Glacier loss and hydro-social risks in the Peruvian Andes, *Global and Planetary Change,* vol. 159, pp. 61-76.

Markstrom, S.L., Niswonger, R.G., Regan, R.S., Prudic, D.E. & Barlow, P.M. (2008). GSFLOW-

Coupled Ground-Water and Surface-Water Flow Model Based on the Integration of the Precipitation-Runoff Modeling System (PRMS) and the Modular Ground-Water Flow Model (MODFLOW-2005). *U.S. Geological Survey Techniques and Methods 6-D1*, p.240.

McClymont, A. F., Hayashi, M., Bentley, L. R., Muir, D., & Ernst, E. (2010). Groundwater flow and storage within an alpine meadow-talus complex. *Hydrology and Earth System Sciences, 14*(6), 859-872. doi:10.5194/hess-14-859-2010

Moriasi, D.N., Arnold, J.G., Van Liew, M.W., Bingner, R.L., Harmel, R.D. & Veith, T.L. (2007). Model evaluation guidelines for systematic quantification of accuracy in watershed simulations. *American Society of Agricultural and Biological Engineers* 50, no.3: 885-900.

Mountain Research Initiative EDW Working Group (2015). Elevation-dependent warming in mountain regions of the world, *Nature Climate Change*, 5, 424-430. DOI: 10.1038/NGEO1356

Ng, G.-H. C., Wickert, A. D., Somers, L. D., Saberi, L., Cronkite-Ratcliff, C., Niswonger, R. G., & McKenzie, J. M. (2018). GSFLOW-GRASS v1.0.0: GIS-enabled hydrologic modeling of coupled groundwater–surface-water systems, *Geoscience Model Development*, 11, 4755-4777. DOI:10.5194/gmd-11-4755-2018.

Paul, F., Kääb, A., Maisch, M., Kellenberger, T. & Haeberli, W. (2004). Rapid disintegration of Alpine glaciers observed with satellite data, *Geophysical Research Letters,* vol. 31, no. 21, pp. L21402 1-4.

Pritchard, H. D. (2017). Asia's glaciers are a regionally important buffer against drought. *Nature, 545*(7653), 169-174. doi:10.1038/nature22062

Quick, M.C. & Pipes, A., (1977). UBC watershed model. *Hydrological Sciences Bulletin,* 221, 153–161

Rabatel, A., Francou, B., Soruco, A., Gomez, J., Cáceres, B., Ceballos, J.L., Basantes, R., Vuille, M., Sicart, J.-., Huggel, C., Scheel, M., Lejeune, Y., Arnaud, Y., Collet, M., Condom, T., Consoli, G., Favier, V., Jomelli, V., Galarraga, R., Ginot, P., Maisincho, L., Mendoza, J., Ménégoz, M., Ramirez, E., Ribstein, P., Suarez, W., Villacis, M. & Wagnon, P. (2013). Current state of glaciers in the tropical Andes: A multi-century perspective on glacier evolution and climate change. *Cryosphere,* vol. 7, no. 1, pp. 81-102.

Ragettli, S., Cortés, G., McPhee, J., & Pellicciotti, F. (2014). An evaluation of approaches for modelling hydrological processes in high-elevation, glacierized Andean watersheds. *Hydrological Processes*. 28(2014): 5674-5695. doi: 10.1002/hyp.10055

Saberi, L., McLaughlin, R., Ng., G.-H. C., La Frenierre, J., Wickert, A., Baraer, M., Zhi, W., Li, L. & Mark, B.G. (2019). Multi-scale temporal variability in meltwater contributions in a tropical glacierized watershed. *Hydrol. Earth Syst. Sci*., 23, 405-425. DOI: 10.5194/hess-23-405-2019.

Sadler, M., L.D. Somers, J.M. McKenzie, B. Mark, P. Lagos, M. Baraer (in review). The distribution and hydrological function of land cover types within a proglacial Andean watershed. Submitted to *Hydrological Processes* Jan 31, 2019. Submission HYP-19-0083

Seth, A., Thibeault, J., Garcia, M., & Valdivia, C. (2010). Making sense of twenty-first-century climate change in the Altiplano: Observed trends in CMIP3 projections. *Ann. Assoc. Am. Geogr.* 100 (4), 835 – 847.

Smitha, P. S., Narasimhan, B., Sudheer, K.P. & Annmalai, H. (2018). An improved bias correction method of daily rainfall data using a sliding window technique for climate change impact assessment. *Journal of Hydrology*, 556, 100-118, doi: 10.1016/j.jhydrol.2017.11.010.

Tachikawa, T., Kaku, M., Iwasaki, A., Gesch, D., Oimoen, M., Zhang, Z. & Meyer, D. (2011). *ASTER Global Digital Elevation Model version 2—Summary of validation results*. NASA Land Processes Distributed Active Archive Center and the Joint Japan-US ASTER Science Team. Retrieved from: https://lpdaacaster.cr.usgs.gov/GDEM/Summary_GDEM2_validation_report_final.pdf

Tague, C., Grant, C., Farrell, M., Choate, J. & Jefferson, A. (2008). Deep groundwater mediates streamflow response to climate warming in the Oregon Cascades. *Clim. Change* 86, 189-210.

Teng, J., Vaze, J., Chiew, F.H., Wang, B. & Perraud, J. (2012). Estimating the Relative Uncertainties Sourced from GCMs and Hydrological Models in Modeling Climate Change Impact on Runoff. J. Hydrometeor., 13, 122–139, https://doi.org/10.1175/JHM-D-11-058.1 United Nations Development Report (UNDP) (2006). *Human Development Report, beyond scarcity: Power, poverty and the global water crisis*. New York, NY, USA. ISBN: 0-230-50058-7.

Urrutia, R. & Vuille, M. (2009). Climate Change projections for the tropical Andes using a regional climate model: Temperature and precipitation simulations for the end of the 21st century. *Journal of Geophysical Research –Atmos*. 114, 1-15.

Viviroli, D., Durr, H.H., Messerli, B., Meybeck, M. & Weingartner, R. (2007). Mountains of the world, water towers for humanity: Typology, mapping, and global significance. *Water Resources Research.* vol. 43, W07447, doi:10.1029/2006WR005653

Voss, C.I. (2011). Editor's message: Groundwater modeling fantasies-part 1, adrift in the details. *Hydrogeol J.,* 19: 1281. https://doi.org/10.1007/s10040-011-0789-z

Vuille, M., Carey, M., Huggel, C., Buytaert, W., Rabatel, A., Jacobsen, D., Soruco, A., Villacis, M., Yarleque, C., Elison Timm, O., Condom, T., Salzmann, N. & Sicart, J. (2018). Rapid decline of snow and ice in the tropical Andes – Impacts, uncertainties and challenges ahead, *Earth-Science Reviews,* vol. 176, pp. 195-213.

Weertman, J. (1961). Stability of ice-age ice sheets. *J. Geophys. Res*. 66:3783–3792, doi:10.1029/JZ066i011p03783.

Yarleque, C., Vuille, M., Hardy, D.R., Timm, O.E., De la Cruz, J., Ramos, H., & Rabatel, A. (2018). Projections of the future disappearance of the Quelccaya Ice Cap in the Central Andes, *Scientific Reports* 8:15564, DOI:10.1038/s41598-018-33698-z.

Zheng, C., & Bennett, G.D. (2002). *Applied Contaminant Transport Modeling, 2 nd ed.* John Wiley and Sons Inc., New York, NY. 343-347.

Eaton, A., Rouse, W.R., Lafleur, P.M., Marsh, P. & Blanken, P.D. (2001). Surface energy balance of the western and central Canadian subarctic: variations in the energy balance among five major terrain types. *J. Clim*. 14, 3692-3703.

Heath, R.C. (1983). Basic ground-water hydrology, U.S. Geological Survey Water-Supply Paper 2220, 86p.

Saunders, I.R., Bailey, W.G. & Bowers, J.D. (1997). Evaporation regimes and evaporation modelling in an alpine tundra environment. *J. Hydrol*.195, 99-113.

Wilby, R.L. (2005). Uncertainty in water resource model parameters used for climate change impact assessment. *Hydrological Processes* 19, 3201-3219. DOI: 10.1002/hyp.5819

Chapter 4. Does hillslope trenching enhance groundwater recharge and baseflow in the Peruvian Andes?

Authors: Lauren D. Somers, Jeffrey M. McKenzie, Samuel C. Zipper, Bryan G. Mark, Pablo Lagos, Michel Baraer

4.1 Context within thesis

Hydrologic projections for the Shullcas Watershed in central Peru from Chapter 3 indicate that the glaciers at the river headwater are likely to disappear before the end of the 21st century. These results are comparable to other studies projecting glacier retreat in the tropical Andes (e.g. Yarleque *et al*., 2018) and are likely representative of the many glaciers under 5500 m above sea level in the region. Furthermore, changes in precipitation patterns and increased evapotranspiration will likely decrease groundwater recharge. Meanwhile, downstream users (e.g. the population of the city of Huancayo in this case) are searching for adaptation strategies to alleviate intensifying dry season water shortages.

In this manuscript, we assess the effectiveness of hillslope trenching, a climate change adaptation strategy that has been implemented in the Shullcas Watershed. We employ newfound understanding of groundwater flow developed in the previous manuscripts to model the effect of infiltration trenching on dry season baseflow and thus its ability to increase water supply during dry periods.

4.2 Abstract

As Andean glaciers rapidly retreat due to climate change, the balance of groundwater and glacial meltwater contributions to stream discharge in tropical, proglacial watersheds will change,

potentially increasing vulnerability of water resources. The Shullcas River Watershed, near Huancayo, Peru, is fed only partly by the rapidly receding Huaytapallana glaciers (<20% of dry season flow). To potentially increase recharge and therefore increase groundwater derived baseflow, the government and not-for-profit organizations have installed trenches along large swaths of hillslope in the Shullcas Watershed. Our study focuses on a non-glacierized sub-catchment of the Shullcas River Watershed, and has two objectives: (1) create a model of the Shullcas groundwater system and assess the controls on stream discharge; and (2) investigate the impact of the infiltration trenches on recharge and baseflow. We first collected hydrologic data from the field including a year-long hydrograph (2015-2016), meteorological data (2011-2016), and infiltration measurements. We use a recharge model to evaluate the impact of trenched hillslopes on infiltration and runoff processes. Finally, we use a three-dimensional groundwater model, calibrated to the measured dry season baseflow, to determine the impact of trenching on the catchment. Simulations show that trenched hillslopes receive approximately 3.5% more recharge, relative to precipitation, compared with unaltered hillslopes. The groundwater model indicates that because the groundwater flow system is fast and shallow, incorporating trenched hillslopes (~2% of study sub-catchment area) only slightly increases baseflow in the dry season. Furthermore, the location of trenching is an important consideration: trenching higher in the catchment (further from the river) and in flatter terrain provides more baseflow during the dry season. The results of this study may have important implications for Andean landscape management and water resources.

4.3 Introduction

Mountain regions play an important role in global water supply and are highly sensitive to climate change (Barnett *et al*., 2005; Bradley *et al*., 2006; Viviroli *et al*., 2007; Viviroli *et al*., 2011;

Rangwala and Miller, 2012). In the Peruvian Andes, communities and industries along the cordillera and on the arid coast depend on proglacial alpine watersheds for water resources. Glacial meltwater and stored groundwater supply consistent stream discharge during the dry season when precipitation is minimal (Mark *et al*, 2005; Baraer *et al.*, 2009; Baraer *et al*., 2012; Bury *et al*. 2013).

In Peru, glaciological and hydrological research in the Cordillera Blanca has explored the rapid recession of glaciers (Georges, 2004; Mark and Seltzer, 2005; Schauwecker *et al*., 2014) and their threat to water resources (Mark *et al*., 2010; Baraer *et al*., 2012), as well as the mediating influence and importance of groundwater discharge to alpine streams (Baraer *et al*., 2009; Gordon *et al*., 2015; Somers *et al*., 2016).

Similarly, the smaller and less studied Cordillera Huaytapallana in the central Peruvian Andes has undergone extensive glacial recession in recent decades (IGP, 2010; ANA, 2014; Lopez-Moreno *et al*. 2014). Meltwater from the Huaytapallana glaciers feeds the Shullcas River, which in turn provides municipal water to the city of Huancayo and irrigation water to local agricultural operations (ANA, 2010). Previous work has indicated that glacial melt accounted for less than 20% of dry season discharge in 2014 (Crumley, 2015), with the remainder coming from groundwater discharge to the Shullcas River. As the Huaytapallana glaciers continue to retreat, dry season stream discharge is expected to decrease, making groundwater discharge an increasingly significant source of water for this economically and socially important watershed.

While dams or reservoirs are effective and are typically constructed in response to this type of seasonal water shortage, they can also be costly, induce evaporation, and be ecologically harmful (Nilsson *et al*., 2005). Increasing groundwater recharge in times of excess surface water supply is one alternative method for increasing dry season water availability. Several different schemes have been proposed, and are referred to in general as artificial aquifer recharge or managed aquifer recharge (MAR). While some systems divert excess river water to injection wells (Bouwer, 2002, and references therein; Dillon, 2005), others divert excess water to infiltration fields, channels or basins (HeilWeil *et al*., 2015; Mastrocicco *et al*., 2015; Heviánková *et al*., 2016).

The Peruvian government and not-for-profit organizations have installed infiltration trenches over large swaths of hillslope in the Shullcas River watershed. Unlike most MAR schemes, the purpose of these trenches is to capture surface runoff (as opposed to diverted river water) during the rainy season and allow more time for infiltration. In theory, this passive aquifer recharge scheme could increase recharge to groundwater, thereby increasing groundwater baseflow to the river during the dry season with the additional benefit of reducing erosion (CARE Peru, 2013). However, direct measurement of recharge is challenging and very little research has been done to determine the effectiveness of this strategy.

Techniques for measuring groundwater recharge include use of lysimeters, tracers, and water table fluctuations (Scanlon, 2002). However, these techniques are not easily applied to a hillslope scale application. Furthermore, recharge can be divided into distinct processes which occur heterogeneously in time and space, and may not be adequately captured by point measurements. Meixner *et al.* (2016) suggest a four-fold classification of recharge processes: diffuse; focused; mountain system recharge; and irrigation. The addition of infiltration trenches essentially changes the proportions of diffuse and focused recharge. Since direct measurement of groundwater recharge is difficult, researchers often rely on various estimation techniques, including numerical modeling of hydrological processes at the land surface and the unsaturated zone (Scanlon, 2002).

Furthermore, it is hypothesized that a change in recharge caused by the installation of trenches should affect groundwater baseflow to the stream. However, mountain hydrogeological systems are highly heterogeneous and still relatively poorly understood (e.g. Clow *et al*., 2003; Roy and Hayashi, 2009; Harpold *et al*, 2010). Therefore the impacts on the annual stream hydrograph are unknown.

The objectives of this paper are to better understand and quantify the groundwater flow system in the Shullcas River watershed and to determine if and how infiltration trenches increase groundwater discharge during the dry season. To test the hypothesis that hillslope trenching will increase baseflow, we incorporate surface trenching into an infiltration and recharge model in order to estimate the difference in groundwater recharge between trenched and non-trenched terrain. The model is driven by high-frequency meteorological data and incorporates measurements of soil infiltration capacity and observations on vegetation and trench configuration. We then apply the resulting recharge rates to a groundwater model of a study catchment to estimate the change in quantity and timing of groundwater baseflow to the stream. Sensitivity analysis is performed on both models to quantify uncertainty and determine what conditions are favorable for infiltration trenches.

4.4 Study Area

The Shullcas River Watershed is a high-altitude proglacial watershed within the Huaytapallana Conservation Area in the Cordillera Central and is a tributary to the Mantaro River in the Amazon Basin (Figure 4.1 inset). The river provides the city of Huancayo, Junín Region, central Peru (latitude ~12.1°S, longtitude ~75.2°W, population: 466 000), with 60% of its municipal water as well as irrigation water for local agricultural projects (Crumley, 2015). Due to these diversions, the Shullcas River runs dry or almost dry before it reaches the city of Huancayo during the dry season. Average annual precipitation in the Shullcas Basin is approximately 800 mm and varies with elevation (ANA, 2010). Precipitation is highly seasonal, with most of the annual precipitation during the rainy season from October to April. Conversely, air temperature stays almost constant throughout the year.

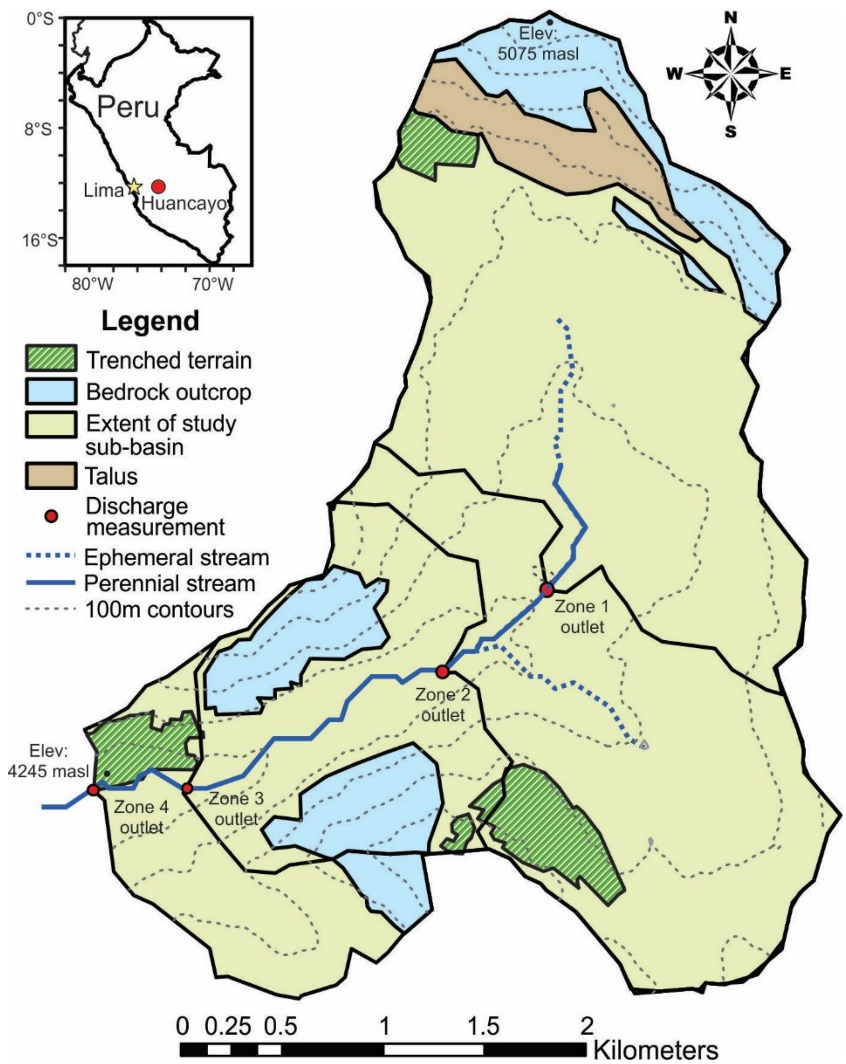

Figure 4.1: *Map of study catchment within a non-glacierized basin of the Shullcas watershed. The ephemeral streams shown are not included in the groundwater model as river nodes.*

The watershed is mainly composed of steep alpine grasslands with some bedrock outcropping, flatter hummocky wetlands known as bofedales (see Fonkén, 2015), and valley bottom alpine meadows known as pampas. Aerial photography and satellite imagery have shown a 55 percent decrease in glacial area from 1984 to 2011 (López-Moreno *et al*., 2014). Additionally, Crumley (2015) performed a hydrochemical mass balance analysis for the watershed (using HBCM method from Baraer *et al*., 2009) and found that glacier meltwater contributed approximately 9-16 percent of dry season stream discharge in 2014.

Between 2009 and 2012, the Peruvian Ministry of Agriculture, in collaboration with non-government organizations CARE and the World Bank, undertook a project entitled "Adaptation to the Impact of Rapid Glacier Retreat in the Tropical Andes," known in Spanish as PRAA. Among other components, this project included the excavation of infiltration trenches in the Shullcas Watershed where 800 hectares of land were covered in trenches (CARE Peru, 2013). Local communities were employed to manually dig trenches in several areas of the catchment. The trenches are trapezoidal in shape, roughly 30 cm deep, 40 cm wide at the top and are spaced 9-10 meters apart on steep grassy hillslopes (Figure 4.2). It has been suggested that channels known as *mamanteo* were used in a similar manner by pre-Incan peoples in the Andes, but instead would drain into an infiltration pond (Fraser, 2015; Bardales *et al*., n.d.).

Figure 4.2: *a. Construction of infiltration trenches as part of the World Bank and Care funded PRAA project. Photo taken from Comunidad Andina presentation; b. Infiltration trench with ponded water; c. Aerial view of trenched hillslope in the Shullcas Watershed, from Google Earth™*

In order to isolate the hydrologic influence of trenches from glacier melt, a non-glacial sub-basin of the Shullcas River Watershed was chosen for this study (Figure 4.1). Table 4.1 shows total, trenched and bedrock outcrop area of the study catchment, as determined from 2014 satellite imagery (Landsat imagery accessed through Google Earth™). Bedrock outcrop area is listed because of its potential relationship to soil depth and runoff characteristics.

Table 4.1: *Basin and Sub-basin properties and discharge*

Zone	Zone Area (km^2)	Trenched Area (km^2)	Outcrop Area (km^2)	Stream discharge change (total) Aug, 2016 (L/s)
1	4.39	0.09 (2%)	0.59 (13%)	14 (14)
2	2.85	0.23 (8%)	0 (0%)	0 (14)
3	2.02	0.03 (1.5%)	0.66 (33%)	4 (18)
4	1.14	0.14 (12%)	0.12 (10%)	5 (23)
Total	10.40	0.49 (5%)	1.37 (13%)	23

4.5 Methods

Our study employs both field and numerical modeling approaches to explore the recharge and hydrogeological regime in the study catchment.

4.5.1 Data collection

Field data was collected between 2011 and 2017. In August 2016, stream discharge was measured at 4 locations along the stream (shown in red on Figure 4.1) to correlate stream discharge with the contributing trenched area. The hypothesis to be tested with the discharge measurements is that zones with more trenched area should contribute more baseflow to the stream during the dry season. (It should be noted that differential gaging can have large errors in estimating groundwater inflows; e.g. Briggs *et al*., 2012).

Infiltration capacity was measured with a double ring infiltrometer during the dry season (August 2016) and the rainy season (March 2017) at a variety of sites in the Shullcas Watershed. The infiltrometer had an outer ring diameter of 40 cm and an inner ring diameter of 25 cm. At each test site, the infiltrometer was inserted 5 cm into the ground and infiltration measurements were carried out as described in Bodhinayake (2004), mostly reaching steady state between 25 – 60 minutes.

High frequency meteorological data was obtained from SENAMHI, the Peruvian national weather service, from January 2011 to June 2014. This data includes precipitation, air temperature, humidity, wind speed, shortwave and long wave radiation at 30 minute intervals from the Lazo Huntay automatic weather station, located less than 2 km outside of the study catchment. From July 2015 to August 2016, daily precipitation measurements for the Lazo Huntay station were obtained from SENAMHI's online data base (http://www.senamhi.gob.pe/?p=data-historica; visited Oct. 10, 2016).

Because the Lazo Huntay weather station is located at an elevation of approximately 4650 masl and most of the study catchment is between 4200 and 4700 masl with a midpoint of 4450 masl, the temperature was corrected using the dry adiabatic lapse rate of the atmosphere (1°C per 100m x 200m elevation difference), adding 2°C over the entire record. Similarly, precipitation varies with elevation. However, precipitation was not corrected for elevation because, at the time, precipitation data from a second weather station was not available.

Stream discharge was recorded from July 2015 to August 2016 at 15 minute intervals at our gauging station located approximately 700 m below the outlet of the study catchment using a Solinst LTC Levelogger and Barrologger. A correction was applied to the discharge data to compensate for the difference in gauging location such that the study area outlet discharge is 82%

of the discharge recorded at the gauging station, based on simultaneous discharge measurements at the two sites.

4.5.2 Recharge model

We created and applied an un-calibrated, one-dimensional infiltration model which is used as input to MODFLOW's Unsaturated Zone Flow (UZF) package to estimate recharge to the groundwater system (Figure 4.3).

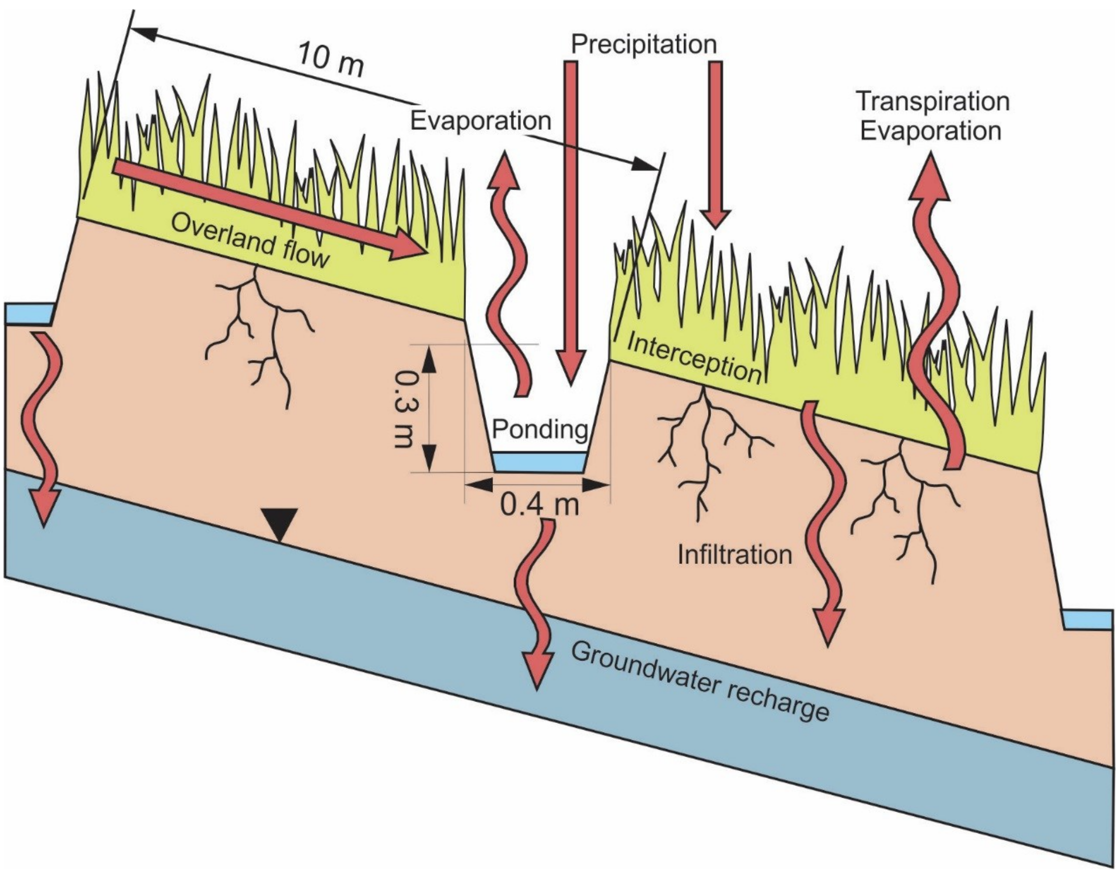

Figure 4.3: *Recharge model schematic. Red arrows indicate movement of water through the relevant hydrological processes.*

For each 30 minute time step, incoming precipitation may first be intercepted by vegetation up to the available interception storage. Intercepted water stored on the vegetation is evaporated over time, creating space for interception in future time steps. Precipitation which exceeds the available interception capacity reaches the ground surface and infiltrates at a rate less than or equal to the infiltration capacity. Runoff is generated when the precipitation that reaches the ground surface exceeds infiltration capacity as follows:

$$R = P - IS_f - I \tag{4.1}$$

Where R is runoff, P is precipitation, IS_f is available interception storage and I is infiltration, all expressed as depth of water per unit area. In the non-trenched, base case scenario, runoff is lost to the stream and therefore eliminated from the model domain. In the trenched scenario, runoff is ponded in ditches where it is evaporated and infiltrated according to:

$$\frac{PV}{W_t} = P + R \times W_n - I - E \tag{4.2}$$

Where PV is volume of ponded water (per unit section of hillslope), W_t is the width of the trench, W_n is the width of hillslope between trenches, E is evaporation from the surface of the ponded water. Potential evaporation from the ponded water in trenches is calculated using a Dalton-Type equation for open water evaporation (Dingman, 2002, Eq. 7-18a) and potential evapotranspiration from the grass land is calculated using the Penman-Monteith Formulation as outlined in Dingman (2002, Eq. 7-56).

The MODFLOW UZF package is then used for conditions representing an idealized hillslope to calculate recharge from infiltration. In the UZF package, a maximum ET rate is assigned at the ground surface and decreases linearly with depth to an assigned extinction depth. Infiltrated water moves from the ground surface towards the water table according to a kinematic wave approximation of the Richards' Equation (Niswonger *et al*., 2006). The UZF package also requires a vertical hydraulic conductivity, and Brooks-Corey Epsilon Exponent value (Niswonger *et al*., 2006). Input parameters for the UZF package are calculated or estimated based on field observations when possible or sourced from literature otherwise (Table 4.2). The UZF module is applied to a two-dimensional, 100 m wide, idealized hillslope that is representative of catchment terrain so that the results represent average recharge rate over the entire slope. More details on the UZF domain setup is included in the supporting information.

This coupled recharge model is driven by three and a half years of high temporal resolution meteorological data (including precipitation, temperature, solar radiation, longwave radiation, humidity and wind speed) to estimate the proportion of precipitation that becomes groundwater recharge for two scenarios: the base case (no trenching) and trenched case.

4.5.3 Groundwater model

Once the net recharge for the base case and trenched scenarios is determined, a three-dimensional groundwater model of the study catchment is used to evaluate the impact of trenching on groundwater baseflow to the stream. The ASTER Global Digital Elevation Model (DEM) with 30 m resolution (https://asterweb.jpl. nasa.gov/gdem.asp; Tachikawa *et al*., 2011) was used to define the model domain and 2014 satellite imagery accessed through Google Earth™ was used to define the location of trenched hillslopes and bedrock outcrop.

The groundwater model was constructed using MODFLOW-NWT (Niswonger, 2011) and uses two MODFLOW Packages: the Recharge Package (RECH) and River Package (RIV). The surface of the model has 1034 square grid cells with a side length of 100 m representing an area of 10.34

km^2. The model has two layers that are each discretized into two levels, for a total of 4136 grid cells (4 x 1034). The top layer of the model is unconfined and represents unconsolidated silty sand and gravel glacial and fluvial deposits and has a depth between 1 and 30 m. Surficial layer depths are based on topography, satellite imagery of rock outcrops and field observation of sediment depth, such as road cuts. The surficial layer is considered isotropic because of the coarse and poorly sorted nature of the deposits. The bottom layer represents fractured bedrock and is simulated as confined to help with model convergence. Rock below 60 m in depth is considered impermeable. Bedrock fracture flow is considered isotropic in absence of detailed bedding information and to simplify calibration. An orthographic view of the model domain, is included in Figure 4.9 of the supporting information.

The model is run with daily time steps. The initial conditions are set by a steady state spin-up that uses long term average conditions followed by one year of transient spin-up to allow the model to reach dynamic equilibrium. Then the model is run for a period of 428 days between July 1, 2015 and August 31, 2016.

Because of limitations in the available data, the high temporal resolution meteorological data (January 2011- July 2014) does not overlap with the stream discharge record (July 2015 – August 2016), and only a daily precipitation record was available during this time period. Therefore, the overall relationship observed between precipitation and recharge for the high temporal resolution run of the recharge model is recreated empirically for the 2015-2016 period, preserving the overall recharge amount as a percentage of precipitation.

Ten day intervals were used to average the relationship between amount of precipitation and recharge during the recharge model run. These coefficients were then applied to the 2015-2016 precipitation data to produce a recharge data set, also with 10 day intervals. The recharge data set was adjusted manually to smooth outliers resulting from periods of unusual or extreme weather in the 2011-2014 data and lag time between precipitation and recharge was reduced to improve model fit. The average proportions of precipitation that becomes recharge for the base case and trenched case, as found in Section 3.2 were preserved over the entire model period and are used along with the daily precipitation record to create two daily recharge time series for the period from July 2015 to August 2016.

The base case and trenched case recharge time series are applied to the appropriate model area according to the presence or absence of trenching. The model output, groundwater baseflow to the stream, is calibrated to dry season stream discharge. Three calibration variables are used to achieve the best fit: hydraulic conductivity of the surficial layer, specific yield of the surficial layer and hydraulic conductivity of the fractured bedrock layer.

A simple surface runoff component is added to the baseflow hydrograph in order to compare with the observed stream discharge. Precipitation depth is multiplied by the area of the catchment, combined into three day intervals and lagged by two days to smooth the runoff response. Several different intervals and lag times were tried to optimize the fit. The percentage of precipitation becoming runoff is then varied to find the best fit to the observed hydrograph. This simple runoff estimate is used because the goal is to roughly compare to the hydrograph and not to investigate in detail the precipitation-runoff response. Furthermore, the dry season discharge, which is of particular interest, is dominated by baseflow.

The ZONEBUDGET and MODPATH modules are used to post-process the MODFLOW-NWT model results. ZONEBUDGET (Harbaugh, 1990) is used to analyze the water budget entering and leaving different zones of the model. MODPATH (Pollock, 2012) is used to analyze flow paths and travel times through the subsurface. This module tracks particles of water from some assigned launch point until they exit the model domain, in our case, through the river. Ten sites were randomly selected throughout the catchment and two particles were released at different depths at each site, vertically distributed between the top-most active layer and the model bottom. The flow paths and travel times were analyzed for each particle.

4.5.4 Sensitivity Analysis

To quantify uncertainty and determine the optimal setting for hillslope trenching, sensitivity analysis is applied to the recharge and groundwater models.

For the recharge model, a one-at-a-time sensitivity analysis is used (Hamby, 1994; Pianosi *et al*., 2016). A range of plausible values is selected for each input variable and the model is run repeatedly, changing one variable while all others remained the same. For each sensitivity run, three results are recorded: the percentage of precipitation that becomes recharge for the base case scenario, the trenched scenario and the difference between the two. Sensitivity is ranked based on the difference between the two scenarios which can be thought of as an indicator of the benefit of trenching.

For the 3-dimensional groundwater model, sensitivity analysis is performed on the configuration of trenching within the catchment. Within the model domain, the trenched area is moved or expanded for consecutive model runs and the impact on the timing and magnitude of groundwater discharge to the river is examined.

4.6 Results

4.6.1 Data collection

Measured stream discharges at several points along the stream from August 2016 are shown in Table 4.1. However, there is no clear connection between the trenched area and the increase in stream discharge from a given zone of the catchment. We must, therefore, rely on the modeling results.

Thirteen infiltration measurements were taken with the double ring infiltrometer. The dry season measurements were performed between August 15 and 19, 2016 and ranged from 0.07 to 5.76 with an average of 2.4 m/d (n = 9). Rainy season measurements were taken between March 7 and 10, 2017 and ranged from 0.17 to 0.24 with an average of 0.20 m/d (n = 4). These measured infiltration capacities are within range of literature values for mountain grassland (Gaither and Buckhouse, 1983; Leitinger *et al*., 2010; Roa-Garcia *et al*., 2011).

Meteorological data from the Lazo Huntay automatic weather station was obtained from SENAMHI. The data set from January 14, 2011 to June 17, 2014 was recorded at 30 minute intervals. Precipitation followed the typical seasonal pattern with the majority of precipitation falling between November and April while air temperature stayed relatively constant throughout the year (Figure 4.4a). Due to field malfunction, there is a data gap from January 29 to April 1, 2013. For the three complete years recorded, the total annual rainfall was 1390 mm, 1240 mm and 1250 mm for 2011, 2012 (starting January 14 of each year) and 2013-2014 (April 1, 2013 – April 1 2014) respectively. These values were substantially higher than the literature value for average annual rainfall in the Shullcas Basin of 800 mm (ANA, 2010), likely because of the location of the weather station higher in the catchment.

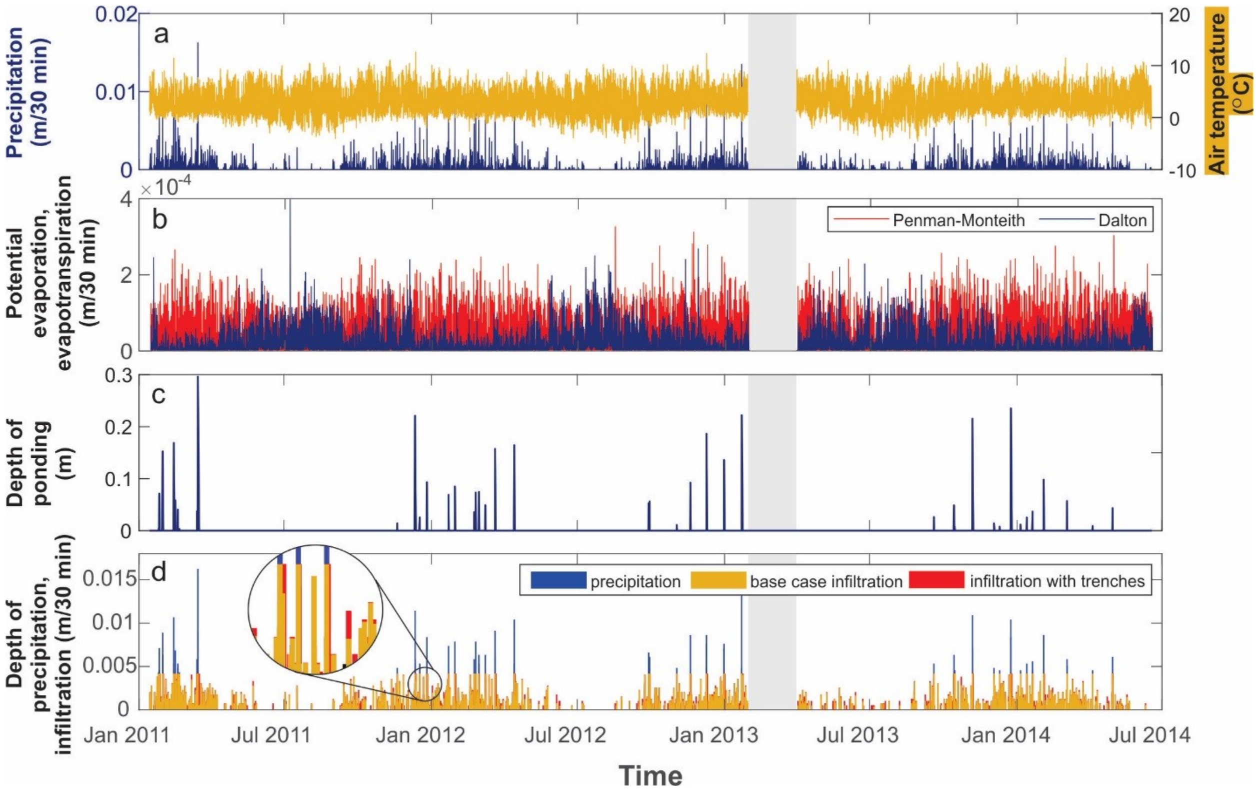

Figure 4.4: *Input variables and results for the recharge model for an idealized grassy hillslope. a. Precipitation and air temperature; b. Potential evapotranspiration as calculated using the Penman-Monteith Formulation (red) and potential evaporation as calculated using the Dalton-type Equation (blue); c. Depth of ponding; d. Depth of precipitation and infiltration, where red indicates times where the trenched case infiltration exceeds the base case. Grey area indicates missing input data.*

For the period between July 1, 2015 and August 31, 2016, daily precipitation measurements for the Lazo Huntay station were taken from SENAMHI's online data base and showed the same seasonal pattern with a total annual precipitation of 736 mm recorded between July 1, 2015 and July 1, 2016. The measurement period coincided with El Niño, which is associated with anomalous weather in Peru. While El Niño often results in excess precipitation in the northern coastal desert, the impact in Huancayo can be either an excess or deficit of precipitation (Kane, 2000) and may explain a drier rainy season than usual in the Shullcas Basin.

Stream discharge was recorded from July 21, 2015 to August 17, 2016 at 15 minute intervals (Figure 4.5). The peak flow of 1.040 m^3/s was recorded on March 10, 2016 and the minimum flow of 0.016 m^3/s was recorded on August 20, 2015. Due to field malfunction, there is a gap in the data between January 3 and March 5, 2016. The stream discharge during this period was estimated using an empirical relationship between the study gauging station and a gauging station in an adjacent catchment ($r^2 = 0.53$).

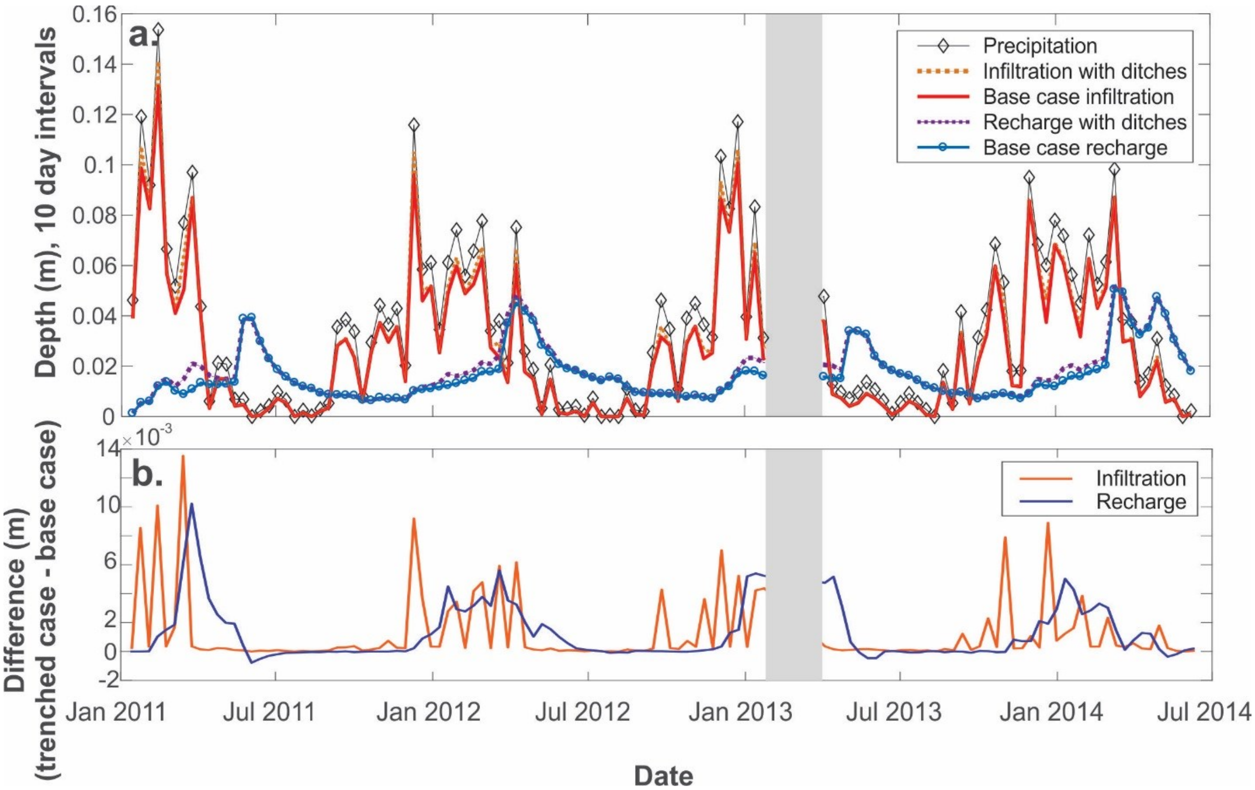

Figure 4.5: *a. Precipitation, infiltration and recharge for the base case and trenched scenarios. b. Difference in infiltration and recharge amounts for the base case and trenched case. Both plots are aggregated over ten day periods. Grey area indicates missing input data.*

4.6.2 Recharge model

Input variables for the recharge model were selected based on field observations and literature values (Table 4.2). The rainy season infiltration capacity was used because this is the only time that the precipitation intensity exceeds the infiltration capacity and runoff is generated.

***Table 4.2**: Model input parameters*

Infiltration Input Variable	Value	Source
Infiltration capacity	0.2 m/d	Rainy season double ring infiltrometer measurements
Interception storage	1 mm	Burgy and Pomeroy, 1958; Dunkerley and Booth, 1999; Zou et al., 2015.
Width, spacing of trenches	0.4 m, 9 m	Field measurement, CARE Peru, 2013.
Potential Evapotranspiration time series	0 – 16 mm/d (average 1 mm/d)	Calculated using Penman-Monteith Formulation. Eq. 7-18a in Dingman, 2002.
Open water evaporation	0-19 mm/d Average (0.8mm/d)	Calculated using Dalton-type Equation. Eq. 7-56 in Dingman, 2002.
Recharge Input Variable		
Maximum ET	1 mm/d	Average of ET time series
ET extinction depth	2 m	Shah, 2007 (approximate value for sandy loam with grass cover)
ET extinction water content	0.05	USDA, 1955. (approximate wilting point for sandy, silty loam)
Vertical hydraulic conductivity of the unsaturated zone	1 m/d	Table 3.7 in Fetter, 2001. (order of magnitude estimation for sandy, silty loam)
Brooks Corey Epsilon	3.5	Niswonger et al., 2006
Saturated water content	0.3	Table 3.4, Fetter, 2001. Estimation for porosity of silty soil

The one-dimensional model was run for the three and a half year period from January 14, 2011 to June 17, 2014 using 30 minute interval meteorological data. The calculated potential evaporation from ponded water, calculated using the Dalton-type Equation, and the potential evapotranspiration from the grassland, calculated using the Penman-Monteith Formulation (Figure 4.4b), had average values of 0.8 and 1.0 mm/d respectively. Ponding occurred during only the highest intensity precipitation events (Figure 4.4c) and trench overflow occurred only once during the model run.

The pattern of infiltration closely follows that of precipitation (Figure 4.5). Infiltration for the trenched scenario exceeded the base case scenario at times of heavy precipitation when runoff is captured and at times when vegetation cover is dry. This is because ditches are not subject to interception, while grassland is (Figure 4.4d). The pattern of recharge is dampened and delayed relative to infiltration, with peak recharge occurring towards the end of the rainy season. Like infiltration, recharge in the trenched scenario exceeds the base case during times of high precipitation and particularly on the rising limb of the recharge curve.

The results of the recharge model indicate that in non-trenched hillslopes, 79.6% of precipitation infiltrates into the ground and 48.6% becomes groundwater recharge (reaches the water table). Whereas for trenched hillslopes, 83.3% of precipitation becomes infiltration and 52.1% becomes recharge. This value is fairly high compared to some studies (Jodar, 2017) but is within range of other studies that have estimated recharge relative to precipitation in alpine catchments (Crosbie *et al*., 2010; Voeckler *et al*., 2014; Fan, 2014).

4.6.3 Three dimensional groundwater model

The model output, net groundwater discharge to the river, served as the target variable for calibration. The model was visually calibrated to the dry season stream discharge from July 21 to October 15, 2015 and May 1 to August 17, 2016 (Figure 4.5), by varying the hydraulic conductivity of the two layers and specific yield of the surficial layer. The calibrated hydraulic conductivities are 7 m/d and 0.5 m/d for the surficial deposits and fractured bedrock respectively. The calibrated specific yield of the surficial deposits is 0.09.

Once calibrated, modeled groundwater baseflow compares well with the measured dry season stream discharge, specifically during baseflow recession at the beginning of the dry season (May - June). The root mean square error (RMSE) of the model base flow during the dry season was

0.011 m^3/s and the normalized RMSE (NRMSE) was 7.5%.

Three "peaks" in baseflow can be observed in the modeled baseflow hydrograph, the first in early January, the second and largest in early March and the third in late April (indicated in Figure 4.6). These peaks correspond to periods of heavy precipitation and are followed by periods where baseflow becomes the dominant water source (baseflow recession), as is expected.

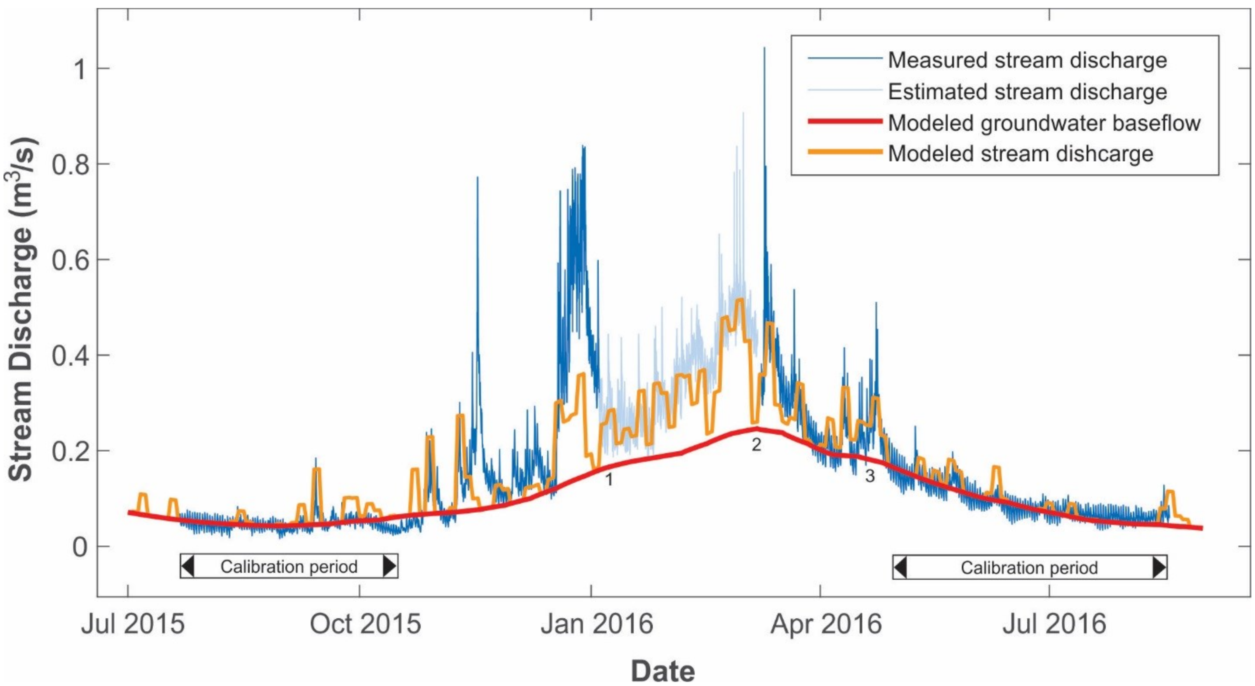

Figure 4.6: *Measured stream discharge compared to modeled baseflow and modeled stream discharge over the 14 month groundwater simulation period. The estimated stream discharge fills the data gap by regressing to a nearby stream gauge.*

In order to compare to the measured hydrograph throughout the rainy season, a simple runoff component was added to the modeled baseflow (Figure 4.6). Using 20% of precipitation to represent aggregate runoff and shallow interflow over the study catchment provided the best fit to the measured hydrograph. This combined modeled hydrograph is generally slightly lower than the measured hydrograph during the rainy season and slightly higher during the dry season. This is likely because the simple runoff model does not include any treatment for antecedent moisture content of the soil and vegetation.

During the simulation, the groundwater table was generally shallow closer to the stream and deeper higher up on the hillslopes. In these higher and steeper areas of the catchment, the surficial layer was never saturated and groundwater flow was channeled through the fractured bedrock. Once the groundwater flow meets the valley, part of it flows into the saturated surficial layer and then to the stream.

In this way, most of the groundwater flow reaching the river did so through the surficial layer due to its higher hydraulic conductivity. Using ZONEBUDGET, the river zone was delineated as the cell containing the river, plus one 100m cell on either side, in all layers. Averaged over the modeled period, 72% of groundwater flow to the river zone was transmitted through the surficial layer and 28% was transmitted through the fractured bedrock layer. Slightly more groundwater reached the river zone through the fractured bedrock layer during the early rainy season from December to January (maximum 33% bedrock flow, 67% surficial flow) and slightly less during the early dry season from May to June (minimum 25% bedrock flow, 75% surficial flow).

Flow paths were analyzed for 20 particles using MODPATH. Two particles were launched at each of ten locations randomly chosen throughout the catchment. Travel times ranged from 198 days to 1859 days (~5 years), from release until reaching the river. The average travel time for the top most particle at each of the ten locations was 545 days (1.5 years). A map of the resulting flow paths is included in Figure 4.10 of the supporting information. This is compatible with a conceptual model based on hydrochemical analysis by Baraer et al. (2015) in which, the retention time is estimated to be long enough to maintain lateral springs through the dry season in glaciated valleys of the Cordillera Blanca.

4.6.4 Sensitivity Analysis

Sensitivity analysis was used for both models. For the recharge model, two types of sensitivity were evaluated: first, the sensitivity of the amount of recharge, in both scenarios, to the input variables; and second, the sensitivity of the difference in recharge between the base case and trenched scenarios to the input variables. For example, increasing the maximum ET decreases the amount of recharge for both the trenched and non-trenched scenarios (sensitive to max ET). However, increasing max ET does not greatly change the difference in recharge between the trenched and non-trenched scenarios (not sensitive to max ET).

Table 4.3 shows the range of likely values selected for each input variable and the resulting recharge rates and difference in recharge between the base case and trenched scenarios. The resulting recharge rates (column 3 and 4 of Table 4.3) are most sensitive to maximum ET, followed by infiltration capacity, ET extinction water content, interception storage, ET extinction depth and the potential ET time series. All other input variables had little impact (<0.1% difference) on the overall recharge rate.

Table 4.3: *Hillslope sensitivity analysis*

1. Sensitivity Variable (original value)	2. Range of values	3. Recharge base case (%)	4. Recharge with trenching (%)	5. Difference between base case and trenched case (%)
Unperturbed (from section 4.2)	-	48.51	52.05	3.54
Infiltration capacity (0.2 m/d)	0.3 m/d	50.69	52.53	1.84
	0.1 m/d	42.07	50.66	8.59
Interception storage (1 mm)	1.5 mm	47.00	50.58	3.58
	0.5 mm	51.84	55.26	3.42
Width of trenches (0.4 m)	0.6	48.56*	52.40	3.84
	0.2	48.56*	51.37	2.81
Spacing of trenches (9 m)	15	48.56*	51.96	3.40
	5	48.56*	53.24	4.68
Potential Evapotranspiration time series (-22 – 16 mm/d, average 1 mm/d)	+10%	47.77	51.32	3.55
	-10%	49.41	52.92	3.51
Open water evaporation (0-19 mm/d, average 0.8 mm/d)	+10%	48.56*	52.09	3.53
	-10%	48.56*	52.09	3.53
Maximum ET (1 mm/d)	1.5 mm/d	40.70	44.15	3.45
	0.5 mm/d	57.97	61.49	3.52
ET extinction depth (2 m)	1 m	49.53	53.01	3.48
	3 m	47.79	51.26	3.47
ET extinction water content (0.05)	0.075	53.55	57.02	3.47
	0.025	48.56	52.03	3.47
Vertical hydraulic conductivity of the unsaturated zone (1 m/d)	1.2 m/d	49.09	52.57	3.48
	0.8 m/d	47.85	51.33	3.48
Brooks Corey Epsilon (3.5)	4	46.32	49.79	3.47
	3	51.13	54.60	3.47
Saturated water content (0.3)	0.35	48.79	52.27	3.48
	0.25	72.38	75.81	3.43

*Unchanged because parameter does not affect base case

The difference in recharge between the two scenarios (column 5) is most sensitive to infiltration capacity followed by the spacing of trenches and then the width of trenches. All other input parameters had minimal impact on the difference in recharge between the two scenarios meaning that they affect the base case and trenched hillslopes similarly.

Sensitivity analysis was also performed on the groundwater model for different trenching configurations. Six different scenarios were tested and compared to a scenario with no trenching. Figure 4.7 shows the difference (increase) in base flow between each different trenching configuration and the base case. Doubling the trenched area approximately doubled base flow, as expected and did not greatly change timing. Trenching low in the catchment or in steep areas made the baseflow increase flashier, with increases higher in the rainy season but then dropping off to almost zero in the dry season. Alternatively, trenching high in the catchment and trenching in flat areas both had the effect of delaying the peak baseflow increase and providing more base flow longer into the dry season. A similar plot showing the difference in baseflow expressed as a percent difference is included in the supporting information (Figure 4.11).

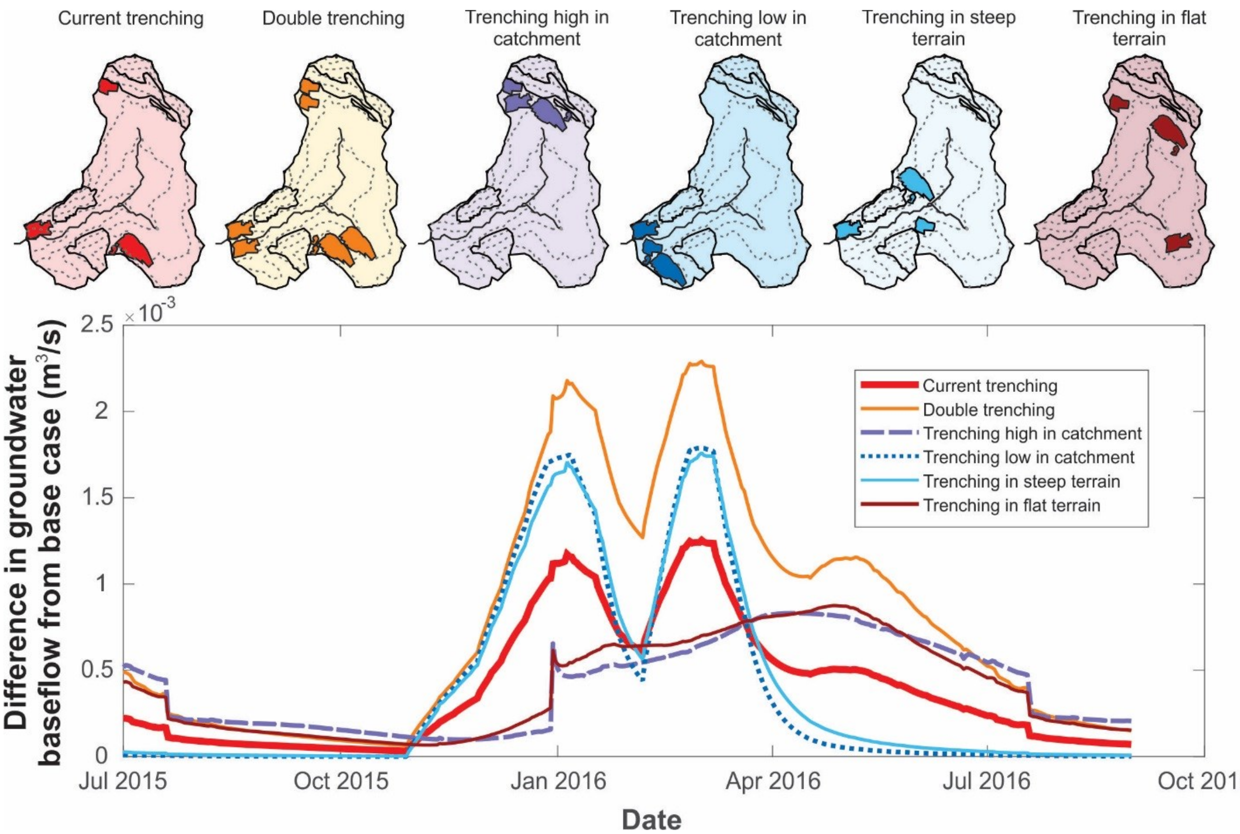

Figure 4.7: *Sensitivity to trenching configuration, demonstrating how location and area of trenching can affect groundwater baseflow generation. Six different trenching scenarios were compared to the base case (no-trenching) baseflow hydrograph and the differences are plotted.*

4.7 Discussion

4.7.1 Groundwater flow system

The calibration of the MODFLOW groundwater model yielded relatively high hydraulic conductivities (K) for both the surficial deposits and the fractured bedrock layer. These parameters are reasonable considering the coarse, gravel-rich nature of much of the surficial layer and the fractured nature of the shallow metamorphic bedrock. Our surficial deposit K is lower than the range reported by Langston *et al*. (2013) for a moraine in the Canadian Rockies (0.3–3 × 10^{-3} m/s) and is similar to that reported by Magnusson *et al*. (2014) for a glacier forefield deposit in the Swiss Alps (0.8 - 5 $\times 10^{-4}$ m/s). The specific yield value on the other hand was low compared to typical values for the mixed silt, sand and gravel soil. Fetter (2001) suggests values ranging from 0.03 to 0.19 for silt and 0.20 to 0.35 for gravelly sand.

The calibrated model indicated that the catchment is dominated by relatively fast and shallow groundwater flow. This agrees with hydrogeological research done in mountain regions elsewhere. McClymont *et al*. (2010) used geophysics to examine groundwater flow paths in a talus and meadow complex in the Canadian Rockies. They found that unconsolidated deposits were less than 10 m thick and that precipitation inputs well exceeded the groundwater storage capacity of the small headwater catchment, meaning that the stored groundwater was replenished on a sub-annual basis. Voeckler *et al*. (2014) used a coupled groundwater-surface water model (MIKE SHE by DHI) to investigate the role of deep groundwater flow in a headwater catchment in the Okanagan highlands of British Columbia, Canada. They found that outward groundwater flux through the deep bedrock layer amounted to only 2% of the annual water budget. However, other research has emphasized the importance of deep groundwater flow in mountain environments (Gleeson and Manning, 2008; Graham *et al*., 2010). Welch and Allen (2012) simulated groundwater flow in different mountain topographic scenarios and looked at how the groundwater recharge is partitioned into baseflow and mountain block recharge (MBR). They estimated 12 to 15 (reported as BF/MBR ratios from 5.8 to 7.3) percent of groundwater recharge goes to mountain block recharge.

During model development, incorporating deeper groundwater flow through intact bedrock with a realistic hydraulic conductivity dampened the annual pattern in baseflow such that the model's prediction of dry season baseflow well exceeded the measured value (not shown). Therefore it was determined that shallow subsurface flow through the surficial and fractured bedrock layers dominates baseflow to the stream.

Our characterization of the montane groundwater flow regime suggests that the Shullcas system does not have significant multi-year groundwater storage and may be sensitive to changes in precipitation and temperature. This agrees with Carey *et al*. (2010) who looked at ten cold regions catchments in North America and Northern Europe, and found that steep catchments had stronger correlations between monthly precipitation and stream discharge, meaning that they were less resistant to hydrologic perturbations. Furthermore, as the Huaytapallana Glaciers continue to retreat, glacial meltwater contribution to streamflow will decrease, strengthening the coupling of precipitation and stream discharge and decreasing the ability of the catchment to resist hydrologic change. Conversely, the strong seasonality of precipitation in the Shullcas Basin could mean that the shallow aquifers are fully replenished each rainy season and that changes in rainy season precipitation do not greatly affect dry season stream discharge. In this case, the addition of trenches would provide no benefit. Multi-year streamflow analysis is needed to tackle this question.

4.7.2 Effectiveness of infiltration trenches

The recharge model showed that the difference in recharge between the base case and trenched scenarios was small, only 3.5% relative to precipitation. This small increase in recharge over the trenched area of the study catchment, results in increased groundwater discharge to the stream (Figure 4.7). For current trenching conditions, the maximum increase in groundwater contribution is 1.3 L/s (112 300 L/d) and occurs in early March during the late rainy season in the Peruvian Andes. The dry season increase is smaller at approximately 0.1 L/s (8 640 L/d). Given that the average Peruvian uses 175 litres of water per day (UNDP, 2006), the dry season baseflow increase discharge could theoretically supply 49 more people with water during the dry season. Furthermore, the study catchment is only a small part of the Shullcas Basin which has a total of 8 km^2 of trenches. Multiplying our result over the total trenched area of the Shullcas Basin, 806 more people could be served during the dry season, ignoring losses in the distribution system which are often significant in municipal water systems.

While direct field measurement would be ideal to demonstrate the effectiveness of these infiltration trenches and compare to our modeling results, this is very difficult in practice. We hypothesized that one way of doing this could be to install a series of soil moisture meters below adjacent trenched and non-trenched hillslopes for a comparison. However, heterogeneity in soil textures, installation technique and even incoming precipitation mean the noise would almost certainly be greater than the difference between the two slopes. Furthermore, a large number of sensors would be required to achieve a statistically significant result if a difference was present. A similar problem was encountered by Mastrocicco *et al*. (2016) when attempting to measure the resulting groundwater mound from an MAR scheme in Italy. The calculated expected mound was well within natural variations in the water table and it was not possible to distinguish the impact of the enhanced recharge.

The effectiveness of the trenches is also likely to change over time. For example, vegetation will re-colonize the trenches as was observed in some areas of the catchment, such that interception will return to pre-trenching levels. Mastrocicco *et al*., (2016) also suggested that the effectiveness of MAR schemes may be affected by pore size reduction from clogging and biologic activity.

4.7.3 Best settings for infiltration trenches

Sensitivity analysis indicated that infiltration trenches provided differing benefits depending on the setting. Most prominently, trenching is more effective in areas with low infiltration capacity and therefore more overland flow for the trenches to intercept, provided that the density of trenches and infiltration capacity is sufficiently high to accommodate all the overland flow generated without additional spillover. This is the opposite of MAR systems which require high infiltration capacities to work (Bouwer, 2002). For the same reason, areas that receive higher intensity precipitation are better candidates for hillslope trenching. Otherwise stated, hillslopes that do not generate overland flow would receive no added benefit from this type of hillslope trenching.

However, if the infiltration capacity is too low, trenches may be filled with water for extended periods of time, overflowing during precipitation events and limiting their effectiveness. For example, in March, 2016, the higher elevation trenched area in the northwest corner of the study catchment was observed to have ponding in trenches at a time when the lower elevation trenched area in the south west corner of study area was not. This likely has to do with differing infiltration capacities where the high elevation trenched area has a siltier soil and low vegetation cover while the lower trenched area has a rockier soil and tall grass. It should be noted that the difference in ponding is probably also a function of elevation difference between the two sites, resulting difference in orographic precipitation and general heterogeneity of mountain weather.

Trenching configuration is also an important consideration. Trench spacing and width should correspond to the anticipated volume of runoff based on land cover and soil properties. Our recharge model (or a similar code) could serve as a tool for selecting the width and spacing of trenches. Furthermore, the sensitivity analysis of the groundwater model indicated that trenching higher in the catchment, further from the stream, or in flatter terrain is better for delaying the peak and increasing dry season baseflow. Differentiating between the impact of the trenching location and the flat terrain is difficult because of the overlap in these terrain characteristics. This is consistent with Smith *et al.* (2014) which found that the spatial distribution of inputs, in their case snow melt, is an important control on stream response.

Here we have outlined some practical considerations for hillslope trenching but many additional concerns exist including the risk of water logging, changes to slope stability, ecosystem damage from modifying large areas of the land surface (Dillon, 2005) and impact on local herding communities.

4.7.4 Assumptions and Limitations

Infiltration capacity is a highly heterogeneous physical property (Haws, 2004). One limitation of the recharge model is that the results represent a small margin of increase compared to the uncertainty on the input variables. While many infiltration observations were performed in order to obtain a representative value, it should be emphasized that the uncertainty in this input parameter has the potential to change the model results significantly. However, the one-dimensional model was only sensitive to three input variables, increasing confidence in our results.

Additionally, our precipitation input data does not vary spatially. Mountain weather is highly heterogeneous but we depended on a single weather station to drive the model and therefore could not apply an orographic correction based on multiple stations. However, this source of error is partially mitigated by the facts that the study area is fairly small (10.4 km^2) and the weather station is close by (<2km).

Roy and Hayashi (2009) showed that multiple complex flow paths exist in mountain groundwater systems, complicating the modeling process. One limitation of our groundwater model is that we lack detailed hydrogeological data including the depth of sediments and permeability field test information. Due to the remote location of the Shullcas Watershed inside a conservation area and the heterogeneity of the hydrogeological materials in the catchment, it was not feasible to execute a field program to gather this information in detail. Therefore, the groundwater model is non-unique, meaning that there is more than one possible combination of input parameters that could provide the same or similar solution. However, fast and shallow groundwater flow is a consistent result across different parameter sets.

Furthermore, our groundwater model set-up assumes that all water leaving the model domain flows out through the river. However, in reality, there is likely some minor groundwater flow out of the catchment through the valley bottom sediments below the river and through the intact bedrock that we did not attempt to account for.

While these limitations may affect our ability to duplicate exactly what was observed in the field, the recharge and groundwater modeling exercises do allow us to better understand the groundwater system and the role of trenching on the hydrological regime as per the goal of this study.

4.8 Conclusions

We used a recharge model to evaluate the potential impact of hillslope trenching on groundwater discharge to a stream in the Shullcas River Watershed in the Peruvian Andes. Simulations showed that trenched hillslopes received approximately 3.5% more recharge than the base case, relative to precipitation, compared with unaltered hillslopes. We then applied the calculated recharge rates to a groundwater model of the study-basin. The MODFLOW groundwater model indicated that incorporating trenched hillslopes (~2% of study catchment area) slightly increases baseflow in the mid-late rainy season but has only a small impact on dry season baseflow. If multiplied over the entire trenched area of the Shullcas Watershed, it could result in water service for an additional

800+ people during the dry season, neglecting losses to the distribution system which are substantial for most municipal water systems. Therefore the effectiveness of the trenches in augmenting dry season baseflow is limited and the hydrogeological characteristics of the area should be considered in installing similar technology.

To our knowledge, this constitutes the first scientific study on hillslope trenching as a passive aquifer recharge technology. Additionally, the results indicate that the groundwater flow system in this mountain catchment is relatively fast and shallow and is an important contributor to stream flow which should not be neglected in modeling efforts. Improving our understanding of mountain groundwater systems will allow better projection of the impact of climate change and allow better design of climate change adaptation strategies. The results of this study may have important implications for Andean landscape management and water resources.

4.9 Acknowledgements

The authors would like to thank SENAMHI for the collection of meteorological data. The National Science Foundation and United States Agency for International Development provided funding as part of the NSF-USAID PEER Program (Project 3-127), NSF #EAR-1316432, as well as the Natural Sciences and Engineering Research Council of Canada. We would also like to acknowledge the help of our field assistants Américo and Alvaro González Caldua, Oliver Wigmore, Pierrick Lamontagne-Halle and Nadine Shatilla.

4.10 Supplementary materials

4.10.1 Unsaturated Zone Flow (UZF) Package Setup

After calculating the infiltration for trenched and non-trenched terrain, the MODFLOW UZF Package was used to calculate recharge. The amount and timing of recharge is affected by the depth to the water table, among several factors. In order to calculate representative recharge characteristics, a 2D hillslope cross section was used for the UZF package, that includes a sloped water table.

The two-dimensional hillslope was set up with a 1:2 slope that represents the steep grassy hillslopes that cover much of the study catchment. The hillslope is 100 m wide and 20 m thick with only one unconsolidated layer. A constant head node at the top of the hill and a river node at the bottom maintain a sloped water table. For the trenched case, trenches are spaced 9 m apart based on field observations. Figure 4.8 shows the set up for the trenched case. The base case set-up is identical, only without the trenches.

The amount of water reaching the water table was extracted and averaged over the entire length of the hillslope to calculate the reported recharge rates.

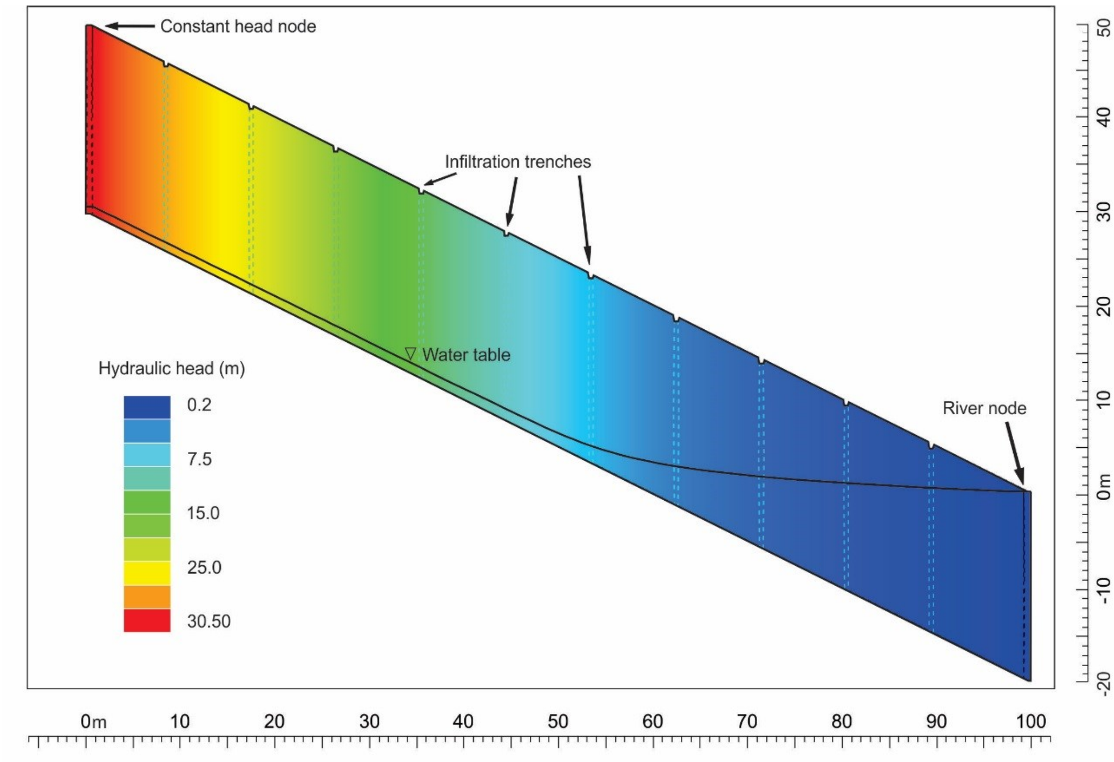

Figure 4.8: *Unsaturated Zone Flow Package 2D model domain for the trenched scenario. Base case scenario is identical, only without trenches.*

4.10.2 MODFLOW-NWT model Setup

The MODFLOW-NWT model was set up using MODELMUSE (Winston, 2009), a graphic user interface for MODFLOW. Figure 4.9 shows the top, front and side views of the model domain.

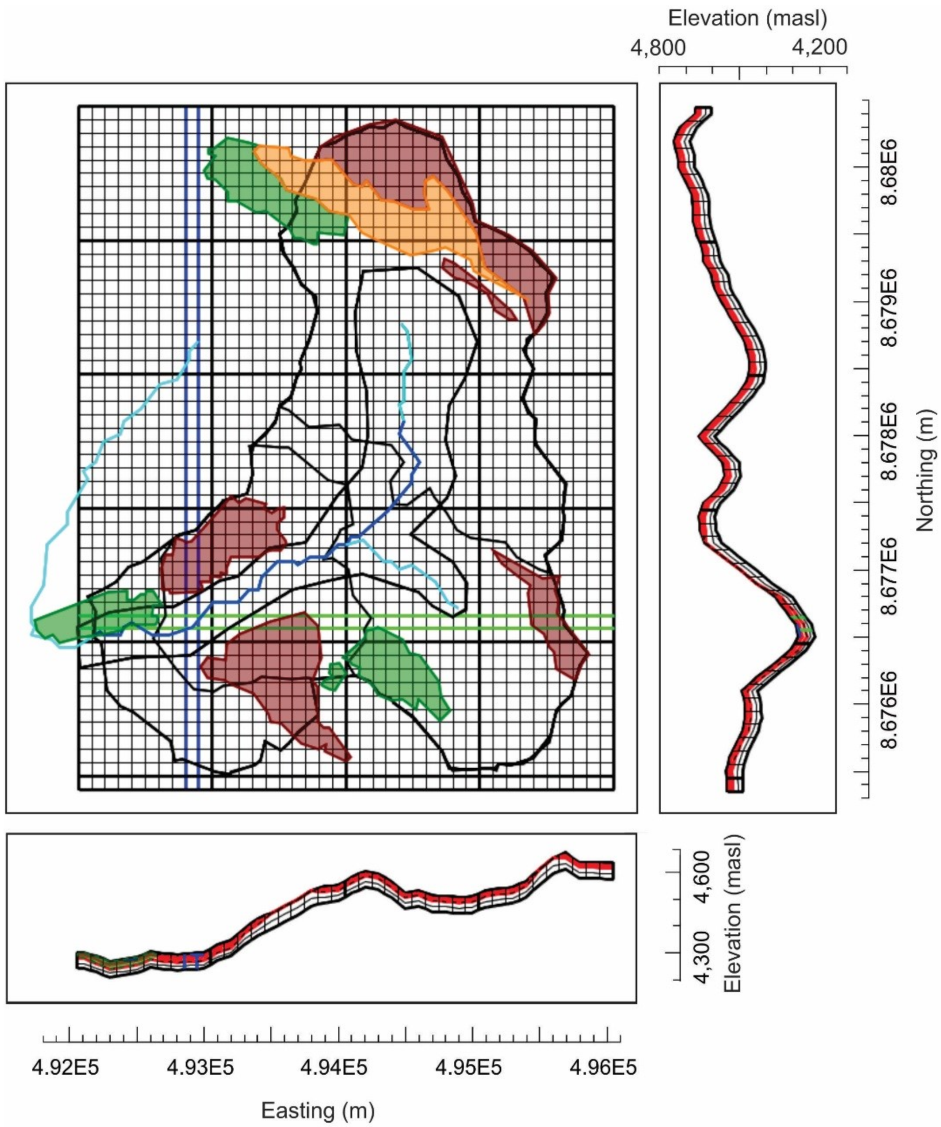

Figure 4.9: *Groundwater flow model domain. Top, front and side views of the MODFLOW-NWT Groundwater flow model as visualized using MODELMUSE, a graphic user interface for MODFLOW. The locations of the cross sections for the front and side views are indicated on the top view by the row and column highlighted in green and blue respectively. The surficial layer, which varies in thickness, is highlighted in red in the front and side views.*

4.10.3 MODPATH Setup and Results

Porosities for the MODPATH analysis were based on the calibrated specific yield of the model layers. A porosity of 0.1 was used for the surficial layer and 0.05 for fractured bedrock. The simulation was set up to repeat the year of inputs used in the main simulation, since travel times exceeded the length of the main simulation (14 months). Particle release locations were chosen randomly in order to get a representative sample. Figure 4.10 shows the particle paths from their release locations to where they exit the model domain in the river nodes. In most cases, the lower of the two particles launched at each location has a longer travel time. Additionally, particles launched farther from the stream and in flatter terrain experienced longer travel times.

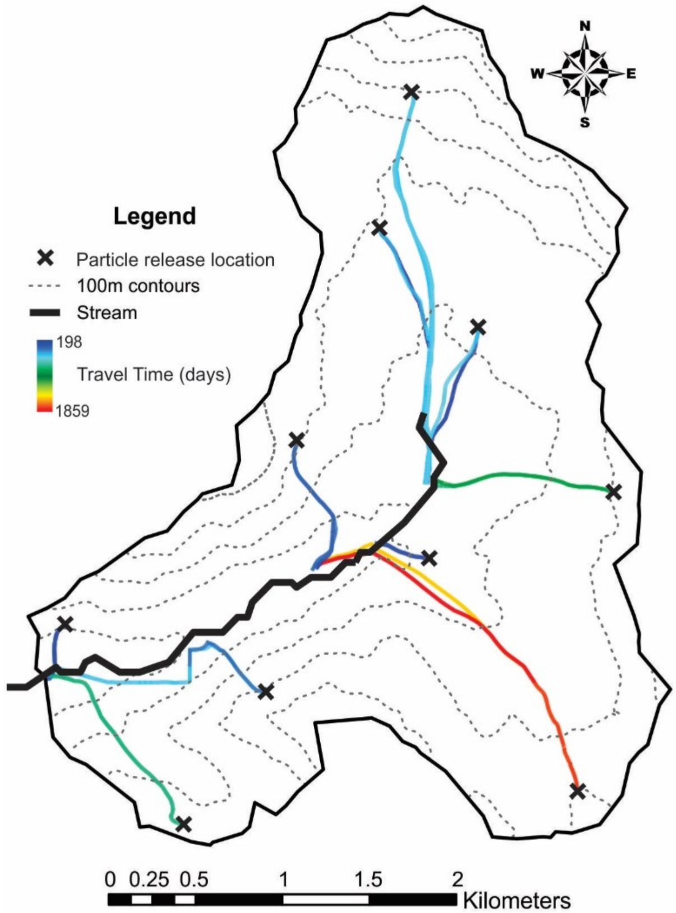

Figure 4.10: *Map of the study catchment showing particle path lines, as calculated using MODPATH. Travel times are indicated by the path colour.*

4.10.4 Groundwater model sensitivity analysis

Figure 4.11 shows an alternative presentation of Figure 4.7 where the difference in baseflow between the base case and trenched scenarios are presented as a percentage of the modeled baseflow instead of absolute flow.

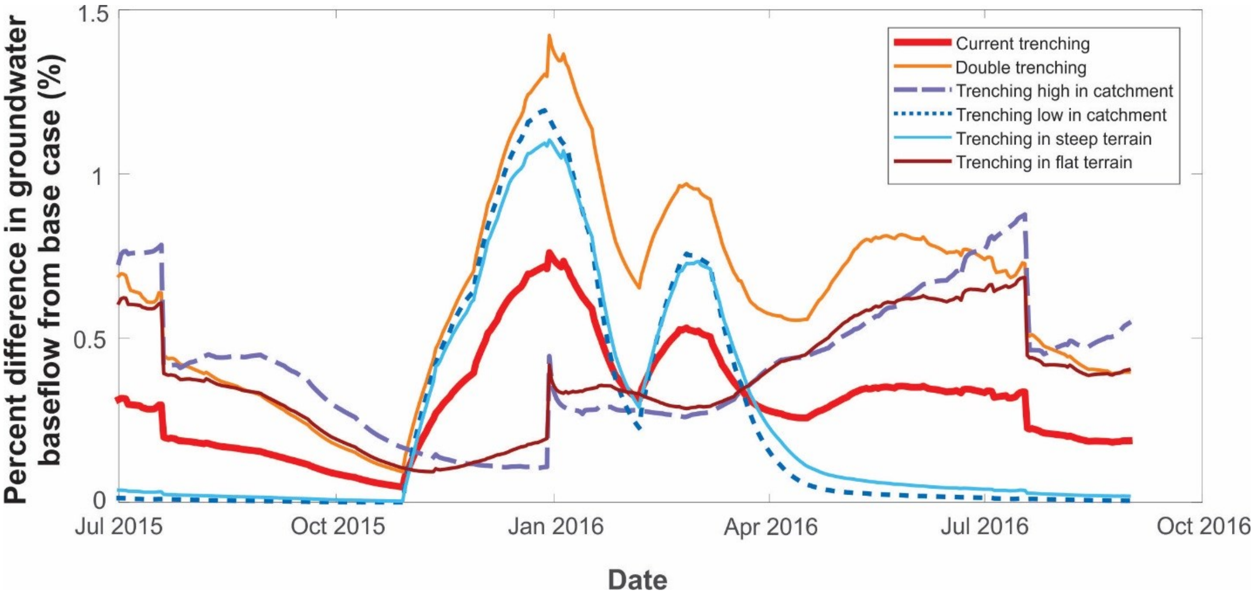

Figure 4.11: *Sensitivity to trenching configuration in percent difference. The six baseflow scenarios shown in Figure 4.7 are plotted here as a percent difference from the base case simulation.*

4.11 References

Autoridad Nacional del Agua (ANA) Ministerio de Agricultura (2010). *Evaluación de recursos hídricos superficiales en la Cuenca del Río Mantaro*. Lima, Perú.

Autoridad Nacional del Agua (ANA) Ministerio de Agricultura y Riego (2014). *Inventario de glaciares del Peru*. Huaraz, Peru.

Baraer, M., McKenzie, J.M., Mark, B.G., Bury, J., & Knox, S. (2009). Characterizing contributions of glacier melt and groundwater during the dry season in a poorly gauged catchment of the Cordillera Blanca (Peru). *Advances in Geosciences*, 22: 41–49.

Baraer, M., Mark, B.G., McKenzie, J.M., Comdom, T., Bury, J., Huh, K., Portocarrero, C., Gomez, J., & Rathay, S. (2012). Glacier recession and water resources in Peru's Cordillera Blanca. *Journal of Glaciology*. 58(207): 134-149.

Baraer, M., McKenzie, J.M., Mark, B.G., Gordon, R., Bury, J., Condom, T., Gomez, J., Knox, S. & Fortner, S.K. (2015). Contribution of groundwater to the outflow from ungauged glacierized catchments: a multi-site study in the tropical Cordillera Blanca, Peru. *Hydrological Processes*, 29:2561-2581, DOI: 10.1002/hyp.10386

Barnett, T.P., Adam, J.C., & Lettenmaier, D.P. (2005). Potential impacts of a warming climate on water availability in snow-dominated regions. *Nature*, 438, 7066: 303–309, doi: 10.1038/nature04141.

Bodhinayake, W., Si, B. C. & Noborio, K. (2004). Determination of hydraulic properties in sloping landscapes from tension and double-ring infiltrometers. *Vadose Zone Journal, 3*(3), 964-970.

Bradley, R.S., Vuille, M., Diaz, H.F., & Vergara, W. (2006). Threats to Water Supplies in the Tropical Andes. *Science*, 312, 5781: 1755–1756.

Briggs, M.A., Lautz, L.K. & McKenzie, J.M. (2012). A comparison of fibre-optic distributed temperature sensing to traditional methods of evaluating groundwater inflow to streams. *Hydrological Processes*, 26:1277-1290, DOI:10.1002/hyp.8200

Bouwer, H. (2002). Artificial recharge of groundwater: Hydrogeology and engineering. *Hydrogeology Journal,* vol. 10, no. 1, pp. 121-142.

Burgy, R. H., & Pomeroy, C. R. (1958). Interception losses in grassy vegetation. *Eos, Transactions American Geophysical Union, 39*(6), 1095-1100. doi:10.1029/TR039i006p01095

Bury, J.M., Mark, B.G., Carey, M., Young, K.R., McKenzie, J.M., Baraer, M., French, A. & Polk, M.H. (2013). New Geographies of Water and Climate Change in Peru: Coupled Natural and Social Transformations in the Santa River Watershed. *Annals of the Association of American Geographers*. DOI: 10.1080/00045608.2013.754665

CARE Peru (2013). *Analisis situacional de la implementacion de los proyectos piloto como medidas de adaptacion*. Retrieved Mar 28, 2017 from http://www.care.org.pe/wp-content/uploads/2014/12/CARE-PERU-Analisis-situacional-implementacion-proyectos-piloto-como-medidas-de-adaptacion.pdf

Clow, D.W., Schrott, L., Webb, R., Campbell, D.H., Torizzo, A., & Dornblaser, M. (2003). Groundwater Occurrence and Contributions to Streamflow in an Alpine Catchment, Colorado Front Range, *Groundwater,* Vol 41, No.7, pp. 937-950.

Crosbie, R. S., Jolly, I. D., Leaney, F. W. & Petheram, C. (2010). Can the dataset of field based recharge estimates in Australia be used to predict recharge in data-poor areas? *Hydrology and Earth System Sciences, 14*(10), 2023-2038. doi:10.5194/hess-14-2023-2010

Crumley, R. (2015). *Investigating glacier melt contribution to stream discharge and experiences of climate change in the Shullcas River Watershed in Peru* (Master's Thesis). The Ohio State University, Columbus, Ohio, USA.

Bardales, J.D., Barriga, L., Saravia, M., & Angulo, O. (n.d.). Análisis preliminar de la funcionalidad de una práctica ancestral de siembra y cosecha de agua en ecosistemas semiáridos. *Consorcio para el Desarrollo Sostenible de la Ecorregión Andina, Perú.*

Dillon, P. (2005). Future management of aquifer recharge, *Hydrogeology Journal,* vol. 13, no. 1, pp. 313-316.

Dingman, S.L. (2002). *Physical Hydrology 2nd edition.* Waveland Press Incorporated, Long Grove Illinois, USA.

Dunkerley, D. L., & Booth, T. L. (1999). Plant canopy interception of rainfall and its significance in a banded landscape, arid western New South Wales, Australia. *Water Resources Research, 35*(5), 1581-1586. doi:10.1029/1999WR900003

Fan, J., Oestergaard, K. T., Guyot, A., & Lockington, D. A. (2014). Estimating groundwater recharge and evapotranspiration from water table fluctuations under three vegetation covers in a coastal sandy aquifer of subtropical Australia. *Journal of Hydrology, 519*(PA), 1120-1129. Doi:10.1016/j.jhydrol.2014.08.039

Fetter, C.W. (2001). *Applied Hydrogeology, Fourth Edition.* Pearson Education International. Prentice-Hall Inc. Upper Saddle River, New Jersay, USA, 07458.

Fraser (2015). Water-supply solutions include pre-Incan approach. *Eco Americas*. Beverly, MA, USA. Vol 17. No 10.

Georges, C. (2004). 20th-century glacier fluctuations in the tropical Cordillera Blanca, Perú. *Arctic, Antarctic, and Alpine Research, 36*(1), 100-107.

Gleeson, T., & Manning, A. H. (2008). Regional groundwater flow in mountainous terrain: Three-dimensional simulations of topographic and hydrogeologic controls. *Water Resources Research, 44*(10) doi:10.1029/2008WR006848

Gordon, R.P., Lautz, L.K., McKenzie, J.M., Mark, B.G., Chavez, D. & Baraer, M. (2015). Sources and pathways of stream generation in tropical proglacial valleys of the Cordillera Blanca, Peru, *Journal of Hydrology*, 522:628-644, DOI: 10.1016/j.jhydrol.2015.01.013

Graham, C. B., Van Verseveld, W., Barnard, H. R., & McDonnell, J. J. (2010). Estimating the deep seepage component of the hillslope and catchment water balance within a measurement uncertainty framework. *Hydrological Processes, 24*(25), 3631-3647. doi:10.1002/hyp.7788

Hamby, D. M. (1994). A review of techniques for parameter sensitivity analysis of environmental models. *Environmental Monitoring and Assessment, 32*(2), 135-154. doi:10.1007/BF00547132

Harbaugh, A.W. (1990). *A Computer Program for Calculating Subregional Water Budgets Using Results from the U.S. Geological Survey Modular Three-dimensional Finite-difference Ground-water Flow Model.* U.S. Geological Survey Open-File Report 90-392.

Harpold, A. A., Lyon, S. W., Troch, P. A., & Steenhuis, T. S. (2010). The hydrological effects of lateral preferential flow paths in a glaciated watershed in the northeastern USA. *Vadose Zone Journal, 9*(2), 397-414. doi:10.2136/vzj2009.0107

Haws, N.W., Liu, B., Boast, C.W., Rao, P.S.C., Kladivko, E.J. & Franzmeier, D.P. (2004). Spatial variability and measurement scale of infiltration rate on an agricultural landscape. *Soil Science Society of America Journal,* vol. 68, no. 6, pp. 1818-1826.

Heilweil, V. M., Benoit, J., & Healy, R. W. (2015). Variably saturated groundwater modelling for optimizing managed aquifer recharge using trench infiltration. *Hydrological Processes, 29*(13), 3010-3019. doi:10.1002/hyp.10413

Heviánková, S., Marschalko, M., Chromíková, J., Kyncl, M. & Korabík, M. (2016). Artificial Ground Water Recharge with Surface Water. *IOP Conference Series: Earth and Environmental Science*.

Instituto Geofísico del Perú (IGP) (2010). *Cambio Climático en la Cuenca del Río Mantaro. Balance de 7 Años de Estudios.* Huancayo, Perú.

Jódar J., Cabrera, J.A., Martos-Rosillo, S., Ruiz-Constán, A., González-Ramón, A., Lambán, L.H., Herrera, C. & Custodio, E. (2017). Groundwater discharge in high-mountain watersheds: A valuable resource for downstream semi-arid zones. The case of the Bérchules River in Sierra Nevada (Southern Spain). *Science of The Total Environment*, Volumes 593–594, pp 760-772, ISSN 0048-9697

Kane, R. P. (2000). El Nino/La Nina relationship with rainfall at Huancayo, in the Peruvian Andes. *International Journal of Climatology, 20*(1), 63-72. doi:10.1002/(SICI)1097-0088(200001)20:1<63::AID-JOC447>3.0.CO;2-J

Langston, G., Hayashi, M., & Roy, J. W. (2013). Quantifying groundwater-surface water interactions in a proglacial moraine using heat and solute tracers. *Water Resources Research, 49*(9), 5411-5426. doi:10.1002/wrcr.20372

López-Moreno, J. I., Fontaneda, S., Bazo, J., Revuelto, J., Azorin-Molina, C., Valero-Garcés, B., Morán-Tejeda, E., Vicente-Serrano, S.M., Zubieta, R., Alejo-Cochachín, J. (2014). Recent glacier retreat and climate trends in cordillera huaytapallana, peru. *Global and Planetary Change, 112*, 1-11. doi:10.1016/j.gloplacha.2013.10.010

Magnusson, J., Kobierska, F., Huxol, S., Hayashi, M., Jonas, T., & Kirchner, J. W. (2014). Melt water driven stream and groundwater stage fluctuations on a glacier forefield (dammagletscher, switzerland). *Hydrological Processes, 28*(3), 823-836. doi:10.1002/hyp.9633

Maldonado-Fonkén, S. M. (2015). An introduction to the bofedales of the Peruvian high Andes. *Mires and Peat, 15*

Mark, B. G., McKenzie, J. M., & Gómez, J. (2005). Hydrochemical evaluation of changing glacier meltwater contribution to stream discharge: Callejon de huaylas, peru. *Hydrological Sciences Journal, 50*(6), 975-988. doi:10.1623/hysj.2005.50.6.975

Mark, B. G., & Seltzer, G. O. (2005). Evaluation of recent glacier recession in the cordillera blanca, peru (AD 1962-1999): Spatial distribution of mass loss and climatic forcing. *Quaternary Science Reviews, 24*(20-21), 2265-2280. doi:10.1016/j.quascirev.2005.01.003

Mark, B.G., Bury, J., McKenzie, J.M., French, A. & Baraer, M. (2010). Climate change and tropical Andean glacier recession: evaluating hydrologic changes and livelihood vulnerability in the Cordillera Blanca, Peru. *Annals of the Association of American Geographers.* DOI: 10.1080/00045608.2010.497369

Mastrocicco, M., Colombani, N., Salemi, E., Boz, B., & Gumiero, B. (2016). Managed aquifer recharge via infiltration ditches in short rotation afforested areas. *Ecohydrology, 9*(1), 167-178. doi:10.1002/eco.1622

McClymont, A. F., Hayashi, M., Bentley, L. R., Muir, D. & Ernst, E. (2010). Groundwater flow and storage within an alpine meadow-talus complex. *Hydrology and Earth System Sciences, 14*(6), 859-872. doi:10.5194/hess-14-859-2010

Meixner T., Manning A.H., Stonestrom, D.A., Allen, D.M., Ajami, H., Blasch, K.W., Brookfield, A.E., Castro, C.L., Clark, J.F., Gochis, D.J., Flint, A.L., Neff, K.L., Niraula, R., Rodell, M., Scanlon, B.R., Singha, K. & Walvoord, M.A. (2016). Implications of projected climate change for groundwater recharge in the western United States, *Journal of Hydrology,* Volume 534, Pages 124-138, ISSN 0022-1694, doi:10.1016/j.jhydrol.2015.12.027.

Nilsson, C., Reidy, C.A., Dynesius, M., & Revenga, C. (2005). Fragmentation and flow regulation of the world's large river systems. *Science, 308*(5720), 405-408. doi:10.1126/science.1107887

Niswonger, R.G. (2011). MODFLOW-NWT, A Newton Formulation for MODFLOW-2005. *United States Geological Survey Techniques and Methods 6-A37.*

Niswonger, R.G., Prudic, D.E., & Regan, S. (2006). Documentation of the Unsaturated-Zone Flow (UZF1) Package for Modeling Unsaturated Flow between the Land Surface and the Water Table with MODFLOW-2005: *United States Geological Survey Techniques and Methods 6-A19*.

Pianosi, F., Beven, K., Freer, J., Hall, J. W., Rougier, J., Stephenson, D. B., & Wagener, T. (2016). Sensitivity analysis of environmental models: A systematic review with practical workflow. *Environmental Modelling and Software, 79*, 214-232. doi:10.1016/j.envsoft.2016.02.008

Pollock, D.W. (2012). User Guide for MODPATH Version 6 – A Particle-Tracking Model for MODFLOW. U.S. Geological Survey Techniques and Methods 6-A41. Reston, Virginia, U.S.A.

Rangwala, I., & Miller, J. R. (2012). Climate change in mountains: A review of elevation-dependent warming and its possible causes. *Climatic Change, 114*(3-4), 527-547. doi:10.1007/s10584-012-0419-3

Roy, J. W., & Hayashi, M. (2009). Multiple, distinct groundwater flow systems of a single moraine-talus feature in an alpine watershed. *Journal of Hydrology, 373*(1-2), 139-150.

doi:10.1016/j.jhydrol.2009.04.018

Scanlon, B.R. Healy, R.W. & Cook, P.G. (2002). Choosing appropriate techniques for quantifying groundwater recharge. *Hydrogeology Journal*, 10(1), 18-39. doi:10.1007/s10040-001-0176-2

Schauwecker, S., Rohrer, M., Acuña, D., Cochachin, A., Dávila, L., Frey, H., Giráldez, C., Gómez, J., Huggel, C., Jacques-Coper, M., Loarte, E., Salzmann, N. & Vuille, M. (2014). Climate trends and glacier retreat in the Cordillera Blanca, Peru, revisited, *Global and Planetary Change,* vol. 119, pp. 85-97.

Shah, N., Nachabe, M., & Ross, M. (2007). Extinction depth and evapotranspiration from ground water under selected land covers. *Ground Water, 45*(3), 329-338. doi:10.1111/j.1745-6584.2007.00302.x

Smith, R.S., Moore, R.D., Weiler, M. & Jost, G. (2014). Spatial controls on groundwater response dynamics in a snowmelt-dominated montane catchment. *Hydrology and Earth Systems Science* 18: 1835–1856.

Somers, L., Gordon, R.P., Lautz, L.K., McKenzie, J.M., Wigmore, O., Glose, A., Glas, R., Aubry-Wake, C., Mark, B., Baraer, M. & Condom, T. (2016). Quantifying groundwater-surface water interactions in a proglacial valley, Cordillera Blanca, Peru. *Hydrological Processes*, DOI:10.1002/hyp.10912

Tachikawa, T., Kaku, M., Iwasaki, A., Gesch, D., Oimoen, M., Zhang, Z., Danielson, J., Krieger, T., Curtis, B., Haase, H., Abrams, M., Crippen, R., Carabajal, C. & Meyer, D. (2011). *ASTER Global Digital Elevation Model Version 2 – Summary of Validation Results.* NASA

Land Processes Distributed Active Archive Center and the Joint Japan-US ASTER Science Team. Retrieved Jan., 2017 from: https://lpdaacaster.cr.usgs.gov/GDEM/Summary_GDEM2_validation_report_final.pdf

United Nations Development Report (UNDP) (2006). *Human Development Report, Beyond Scarcity: Power, poverty and the global water crisis*. New York, NY, USA. ISBN: 0-230-50058-7

US Department of Agriculture (USDA) (1955). *Yearbook.* Washington D.C.

Viviroli, D., Dürr, H. H., Messerli, B., Meybeck, M., & Weingartner, R. (2007). Mountains of the world, water towers for humanity: Typology, mapping, and global significance. *Water Resources Research, 43*(7) doi:10.1029/2006WR005653

Viviroli, D., Archer, D.R., Buytaert, W., Fowler, H.J., Greenwood, G.B., Hamlet, A.F., Huang, Y., Koboltschnig, G., Litaor, M.I., López-Moreno, J.I., Lorentz, S., Schädler, B., Schreier, H., Schwaiger, K., Vuille, M. & Woods, R. (2011). Climate change and mountain water resources: Overview and recommendations for research, management and policy. *Hydrology and Earth System Sciences,* vol. 15, no. 2, pp. 471-504.

Voeckler, H.M., Allen, D.M. & Alila, Y. (2014). Modeling coupled surface water - Groundwater processes in a small mountainous headwater catchment, *Journal of Hydrology,* vol. 517, pp. 1089-1106.

Welch, L. A., & Allen, D. M. (2012). Consistency of groundwater flow patterns in mountainous topography: Implications for valley bottom water replenishment and for defining groundwater flow boundaries. *Water Resources Research, 48*(5). doi:10.1029/2011WR010901

Winston R.B. (2009). ModelMuse – A graphical user interface for MODFLOW-2005 and PHAST. *U.S. Geological Survey Techniques and Methods 6-A29*. Reston Virginia, USA.

Zou, C. B., Caterina, G. L., Will, R. E., Stebler, E., & Turton, D. (2015). Canopy interception for a tallgrass prairie under juniper encroachment. *PLoS ONE, 10*(11) doi:10.1371/journal.pone.0141422

Chapter 5. Discussion

The research presented in this thesis elucidates the details of how, when, and where groundwater contributes to streamflow in proglacial mountain systems and suggests that as glaciers recede, the importance of groundwater in Andean rivers is growing both as a natural phenomenon (Chapters 2 and 3) and as a potential method for human enacted adaptation (Chapter 4). In this section I discuss some of the challenges and opportunities that have arisen through my PhD research and comment on potential future research directions.

5.1 Challenges and opportunities

One of the main challenges in hydrological and hydrogeological research in a mountain watershed – or indeed any watershed - is the inherent heterogeneity in the landscape and hydro-climatic variables (e.g. McDonnell *et al.,* 2007). For example, mountain soils can range from fine clays produced in glacial weathering of rock to moraines and talus deposits consisting of cobbles and boulders (Romeo *et al*, 2015). Thus, constraining hydraulic conductivity in modelling of these environments is difficult. Similarly, precipitation and temperature can vary widely within a watershed with upland areas tending to be colder and wetter (Roe, 2005). Additionally, mountain basins are often remote and the difficulty in accessing them means that both the spatial coverage of field measurements and the length of time series measurements is often a limiting factor in researching them.

Evapotranspiration (ET) is another hydrologic flux that is spatially variable and poorly constrained in mountain basins, adding uncertainty to my results as noted in Chapters 3 and 4. While there are many methods for calculating ET, most are data intensive and are of limited applicability in remote mountain regions. Eddy flux instruments are capable of directly measuring ET but are expensive and not widely used in places like Peru where scientific funding is limited. Constraining the response of ET to future climate conditions is a central limitation of projecting future groundwater recharge and therefore groundwater discharge to surface water bodies. This problem is compounded in the Andes because of the low agreement between climate models on the direction of change of precipitation and humidity, which influence ET (Vuille *et al.,* 2018 and references therin).

In this dissertation, the uncertainty in hydrologic heterogeneity was approached in two ways. First, in Chapter 2, we tackle heterogeneity directly by doing a small-scale field experiment to interrogate spatial patterns in groundwater-surface water interactions. Second, in Chapters 3 and 4, we employ integrated modelling based on a relatively dense network of hydrologic monitoring sites. For example, we benefit from using multiple records of stream discharge, multiple weather stations, multiple boreholes and many observations of infiltration capacity to characterize the watershed. By combining these two approaches, we can improve fundamental scientific understanding while also using that improved understanding to produce results that are useful to policy makers.

In addition to heterogeneity within mountain basins, there is also substantial variability between the hydrological settings of mountain basins in different mountain chains (e.g. Viviroli *et al*., 2007; Glas *et al*., 2018). Furthermore, the results presented in Chapter 3 suggest that the change in water table depth resulting from climate change is not spatially uniform over the Shullcas Watershed and seems to be related to topographic gradients.

Despite the challenges in the spatial and temporal variability of parameters, the climatic setting of the tropical Andes provides some advantages over other mountain regions, to examine the role of mountain groundwater in maintaining streamflow. The lack of precipitation during the dry season effectively isolates groundwater discharge from runoff and interflow. Furthermore, by including analysis of non-glacial sub-basins, as was done in Chapters 3 and 4, we further isolate the groundwater system from the influence of glacier melt. Design of future projects could take further advantage of the natural isolation of different water sources.

5.2 Directions for future research

Modelling in Chapter 3 allows us to estimate the magnitude of glacier sourced groundwater recharge in the Shullcas Watershed. However, only one other study globally presents an estimate of the magnitude of this flux (Saberi *et al*., 2018). Therefore, more work in other mountain basins to determine what controls the relationship between glacier coverage and influence on groundwater is imperative to understand the vulnerability of groundwater reserves to glacier recession. Furthermore, no physical measurement of this flux have been documented in the scientific literature and could be an interesting, if not logistically challenging, future research direction.

While this thesis examines the contribution of groundwater to mountain streams, future work could target the contribution of groundwater recharged in the Andes to higher order streams and to distal groundwater resources. For example, intensive groundwater pumping in Peru's Ica region, south of Lima, has allowed for the rapid expansion of export agriculture in the coastal desert that receives little rain. The underlying aquifer is thought to receive recharge from the Andes and is being rapidly depleted (Williams and Murray, 2018). Despite pressing social and economic consequences, little research has been done to quantify Andean contribution to these groundwater resources. Potential research questions include: What is the residence time of water in coastal aquifers? Can we detect the proportion of Andean water based on water chemistry? Was this water recharged in part when glacial coverage was much larger? And, to what extent will Andean glacier recession impact coastal groundwater resources and on what time scale?

Chapter 6. Conclusions and summary

Mountains play a critical role in global water supply. Over 80% of arid and semi-arid regions depend on water sources that originate in mountains (Messerli, 2001). For instance, villages, cities and industries in the Andes and on the arid western coast of South America depend on a combination of glacier melt and stored groundwater from the Andes to sustain dry-season flow (Bury *et al.,* 2013). As per the objectives listed in Section 1.6, my PhD research has interrogated the current and future role of groundwater in proglacial Andean watersheds as tropical glaciers disappear.

First, I elucidated spatial patterns of groundwater discharge to a stream in the proglacial Quilcayhuanca Valley watershed in the Cordillera Blanca, central Peru. I used a novel procedure for tracing groundwater–surface water interaction using dye and temperature as tracers, to establish that groundwater contributes approximately 30% of stream discharge over a 4 km stream reach. Furthermore, results indicated that stream sections which crossed the steeper and coarse-grained moraines were sites of substantial exchange between the surface and subsurface, but that larger net gains of groundwater to the stream were observed in the flat and fine-grained meadow sections.

Second, I integrated glacier melt, groundwater and surface water modelling techniques to better understand the dominant pathways of streamflow generation in the proglacial Shullcas Watershed in Central Peru. The calibrated model indicated that glacier melt contributed approximately 8% of the outlet streamflow and only 1.9% of groundwater recharge between 1998 and 2018. I applied climate projections to the integrated model to project that the watershed's glaciers would likely disappear before the end of the 21st century and that while groundwater helps to buffer the loss of glacier melt, increasing temperatures and decreasing groundwater recharge act to diminish groundwater storage and thus groundwater discharge to the Shullcas River.

Third, I used field data in conjunction with infiltration and groundwater flow numerical modelling to assess the ability of infiltration trenching to delay the transmission of precipitation to the Shullcas River, thereby increasing dry season baseflow. My results show that infiltration trenching could increase infiltration by around 3%, but is limited because overland flow and thus pooling in the infiltration trenches is only generated by the most intense precipitation events. Furthermore, the additional infiltration translates to less than 1% increase in dry season baseflow because of the limited spatial extent of trenching and rapid baseflow recession. Sensitivity analysis indicates that trenching higher in the watershed and in flatter areas should result in a larger increase in baseflow because of longer groundwater transit times.

The research presented in my thesis contributes to the small but growing body of literature concerning the role of groundwater in high mountain and glaciered watersheds. Where previous work has established that groundwater discharge is an important contributor to streamflow through hydrochemical and hydrograph analyses, I expound the pathways of that contribution as well as the spatial distribution of groundwater storage in Andean mountain watersheds. Furthermore, I use this understanding to improve on projections for climate change implications for water resources in these vulnerable watersheds.

My research has immediate application for water managers in Peru and by extension, the millions of people who depend on Andean water resources. My results will be particularly important in planning for future water stress in cities like Huancayo, central Peru, where further reductions in stream flow are projected beyond the loss of glacier melt water. A workshop disseminating the findings of this research in Huancayo is planned for June 2019. Additionally, the assessment of infiltration trenching will serve to inform further implementation of climate change adaptation strategies by government and non-government organizations.

While my research focuses on two watersheds in the Peruvian Andes, the ideas are applicable for other high mountain regions like the Himalaya, Rocky Mountains and Alps. My results also provide important context for global scale glacier hydrology studies like Huss and Hock (2018) who estimate that glacier peak water has passed for roughly half of large glacierized basins worldwide. Furthermore, many studies focus on surface water processes in mountain basins, but my work suggests that any hydrological modelling in mountain regions should include a well-considered and physically based representation of groundwater processes given its importance in feeding streamflow.

References

Authoridad Nacional del Agua (2014). *Inventario de glaciares del Peru*. Ministerio de agricultura y riego, Huaraz, Peru.

Andermann, C., Longuevergne, L., Bonnet, S., Crave, A., Davy, P. & Gloaguen, R. (2012). Impact of transient groundwater storage on the discharge of Himalayan rivers. *Nature Geoscience,* Vol 5, 2012. doi: 10.1038/NGEO1356.

Baraer, M., McKenzie, J., Mark, B.G., Gordon, R., Bury, J., Condom, T., Gomez, J., Knox, S. & Fortner, S.K. (2015). Contribution of groundwater to the outflow from ungauged glazierized catchments: a multi-site study in the tropical Cordillera Blanca, Peru. *Hydrol. Proc.* 29 (11), 2561–2581.

Barnett, T.P., Adam, J.C., & Lettenmaier, D.P. (2005). Potential impacts of a warming climate on water availability in snow-dominated regions. *Nature*, 438, 7066: 303–309, doi: 10.1038/nature04141.

Bresciani E., Cranswick, R.H., Banks, E.W., Batlle-Aguilar, J., Cook, P.G. & Batelaan, O. (2018). Using hydraulic head, chloride and electrical conductivity data to distinguish between mountain-front and mountain-block recharge to basin aquifers. *Hydrology and Earth Systems Science*, 22, 1629-1648. doi: 10.5194/hess-22-1629-2018

Burns, D. A., McDonnell, J. J., Hooper, R. P., Peters, N. E., Freer, J. E., Kendall, C. & Beven, K. (2001). Quantifying contributions to storm runoff through end-member mixing analysis and hydrologic measurements at the panola mountain research watershed (georgia, USA). *Hydrological Processes,* 15(10), 1903-1924. doi:10.1002/hyp.246

Bury, J.M., Mark, B.G., Carey, M., Young, K.R., McKenzie, J.M., Baraer, M., French, A. & Polk, M.H. (2013). New Geographies of Water and Climate Change in Peru: Coupled Natural and Social Transformations in the Santa River Watershed. *Annals of the Association of American Geographers*. doi: 10.1080/00045608.2013.754665

Romeo, R., Vita, A., Manuelli, S., Zanini, E., Freppaz, M. & Stanchi, S. (2015). *Understanding Mountain Soils: A contribution from mountain areas to the International Year of Soils 2015*. Food and Agriculture Organization of the United Nations (FAO), Rome, Italy.

Frisbee M.B., Phillips, F.M., Campbell, A.R., Liu, F. & Sanchez, S.A. (2011). Streamflow generation in a large, alpine watershed in the southern Rocky Mountains of Colorado: Is streamflow generation simply the aggregation of hillslope runoff responses? *Water Resour. Res.* 47(6) W06512. doi :10.1029/2010WR009391

Glas, R., Lautz, L., McKenzie, J., Mark, B., Baraer, M., Chavez, D. & Maharaj, L. (2018). A review of the current state of knowledge of proglacial hydrogeology in the Cordillera Blanca, Peru. *WIREs Water,* 5:c1299. doi: 10.1002/wat2.1299

Gordon, R.P., Lautz, L.K., McKenzie, J.M., Mark, B.G., Chavez, D. & Baraer, M. (2015). Sources and pathways of stream generation in tropical proglacial valleys of the Cordillera Blanca, Peru. *Journal of Hydrology*, 522:628-644, DOI: 10.1016/j.jhydrol.2015.01.013

Graf, W. L. (2006). Downstream hydrologic and geomorphic effects of large dams on american rivers. *Geomorphology*, 79(3-4), 336-360. doi:10.1016/j.geomorph.2006.06.022

Heilweil, V. M., Benoit, J., & Healy, R. W. (2015). Variably saturated groundwater modelling for optimizing managed aquifer recharge using trench infiltration. *Hydrological Processes,* 29(13), 3010-3019. doi:10.1002/hyp.10413

Heviánková, S., Marschalko, M., Chromíková, J., Kyncl, M. & Korabík, M. (2016). Artificial Ground Water Recharge with Surface Water, IOP *Conference Series: Earth and Environmental Science.*

Hock, R. (2003). Temperature index melt modelling in mountain areas. *Journal of Hydrology,* 282 2003) 104-115. doi:10.1016/S0022-1694(03)00257-9

Hood, J.L. & Hayashi, M. (2015). Characterization of snowmelt flux and groudnwater storage ina n alpine headwater basin. *Journal of Hydrology,* 521, 482-497. doi: 10.1016/j.hydrol.2014.12.04

Instituto Nacional de Estadistica e Informatica (INEI) (2018). *Perú: Perfil Sociodemográfico Informe Nacional, Censos Nacionales 2017*. Lima, Peru.

Instituto Nacional de Estadística (INE) (2012). *Bolivia: Proyecciones de población según departamento y municipio 2012-2020*. Sucre, Bolivia.

IPCC, (2018). *Summary for Policymakers. In: Global Warming of 1.5°C. An IPCC Special Report on the impacts of global warming of 1.5°C above pre-industrial levels […] and efforts to eradicate poverty.* World Meteorological Organization, Geneva, Switzerland, 32 pp. 151. Intergovernmental Panel on Climate Change. IPCC, Geneva, Switzerland.

Juen, I., Kaser, G. & Georges, C. (2007), Modelling observed and future runoff from a glacierized tropical catchment (Cordillera Blanca, Peru). *Global and Planetary Change,* 59(2007): 37-48. Doi:10.1016/j.gloplacha.2006.11.038

Kaser, G. (2001). Glacier-climate interaction at low latitudes. *Journal of Glaciology*, 47(157).

Kelly, C.A., Rudd, J.W.M., Bodaly, R.A., Roulet, N.T., StLouis, V.L., Heyes, A., Moore, T. R., Schiff, S., Aravena, R., Scott, K. J., Dyck, B., Harris R., Warner, B. & Edwards, G. (1997).

Increases in fluxes of greenhouse gases and methyl mercury following flooding of an experimental reservoir. *Environmental Science and Technology* 31: 1334–1344.

Liu, F., Williams, M. W. & Caine, N. (2004). Source waters and flow paths in an alpine catchment, Colorado Front Range, United States. *Water Resources Research*, 40(9), W0940101-W0940116. doi:10.1029/2004WR003076

Loarte, E., Rabatel, A., & Gomez, J. (2015). Determination of the spatio-temporal variations of the glacier equilibrium-line altitude from the snowline altitude in the Cordillera Blanca (Peru). *Rev. Peru. Geo-Atmosferica*, 4, 19-30.

Mastrocicco, M., Colombani, N., Salemi, E., Boz, B., & Gumiero, B. (2016). Managed aquifer recharge via infiltration ditches in short rotation afforested areas. Ecohydrology, 9(1), 167-178. doi:10.1002/eco.1622

McClain, M.E. & Naiman, R.J. (2008). Andean influences on the biogeochemistry and ecology of the Amazon River. *Bioscience*, 8200;58:325-338.

McDonnell, J. J., *et al*. (2007), Moving beyond heterogeneity and process complexity: A new vision for watershed hydrology, *Water Resour. Res.,* 43, W07301, doi:10.1029/2006WR005467

Messerli, B. (2001). Editorial: The International Year of Mountains (IYM). *The Mountain Research Initiative (MRI) News*, vol. 9(3), p. 2. Doi: 10.22498/pages.9.3.2

Mountain Research Initiative EDW Working Group (2015). Elevation-dependent warming in mountain regions of the world, *Nature Climate Change*, 5, 424-430. doi: 10.1038/NGEO1356

Nilsson, C., Reidy, C. A., Dynesius, M., & Revenga, C. (2005). Fragmentation and flow regulation of the world's large river systems. *Science*, 308(5720), 405-408. doi:10.1126/science.1107887

Ochoa-Tocachi, B.F., Bardales, J.D., Antiporta, J., Pérez, K., Acosta, L., Mao, F., Zulkafli, Z., Gil-Ríos, J., Angulo, O., Grainger, S., Gammie, J., De Bièvre, B. & Buytaert, W. (in review). Potential contributions of pre-Inca infiltration infrastructure to Andean water security.

Paul, F., Kääb, A., Maisch, M., Kellenberger, T. & Haeberli, W. (2004). Rapid disintegration of Alpine glaciers observed with satellite data. *Geophysical Research Letters,* vol. 31, no. 21, pp. L21402 1-4.

Pritchard, H. D. (2017). Asia's glaciers are a regionally important buffer against drought. *Nature, 545*(7653), 169-174. doi:10.1038/nature22062

Rabatel, A., Bermejo, A., Loarte, E., Soruco, A., Gomez, J., Leonardini, G., Vincent, C. & Sicart, J.E. (2012). Can the snowline be used as an indicator of the equilibrium line and mass balance for glaciers in the outer tropics? *Journal of Glaciology,* 58(212):1027-1036. Doi: 10.3189/2012JoG12J027

Rabatel, A., Francou, B., Soruco, A., Gomez, J., Cáceres, B., Ceballos, J.L., Basantes, R., Vuille, M., Sicart, J.-., Huggel, C., Scheel, M., Lejeune, Y., Arnaud, Y., Collet, M., Condom, T., Consoli, G., Favier, V., Jomelli, V., Galarraga, R., Ginot, P., Maisincho, L., Mendoza, J., Ménégoz, M., Ramirez, E., Ribstein, P., Suarez, W., Villacis, M. & Wagnon, P. 2013, Current state of glaciers in the tropical Andes: A multi-century perspective on glacier evolution and climate change. *Cryosphere,* vol. 7, no. 1, pp. 81-102.

Ragettli, S., Immerzeel, W. W. & Pellicciotti, F. (2016). Contrasting climate change impact on river flows from high-altitude catchments in the Himalayan and Andes mountains.

Proceedings of the National Academy of Sciences of the United States of America, 113(33), 9222-9227. doi:10.1073/pnas.1606526113

Roe, G. H. (2005). Orographic precipitation. *Annual Review of Earth and Planetary Sciences, Vol. 33: 645-671*, doi:10.1146/annurev.earth.33.092203.122541

Saberi, L., McLaughlin, R., Ng., G.-H. C., La Frenierre, J., Wickert, A., Baraer, M., Zhi, W., Li, L. & Mark, B.G. (2019). Multi-scale temporal variability in meltwater contributions in a tropical glacierized watershed. *Hydrol. Earth Syst. Sci.,* 23, 405-425. doi: 10.5194/hess-23-405-2019.

Shaw, G.D., Conklin, M.H., Nimz, G.J. & Liu, F. (2014). Groundwater and surface water flow to the Merced River, Yosemite Valley, California: ^{36}Cl and Cl^- evidence. *Water Resour. Res.* 50, 1943–1959.

Tague, C., Grant, G., Farrell, M., Choate, J. & Jefferson, A. (2008). Deep groundwater mediates streamflow response to climate warming in the Oregon Cascades. *Climate Change* 86, 189–210.

Tromp-van Meerveld, H. J., Peters, N. E., & McDonnell, J. J. (2007). Effect of bedrock permeability on subsurface stormflow and the water balance of a trenched hillslope at the panola mountain research watershed, Georgia, USA. *Hydrological Processes*, 21(6), 750-769. doi:10.1002/hyp.6265

Veettil, B.K., Wang, S., Florêncio de Souza, S., Bremer, U.F. & Simoes, J.C. (2017). Glacier monitoring and glacier-climate interactions in the tropical Andes: A review. *Journal of South American Earth Sciences*. 77, 218-246. Doi: 10.1016/j.jsames.2017.04.0090895-9811

Viviroli, D., Durr, H.H., Messerli, B., Meybeck, M. & Weingartner, R. (2007). Mountains of the world, water towers for humanity: Typology, mapping, and global significance. *Water Resources Research.* vol. 43, W07447, doi:10.1029/2006WR005653

Vuille, M., Carey, M., Huggel, C., Buytaert, W., Rabatel, A., Jacobsen, D., Soruco, A., Villacis, M., Yarleque, C., Elison Timm, O., Condom, T., Salzmann, N. & Sicart, J. (2018). Rapid decline of snow and ice in the tropical Andes – Impacts, uncertainties and challenges ahead, *Earth-Science Reviews,* vol. 176, pp. 195-213.

Welch, L. A., & Allen, D. M. (2012). Consistency of groundwater flow patterns in mountainous topography: Implications for valley bottom water replenishment and for defining groundwater flow boundaries. *Water Resources Research*, 48(5). doi:10.1029/2011WR010901

Williams, P., & Murray, W. E. (2018). Behind the 'Miracle': Non-traditional agro-exports and water stress in marginalised areas of ica, peru. *Bulletin of Latin American Research*, doi:10.1111/blar.12918

Yarleque, C., Vuille, M., Hardy, D.R., Timm, O.E., De la Cruz, J., Ramos, H., & Rabatel, A. (2018). Projections of the future disappearance of the Quelccaya Ice Cap in the Central Andes. *Scientific Reports* (2018)8:15564, doi:10.1038/s41598-018-33698-z.